# CYTOCHROME P450 METABOLISM INVOLVEMENT IN THE DEVELOPMENT OF HEPATOTOXICITY WITH FIRST-GENERATION NON-NUCLEOSIDE REVERSE TRANSCRIPTASE INHIBITORS

by

Carley Jeanne Sue Heck

A dissertation submitted to Johns Hopkins University in conformity with the requirements for the degree of Doctor of Philosophy

Baltimore, Maryland

June, 2019

**Abstract**

The cytochrome P450 monooxygenase enzymes have been demonstrated to play a role in the metabolism of ~75% of FDA-approved drugs. Though generally thought to facilitate excretion, the metabolism of drugs by P450s generates new molecular entities, which can have differential effects from those of the parent drugs, including off-target, cytotoxic effects. Two hepatotoxic drugs used to treat HIV, efavirenz (EFV) and nevirapine (NVP), are so extensively metabolized by cytochrome P450 enzymes that their main P450 metabolites, 8-hydroxy-EFV (8-OHEFV) and 12-hydroxy-NVP (12-OHNVP), respectively, exist at micromolar concentrations in patient plasma. Previous work suggests that these metabolites play a role in the respective hepatotoxic events observed with these drugs. We probed whether EFV and 8-OHEFV activate hepatic IRE1α-XBP1 signaling, which has been previously demonstrated to activate hepatocyte death under select stimuli. Interestingly, we observed that EFV treatment resulted in a greater magnitude of IRE1α-XBP1 signaling activation in primary hepatocytes than 8-OHEFV. With this, we surveyed other structural changes to EFV and two other compounds (analog 3 and 14) with only single-atom changes from EFV that demonstrated greater activation of IRE1α-XBP1 than EFV itself. Despite all being activators of IRE1α-XBP1, only EFV and analog 3 induced hepatocyte cell death, and only cell death with EFV was inhibited by co-treatment with the IRE1α-XBP1 inhibitor STF083010. Taken together these results suggest that EFV activates IRE1α-XBP1 and that this activation plays a role in the hepatocyte death observed with EFV. In addition,

while other very similar compounds, analogs 3 and 14, are activators of IRE1α-XBP1, they demonstrate variable toxicity or toxicity mechanisms different from that of EFV. We also investigated whether twelfth position deuteration on NVP, generating 12-$D_3$NVP is an effective strategy in controlling hepatic P450 metabolism to 12-OHNVP and ultimately NVP toxicity. A 10.6-fold reduction in production of 12-OHNVP was observed in human hepatocytes during treatments with clinically relevant concentrations of 12-$D_3$NVP (as compared to NVP) with no impact on the formation of other detectable P450 metabolites of NVP. In addition, a kinetic isotope effect of 10.1-fold was measured in incubations with human liver microsomes. Despite this large change in 12-OHNVP production, hepatocyte death was only modestly reduced with 12-$D_3$NVP in primary mouse hepatocytes, as compared to NVP. To investigate potential differences in cell signaling with these compounds we performed relative quantitation proteomics analysis on hepatocytes treated with NVP or 12-$D_3$NVP and observed differential protein expression with these two treatments. These results suggest that deuterium substitution, while an effective strategy for controlling 12-OHNVP production does not drastically reduce NVP hepatotoxicity and that this compound can induce differential protein expression from that observed with NVP.

Doctoral advisor: Dr. Namandjé N. Bumpus

Thesis readers: Dr. Namandjé N. Bumpus

Dr. G. William Wong

Thesis committee: Dr. Namandjé N. Bumpus

Dr. James T. Stivers

Dr. Herschel V. Wade

Dr. G. William Wong

**Copyright Disclaimer**

**Acknowledgements**

First and foremost, I would like to acknowledge my thesis advisor, Namandjé Bumpus. Upon my initial rotation in her lab, it was very clear to me that I could learn and grow immensely both as a scientist and as a person under her guidance. She, of course, did not disappoint. Namandjé has invested countless hours in my development, both in helping me grow in my understanding and implementation of the creative scientific process, but also in my professional development and in my ability to advocate for myself and my ideas. She has also spared no expense in providing me with opportunities to travel and share my research with giants in the field of drug metabolism, as well as explore new and exciting techniques within the lab. I am always constantly impressed with her ability to shift her mentoring style with the various personalities of the individuals that she mentors. Namandjé always made an effort to understand my own individual struggles and motivations, catering her advice and guidance to me personally. She is truly an inspirational presence in my life, and I am confident that I will be able to leverage her teachings throughout the rest of my career. I am so fortunate to have her as a mentor.

Thank you to my thesis committee members, James Stivers, Herschel Wade, and G. William Wong, for their guidance throughout my thesis work. With these individuals on my committee, my meetings were of course scientifically stimulating, but also genuinely fun and enjoyable.

My lab mates, both past and present, have provided me with an excellent work environment. While we don't always agree scientifically, everyone treats

each other with respect, resulting in enjoyable and stimulating conversations that allow us to grow as a group into stronger scientists. I would like to specifically acknowledge a few lab members. Thank you to Allyson Hamlin and Kamal Seneviratne for their contributions to the work outlined in the subsequent chapters. I would also like to thank Julie Lade, who took me under her wing during my first year in the lab, providing me with excellent technical training and professional guidance. In addition, Julie was instrumental in helping me to obtain an internship at Amgen, which was a life-changing experience for me.

The Johns Hopkins Pharmacology and Molecular Sciences graduate program has been a source of immense support during my graduate studies. I would like to acknowledge the excellent departmental leadership by Caren Meyers and James Stivers, who not only work to ensure that we are trained rigorously in the cross-disciplinary study of pharmacology, but also that we are happy while doing so. They are always open to feedback and constantly strive for program growth and improvement. Thank you to Amy Paronto, Mimi Guercio, Brenda Figueroa, and Deborah Saylor for always being there for me when needed assistance and for being sources of years of fun, good natured conversations. These four women work tirelessly to keep this department running and assist student growth and development in every way possible.

The Pharmacology Student Initiative is a student group that I have had the privilege of helping to implement in the department, and through this group have been able to foster meaningful relationships with my fellow graduate students. This group has always strived to foster departmental camaraderie and peer to

peer support systems. Having PSI to for encouragement, fun times, and friendship has been imperative to the successful completion of my thesis work. I look forward to watching PSI grow and improve.

I would like to thank my long-time friends Helen Gassmann, Ethan Goldbach, and Gabrielle Sheller for their love and support. I would also like to acknowledge the friendships I have fostered in graduate school, with Amer Al-Khouja, Nicholas Bienko, Michael Wormald, and Phillip Sanchez, all of whom have been ready to grab a beer or cocktail while we vent, discuss scientific problems, or just laugh and decompress at a moment's notice.

Thank you to Samuel Henager for being a loving and supportive friend and partner. I have the immense privilege of loving a fellow scientist, which means often having my own "Post-Doc" to label my tubes and fetch reagents during weekend lab trips, as well as someone to agonize with me over mass spectrometry fragment structure prediction. In addition, with Sam I have an amazing person to laugh, love, grow, fight, cry, and experience new and wonderful adventures with for the rest of my life.

And finally, thank you to my parents, Patricia and Garth Heck, for their love, and for all of their emotional and financial support during my education. In addition, they have raised me to be patient and open minded- traits that have served me well in the pursuit of my Ph.D. and I believe will continue to allow me to be a rigorous and unbiased scientist throughout the rest of my career. Perhaps most importantly, they have always accepted and forgiven my mistakes and failures without hesitation, something I am extremely grateful for.

**Table of Contents**

## List of Tables

Chapter 3

## List of Figures

## Chapter 1: Introduction

### A Brief History of the Study of Drug Metabolism and Cytochrome P450s

The earliest descriptions of the ability of the human body to chemically modify and excrete a foreign organic compound date back to the mid-1800s, in a pair of publications regarding benzoic acid. Dr. Alexander Ure discovered that following his own oral ingestion of benzoic acid, the structurally similar hippuric acid could be readily detected in his urine (Ure, 1841). This result was verified by Dr. William Keller, who through his own self-experimentation, observed the same result and proposed that the hippuric acid was a product of benzoic acid conjugation by the human body (Keller, 1842). Though in discussing his work Dr. Ure focuses mainly on its implications in the treatment of gout (Ure, 1841), in combination with observations of Dr. Keller, these findings have been cited the beginnings of the study of human drug metabolism (Murphy, 2001). In treating patients with foreign chemical compounds (i.e. drugs), careful characterization of the fate of these drugs following administration is not only scientifically interesting, but is also crucial to the development of safe and effective therapies. Because of this, it is no surprise that the study of drug metabolism has grown significantly and become a vital part of new pharmaceutical development since this early work by Ure and Keller (Murphy, 2001).

An early pioneer in defining the study of human drug metabolism, R.T. Williams, published several works throughout the 1940s-1960s that, in addition to summarizing the work of those before him, helped to define and shape the field of drug metabolism (Jones, 2015). Williams was the first to propose two distinct

phases of drug metabolism: phase I reactions, which consist of drug oxidations, reductions, and hydrolyses; and phase II reactions, which are drug and/or phase I metabolite conjugation reactions. He reasoned that while most drug metabolism reactions were largely inactivating, phase I metabolites may retain biological activity, either against the intended drug target or have an off-target, potentially toxic effect (Figure 1) (Williams, 1959; Jones, 2015).

Many of the first instances of characterized drug and drug metabolite pairings were examples of these phase I oxidation reactions: the conversion of cinnamic acid to benzoic acid (Erdmann and Marchand, 1842), benzene to phenol (Schultzen and Naunyn, 1867), and benzaldehyde to benzoic acid (Wohler and Frerichs, 1848). Almost a century following this initial work, isolated sub-cellular liver fractions, called microsomes, were demonstrated to perform these oxidation reactions in a nicotinamide adenine dinucleotide phosphate (NADPH)-dependent manner (Mueller and Miller, 1949; Axelrod, 1955). Discovered in 1958 and further characterized in 1962 was a novel group of cytochromes in liver microsomal preparations with a strong absorbance peak at 450 nm when carbon-monoxide bound, for which they were given the name “P-450” (hereafter referred to as P450) (Klingenberg, 1958; Omura and Sato, 1962). Not long after this, it was observed that these microsomal cytochrome P450s are able to catalyze the oxidation of small molecules (Estabrook *et al.*, 1963). Since that discovery, 57 different human cytochrome P450 enzymes have been identified and categorized into 18 different families. Cytochrome P450s have been demonstrated to be involved not only in oxidative drug metabolism, but also

in steroid synthesis, cholesterol biosynthesis, bile acid biosynthesis, vitamin degradation, and the metabolism of eicosanoids (Nebert *et al.*, 2013)

Throughout the years of their study, cytochrome P450 nomenclature has been standardized: they are named beginning with “CYP” for cytochrome P450 followed by a number indicating family, a letter indicating subfamily, and finally a number indicating the order of discovery within that subfamily, an example being “CYP1A1” (Nelson, 2006). Cytochrome P450 families 1, 2, 3, and 4 (CYP1, CYP2, CYP3, and CYP4, respectively), are the P450 families implicated in drug metabolism (Nebert *et al.*, 2013). Roughly 75% of approved drugs are metabolized by cytochrome P450 enzymes, and a vast majority (~94%) of these are metabolized by a select few cytochrome P450 enzymes: CYP1A1, -1A2, -1B1, -2A6, -2B6, -2C8, -2C9, -2C19, -2D6, -2E1, -3A4, and -3A5 (Rendic and Guengerich, 2015).

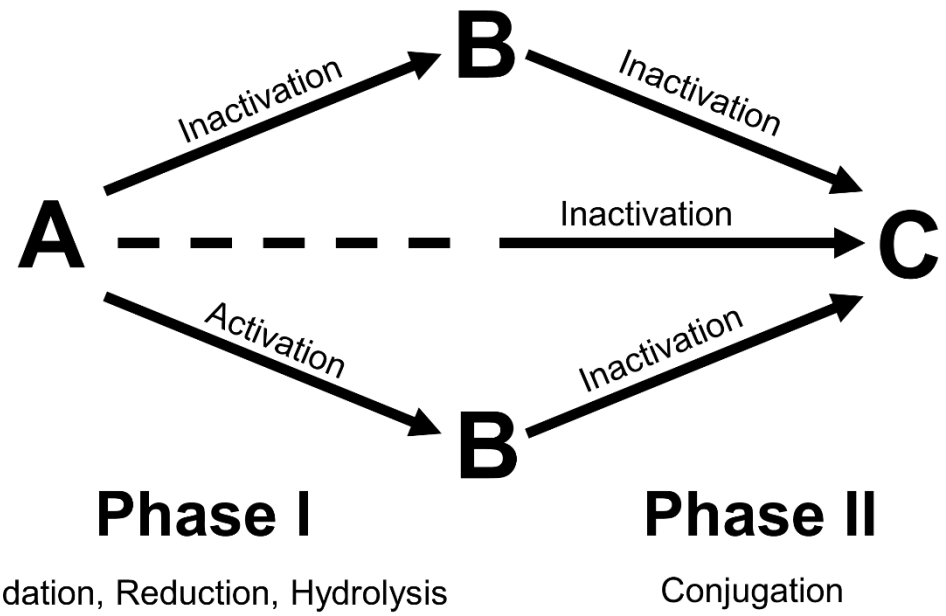


**Figure 1. The two phases of human drug metabolism as described by R.T. Williams.** Drugs (A) can be oxidized, reduced, or hydrolyzed by the human body to form a phase I drug metabolite (B). In addition the drug or phase I metabolite can undergo subsequent conjugation metabolism to form a phase II metabolite (C). Phase I reactions can result in an inactive or biologically active metabolite, while generally phase II reactions are inactivating. This figure has been re-created from Williams, 1959.

## Drug Metabolism by Cytochrome P450s

Following oral ingestion, a drug will be absorbed through the gut wall and into circulation, where the first major organ it encounters is the liver. The liver is home to many different drug metabolizing enzymes, including cytochrome P450s, that will begin to metabolize the drug before it even reaches systemic circulation, an event known as first-pass metabolism (Pond and Tozer, 1984) (Figure 2). The most common result of P450 metabolism is the insertion of an oxygen molecule onto its substrate (Guengerich, 2001). This facilitates foreign compound excretion by increasing hydrophilicity, and therefore clearance from the body via the kidneys, into the urine. Because of this, it has often been reasoned that cytochrome P450s evolved as a defense mechanism against potentially toxic foreign compounds, by metabolically modifying them to facilitate clearance from the body (Gonzalez and Nebert, 1990; Nebert *et al.*, 2013) (Figure 2).

Cytochrome P450s are heme-containing enzymes that catalyze oxygen insertion in an NADPH-dependent fashion. They exist as membrane bound proteins, found largely in the endoplasmic reticulum membrane, on the cytosolic face, and much less so in the mitochondrial membrane (Nebert *et al.*, 2013; Guengerich, 2015). Their activity is facilitated through a complex reaction cycle (Figure 3) that is dependent upon partnering with another membrane bound enzyme, cytochrome P450 reductase. First, the substrate binds near the iron ($Fe^{+3}$)-containing heme causing a conformational shift in the cytochrome P450 enzyme (Figure 3A). P450 reductase utilizes NADPH to donate one electron to

the heme iron (now $Fe^{+2}$) (Figure 3B), which is then able to complex with molecular oxygen ($O_2$) (Figure 3C). Yet another electron is donated by reductase from NAPDH (Figure 3D). Then, through the addition of two protons, one oxygen atom is released as water, during which the iron is reduced, forming a complex of $Fe^{+4}$ and one oxygen atom (Figure 3E and F). In a series of radical-chemistry catalyzed bond breaking/reforming steps, an oxygen is inserted onto the drug substrate (Figure 3G), which can then be released as a novel drug metabolite (Figure 3H) (Guengerich, 2007; Ortiz de Montellano, 2015). These radical-chemistry-based steps are shown in more detail in Figure 4. First, a proton is abstracted from the drug substrate by the iron-bound oxygen. Following this, the carbon radical is then able to abstract the protonated oxygen, resulting in the final oxidized drug metabolite product, and regenerating the initial +3 charge state of the heme iron (Figure 4) (Ortiz de Montellano, 2015).

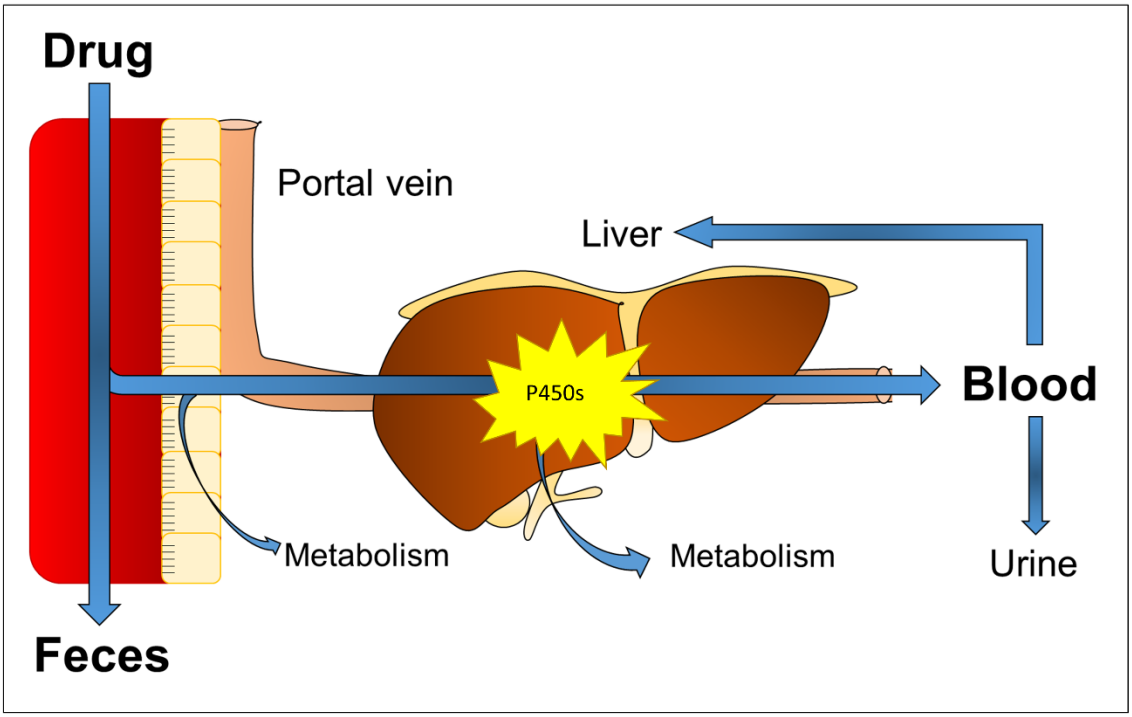


**Figure 2. First-pass metabolism promotes early systemic exposure to drug metabolites.** When orally ingested, a portion of a drug is absorbed through the gut wall and into the portal vein. Before reaching systemic circulation the drug encounters the liver, where it is metabolized by an array of drug metabolizing enzymes, the most common being the cytochrome P450s. This initial act of drug metabolism by the liver, and to some extent also by the gut wall, prior to reaching systemic circulation is known as first-pass metabolism. Following this event, both drug and drug metabolites enter systemic circulation where they can have therapeutic effects, toxic effects, no effect, and/or be excreted in the urine.

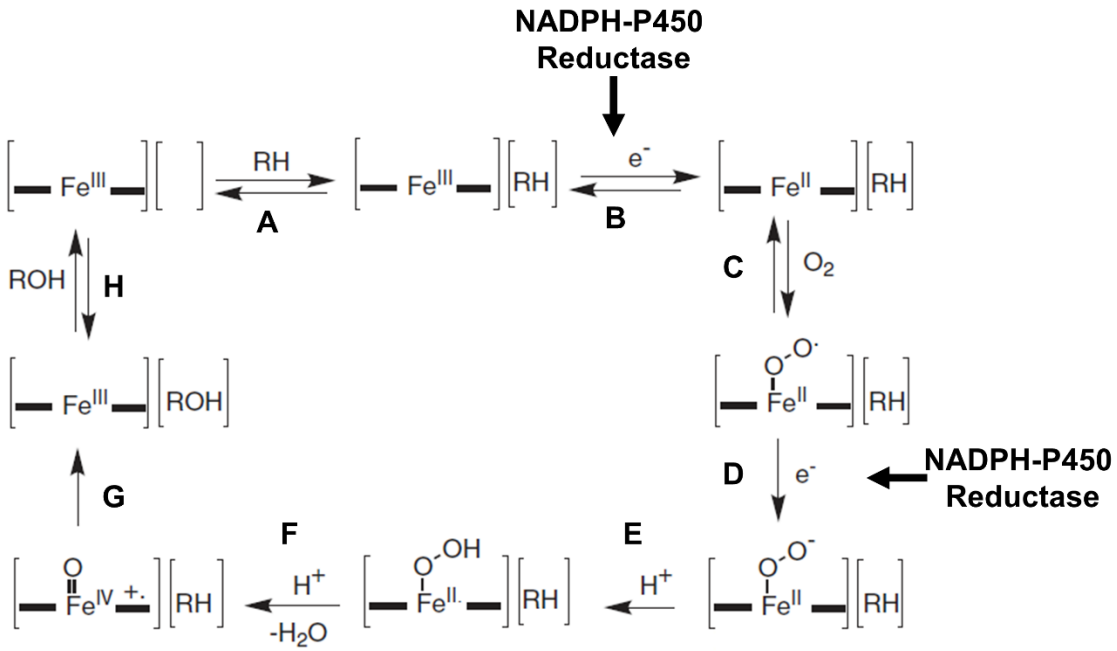


**Figure 3. The cytochrome P450 catalytic cycle.** Upon binding of its substrate (A), a cytochrome P450 will undergo a conformational change that primes it for electron donation by P450 reductase (B). Following this reduction, the P450 can then bind molecular oxygen (C) and be given yet another electron by reductase (D). Through the addition two protons (E and F), one oxygen atom is released in the form of water and the P450 is primed to insert an oxygen onto its substrate (G), which is then released (H). This figure was modified from Ortiz de Montellano, 2015.

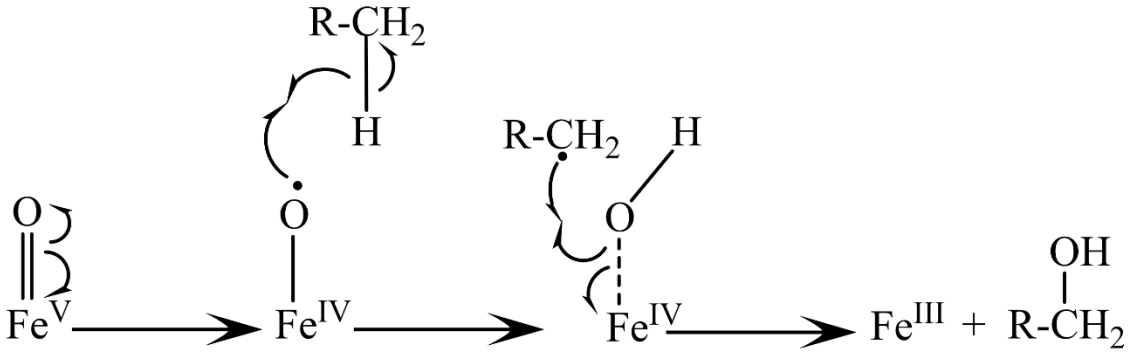


**Figure 4. The mechanism of P450-dependent oxygen insertion onto an organic substrate.** The bound oxygen atom will first donate an electron to reduce the iron of the cytochrome P450 heme. This event primes the oxygen to abstract and proton from the substrate, creating a carbon radical that is then resolved when the substrate subsequently abstracts the protonated oxygen atom bound to the P450 heme iron. This step returns the iron to its initial charge state ($Fe^{+3}$), allowing the P450 to restart its catalytic cycle following substrate release.

## Implications of Cytochrome P450 Metabolism in Drug Toxicity

It is important to emphasize that upon metabolizing a drug, cytochrome P450 oxidation creates a completely new molecular entity. Because of this, there are several possible consequences of P450 drug metabolism. First, the drug metabolite may be rendered completely inactive. If not completely inactivated, the metabolite may retain pharmacologic activity towards the intended drug target that is greater or lesser than the parent drug. In addition to this, the metabolite may also have off-target, potentially cytotoxic effects that could be the same as or different from the parent drug (Williams, 1959; Guengerich, 2001). This last potential outcome is the main focus of the subsequent chapters.

One of the first identified toxic cytochrome P450 metabolites was characterized by G. Dahl *et al.*, in which they demonstrated that bacterial cell death during incubation with vinyl carbamate and metabolically active hepatic microsomes was drastically reduced during co-treatment with cytochrome P450 inhibitors (Dahl *et al.*, 1978). Another example of the toxic effects of P450 metabolites can be seen in formation of neurotoxic protein pyrroles formed from the metabolite of hexane, 2,5-hexanedione (Couri and Milks, 1982; Couri and Milks, 1985; Genter St Clair *et al.*, 1988). Suicide inactivation of cytochrome P450 metabolizing enzymes, in which the drug becomes covalently bound to the P450 itself during the course of the metabolism reaction, has been observed for many different P450 substrates. This often results in unintended increased drug exposure or drug-drug interactions if the inactivated P450 is involved in the metabolism of another drug a given patient is taking. This can also cause the

inactivation of a P450 involved in endogenous small molecule synthesis (Oritz de Montellano and Correia, 1983; Guengerich, 2001; Hollenberg *et al.*, 2008). Some of the first identified incidences of this suicide inactivation involved acetylenic substrates that covalently bind to the P450 heme during metabolism, resulting in altered P450 absorbance spectra (Ortiz de Montellano and Kunze, 1980; Hollenberg *et al.*, 2008). The “grapefruit juice effect” is another representation of suicide inactivation in which bergamottin, a furanocoumarin found in grapefruit, results in the inactivation of several P450s in the 3A and 2B subfamilies (Lin *et al.*, 2005), and can result in decreased drug plasma concentrations in patients following ingestion of grapefruit juice (Edgar *et al.*, 1992; Hollenberg *et al.*, 2008).

Hepatotoxicity with the widely used analgesic acetaminophen is a well-studied example of a drug metabolism-related adverse event. During standard dosing, acetaminophen is extensively cleared (~90 %) through conjugation by uridine 5’-diphospho-glucuronosyltransferase (UGT) or sulfotransferase (SULT) drug metabolizing enzymes. A smaller portion of this drug is also metabolized by CYP2E1 to form N-acetyl-p-benzoquinone imine (NAPQI). NAPQI is toxic but also generally inactivated by conjugation with endogenous glutathione. Under instances of acetaminophen overdose these UGT and SULT enzyme systems become saturated, and glutathione drastically reduced. This results in shunting to metabolism by CYP2E1, causing increased production of NAPQI that can no longer be inactivated by glutathione conjugation. This increase in liver exposure to NAPQI can cause serious hepatotoxicity (Jollow *et al.*, 1973; Mitchell *et al.*,

1973a; Mitchell *et al.*, 1973b; Potter *et al.*, 1973; Guengerich, 2001; James *et al.*, 2003).

One can imagine that the concern for P450 metabolite-related toxicity is that much greater for extensively metabolized drugs, and in addition for drugs that reach high systemic concentrations. Together, these factors may result in exposure to high circulating concentrations of a drug metabolite, which could have serious consequences if that metabolite has harmful effects. This thesis work focuses on two such drugs, which demonstrate high plasma concentrations and are extensively metabolized by cytochrome P450s, within the same drug class: first-generation non-nucleoside inhibitors (NNRTIs) used in the treatment of human immunodeficiency virus (HIV).

Cytochrome P450 Metabolism of Efavirenz and Nevirapine

Nevirapine (NVP) and efavirenz (EFV), approved for use in the United States in 1996 and 1998, respectively, are two of the three first-generation NNRTIs approved for the treatment of human immunodeficiency virus. They function by allosterically inhibiting the reverse transcriptase enzyme vital to successful integration of HIV into the host genome (Usach *et al.*, 2013). Both of these drugs are categorized as essential therapies by the World Health Organization as part of combination therapy for the treatment of HIV; NVP is also used to prevent mother-to-infant transmission of HIV during childbirth (WHO, 2017).

NVP, sold under the trade name Viramune® (Boehringer Ingelheim Pharmaceuticals, 2018), is used in combination therapy with the nucleoside

reverse transcriptase inhibitors zidovudine and lamivudine (WHO, 2017). NVP is dosed at 200 mg per day for the first 14 days of administration, after which the dose is increased to 200 mg twice per day (Boehringer Ingelheim Pharmaceuticals, 2018). EFV is marketed under the name Sustiva® (Bristol-Meyers Squibb Company, 2017). In 2006, the first single-pill formulation combination therapy for the treatment of HIV was released containing EFV with the nucleoside reverse transcriptase inhibitors tenofovir and emtricitabine, marketed under the name Atripla®. EFV is dosed once-daily at 600 mg. (Usach *et al.*, 2013; Gilead Sciences, 2018).

At steady-state, under normal dosing regimens, both EFV and NVP reach circulating concentrations in the micromolar range. NVP has been demonstrated to reach steady-state plasma concentrations averaging 16.0 μM (95% CI [10.0, 19.2]) (Marinho *et al.*, 2014) and 26.7 μM (95% CI [19.1, 50.2]) (Fan-Havard *et al.*, 2013). EFV target plasma concentrations generally range from 3-12 μM (Fayet Mello *et al.*, 2011), though in some instances EFV plasma concentrations have been demonstrated to climb as high as 50 μM (Marzolini *et al.*, 2001; Gounden *et al.*, 2010). In comparison, rilpivrine, a more recently developed second-generation NNRTI that is dosed at 25 mg per day (Usach *et al.*, 2013), has been demonstrated to have circulating plasma concentrations of 0.71 ±0.15 μM (Goebel *et al.*, 2006).

Both EFV and NVP are extensively metabolized by cytochrome P450 monooxygenase enzymes. Nevirapine is metabolized to four mono-oxygenated metabolites: 2-hydroxy- (2-OH), 3-hydroxy- (3OH), 8-hydroxy (8-OH), and 12-

hydroxy-nevirapine (12-OHNVP) (Figure 5) (Erickson *et al.*, 1999). On the other hand, efavirenz is metabolized by P450s to both mono- and dioxygenated metabolites: 7-hydroxy (7-OHEFV), 8-hydroxy (8-OHEFV), 7,8-dihydroxy- (7,8-OHEFV), 8,14-drihydroxy-efavirenz (8,14-OHEFV), as well as a third dioxygenated, metabolite from 8-OHEFV for which the position oxygen insertion has not been fully characterized (Figure 6) (Avery *et al.*, 2013).

Given the high circulating plasma concentrations of EFV and NVP, as well as their extensive metabolism, it is of little surprise that patients are also exposed to micromolar circulating concentrations of the primary monooxygenated metabolites. In patients receiving standard dosing of NVP-containing therapies, circulating levels of 12-OHNVP are the highest of the NVP P450-dependent metabolites. Plasma concentrations of 12-OHNVP have been measured at 1.0 μM (95% CI [0.5, 3.8]) (Fan-Havard *et al.*, 2013), and 1.3 μM (95% CI [0.9, 1.9]) (Marinho *et al.*, 2014). For EFV, 8-OHEFV has been demonstrated to be the primary P450 metabolite (Ward *et al.*, 2003; Grilo *et al.*, 2016). The metabolism of EFV to 8-OHEFV is so extensive that circulating concentrations of this P450 metabolite have been demonstrated to be nearly equimolar to that of EFV. In one study of patients receiving standard EFV- containing therapy, concentrations of EFV and 8-OHEFV were 10.33 ± 0.98 μM and 6.51 ± 0.87 μM, respectively (Ngaimisi *et al.*, 2010). In another, average plasma concentrations were 4.61 μM for EFV and 3.14 μM for 8-OHEFV (Grilo *et al.*, 2016).

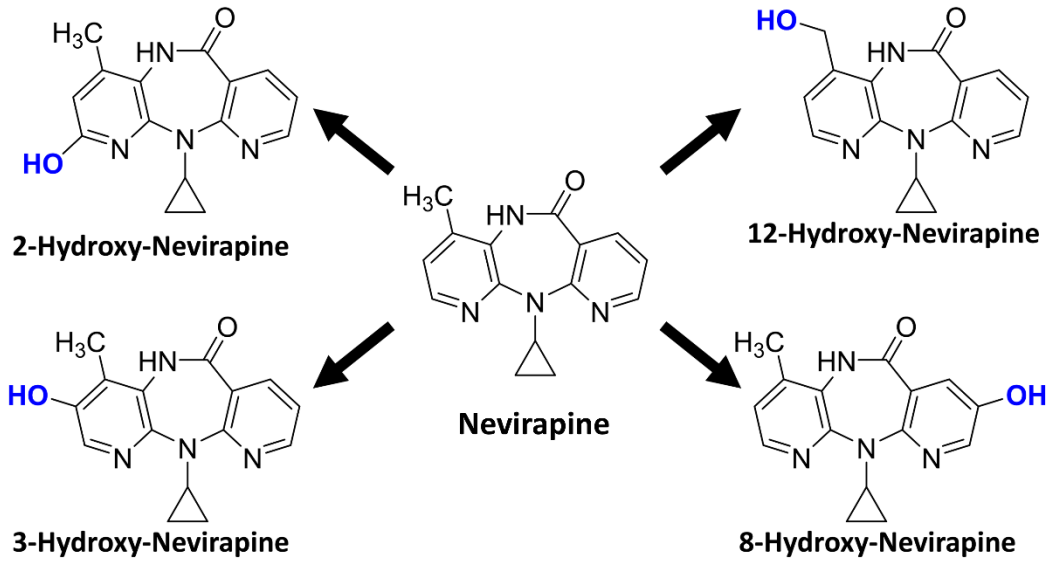


**Figure 5. The monooxygenated human cytochrome P450-dependent metabolites of NVP.** NVP is metabolized by human cytochrome P450 enzymes to four monooxygenated metabolites: 2-, 3-, 8-, and 12-OHNVP.

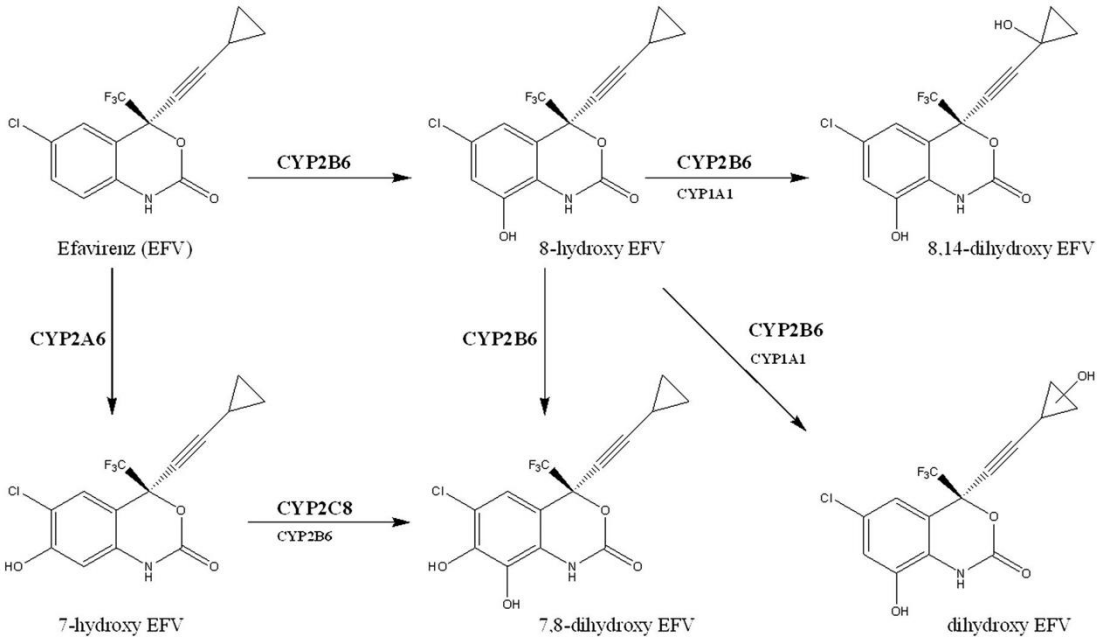


**Figure 6. The mono- and dioxygenated human cytochrome P450-dependent metabolites of NVP.** EFV is metabolized by human cytochrome P450 enzymes to two monooxygenated metabolites: 7- and 8-OHEFV. 8-OHEFV can then undergo further metabolism to 7,8-OHEFV, 8,14-OHEFV, and to a third deoxygenated metabolite. This figure is adapted from (Avery *et al.*, 2013).

## Nevirapine Hepatotoxicity

The prescribing information for NVP contains a black-box warning for potentially fatal hepatotoxic events. In addition, it states that monitoring patients during their initial weeks taking NVP is “essential”, prompting physicians to employ “extra vigilance”. It is because of this that NVP is prescribed with a lead-in dose of 200 mg per day for the first 14 days, after which the dose is increased to 200 mg twice per day (Boehringer Ingelheim Pharmaceuticals, 2018). Nevirapine hepatotoxicity has been characterized as an immune hypersensitivity response (Popovic *et al.*, 2010), resulting in extensive immune-cell infiltration of the liver, promoting hepatic cell death and tissue necrosis (Jao *et al.*, 2010; Adaramoye *et al.*, 2012; Sharma *et al.*, 2012). One mechanism that promotes drug-induced hypersensitivity reactions is the formation of neo-antigens through the adduct formation of reactive drugs or drug metabolites with biomolecules such as DNA or proteins. These form hapten-like neo-antigens that appear foreign to the adaptive immune system, resulting in a potentially cytotoxic immune response towards the cells harboring the novel drug-biomolecule derived antigens (Zhang *et al.*, 2013; Mak and Uetrecht, 2017).

There have been several studies investigating the potential for reactivity of NVP and NVP monooxygenated metabolites with proteins and DNA. Across the board these studies have demonstrated that P450 metabolism to 12-OHNVP plays a role in adduct formation, either by way of promoting downstream metabolism to a potentially reactive 12-sulfoxy-NVP conjugate or through the formation of a reactive intermediate during the production of 12-OHNVP itself

(Chen *et al.*, 2008; Antunes *et al.*, 2010; Sharma *et al.*, 2012; Antunes *et al.*, 2013; Sharma *et al.*, 2013; Zhang *et al.*, 2013; Pinheiro *et al.*, 2016). Rats dosed with 12-OHNVP as compared to NVP show a higher incidence of another NVP hypersensitivity reaction, skin rash formation (Chen *et al.*, 2008). In addition the formation of NVP-protein adducts in human liver fractions has been demonstrated to be drastically reduced or modified using treatments with a pan-CYP inhibitor preventing overall NVP metabolism, and during treatments with equimolar amounts of a tri-deuterated version of NVP that undergoes less P450 metabolism to 12-OHNVP (Sharma *et al.*, 2012). This tri-deuterated NVP (12-$D_3$NVP) has been also demonstrated to reduce NVP skin rash incidence in rats (Chen *et al.*, 2008), and will be the subject of research and discussion in this thesis work investigating P450 metabolite-mediated hepatotoxicity.

**Efavirenz Hepatotoxicity**

Efavirenz, like nevirapine, has also been demonstrated to cause severe hepatotoxic events in patients (Brück *et al.*, 2008), including hepatocyte cell death and dyslipidemia (Feeney and Mallon, 2011; Shubber *et al.*, 2013). Hepatotoxicity has been linked to elevated plasma concentrations of EFV (Yimer *et al.*, 2012), prompting both therapeutic drug monitoring and dose reduction in patients (Fayet Mello *et al.*, 2011). During treatment with EFV patients present ~10% of the time with grade 3 or grade 4 (severe) hepatotoxicity, characterized by highly elevated serum transaminases and cholestasis (Kontorinis and Dieterich, 2003). In severe cases, life-threatening fulminant hepatic failure has occurred (Abrescia *et al.*, 2002).

The metabolism to 8-OHEFV has also been implicated in another adverse reaction of EFV, neurotoxicity, and has been shown to cause cytotoxic effects to primary neuronal cell cultures at concentrations much lower than EFV itself (Tovar-y-Romo *et al.*, 2012). Interestingly, it has also been demonstrated by our lab that treatment of primary human hepatocytes with 8-OHEFV results in the activation of c-Jun N-terminal kinase (JNK)-dependent cell death more readily than treatment with EFV, and that co-treatment with EFV and a pan-CYP inhibitor reduces the levels of EFV-induced hepatocyte death (Bumpus, 2011). It has recently been uncovered that EFV is an activator of the ER stress response (Apostolova *et al.*, 2013), however the contributions of the 8-OHEFV metabolite in this activation has yet to be examined. One pathway of this cell stress response, the inositol requiring enzyme 1α (IRE1α)/ X-box binding protein 1 (XBP1) signaling axis, can result in the activation of JNK-dependent cell death (Urano *et al.*, 2000), as we have observed with EFV and 8-OHEFV treatment in hepatocytes. Given this information, it is important to understand whether EFV or 8-OHEFV are activators of IRE1α-XBP1 and if activation of this pathway by either compound is playing a part in the hepatocyte death observed with EFV.

**Summary**

Given the similarities between EFV and NVP (high systemic concentrations, extensive P450 metabolism, and serious adverse hepatotoxic events), I feel that these first-generation NNRTIs present an intriguing opportunity to study the chemical and molecular mechanisms of drug-induced hepatotoxicity, and the potential role of cytochrome P450 metabolism in these

toxicities. Patients are exposed to micromolar concentrations of both the parent drug compound (EFV or NVP) and of the primary monooxygenated metabolites (8-OHEFV and 12-OHNVP), and previous work suggests that these monooxygenated metabolites may play a role in promoting the toxicity of these compounds. With this work, I aim to investigate potential contributions of these P450 metabolites and the dynamics of P450 metabolism in the hepatotoxicity of EFV or NVP (Figure 7).

Furthering our scientific understanding of drug metabolism has been a point of genuine curiosity not only for myself but for over a century's worth of scientists; from the early identification of drug and oxidized drug metabolite pairs, followed by the discovery of the cytochrome P450 monooxygenase drug metabolizing enzymes, to the characterization of P450s significant contributions to drug metabolism of the vast majority of approved pharmaceuticals. Cytochrome P450 drug metabolism is an imperative topic of investigation should we desire to continue to develop safer and more efficacious small molecule therapies.

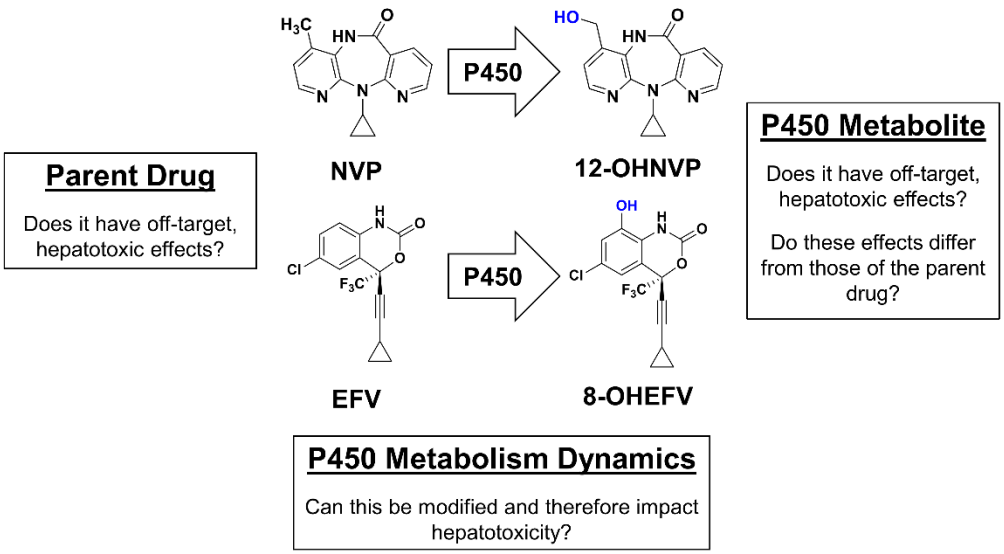


**Figure 7. A visual summary of the questions and principles guiding this work.** The extensive P450 metabolism of the hepatotoxic first-generation NNRTIs NVP and EFV (NVP to 12-OHNVP and EFV to 8-OHEFV) provides an interesting opportunity to study the contributions of both drug and drug-metabolite in promoting hepatotoxicity. In addition, I also am interested in modifying the dynamics of P450 metabolism to observe any potential impact on drug hepatotoxicity.

## References


Abrescia N, D'Abbraccio M, Figoni M, Busto A, Butrico E, De Marco M and Viglietti R (2002) Fulminant hepatic failure after the start of an efavirenz-based HAART regimen in a treatment-naive female AIDS patient without hepatitis virus co-infection. J Antimicrob Chemother 50:763-765.

Adaramoye OA, Adesanoye OA, Adewumi OM and Akanni O (2012) Studies on the toxicological effect of nevirapine, an antiretroviral drug, on the liver, kidney and testis of male Wistar rats. *Hum Exp Toxicol* **31**:676-685.

Antunes AM, Godinho AL, Martins IL, Justino GC, Beland FA and Marques MM (2010) Amino acid adduct formation by the nevirapine metabolite, 12-hydroxynevirapine--a possible factor in nevirapine toxicity. *Chem Res Toxicol* **23**:888-899.

Antunes AM, Wolf B, Oliveira MC, Beland FA and Marques MM (2013) 2'-Deoxythymidine adducts from the anti-HIV drug nevirapine. *Molecules* **18**:4955-4971.

Apostolova N, Gomez-Sucerquia LJ, Alegre F, Funes HA, Victor VM, Barrachina MD, Blas-Garcia A and Esplugues JV (2013) ER stress in human hepatic cells treated with Efavirenz: Mitochondria again. *Journal of Hepatology* **59**:780-789.

Avery LB, VanAusdall JL, Hendrix CW and Bumpus NN (2013) Compartmentalization and antiviral effect of efavirenz metabolites in blood plasma, seminal plasma, and cerebrospinal fluid. *Drug Metab Dispos* **41**:422-429.

Axelrod J (1955) The enzymatic deamination of amphetamine (benzedrine). *J Biol Chem* **214**:753-763.

Boehringer Ingelheim Pharmaceuticals I (2018) VIRAMUNE® [Prescribing Information], in, Boehringer Ingelheim Pharmaceuticals, Inc., Ridgefield, CT.

Bristol-Meyers Squibb Company (2017) SUSTIVA ® [Prescribing information], in, Bristol-Myers Squibb Company, Princeton, NJ.

Brück S, Witte S, Brust J, Schuster D, Mosthaf F, Procaccianti M, Rump JA, Klinker H, Petzold D and Hartmann M (2008) Hepatotoxicity in patients prescribed efavirenz or nevirapine. *Eur J Med Res* **13**:343-348.

Bumpus NN (2011) Efavirenz and 8-hydroxyefavirenz induce cell death via a JNK- and BimEL-dependent mechanism in primary human hepatocytes. *Toxicol Appl Pharmacol* **257**:227-234.

Chen J, Mannargudi BM, Xu L and Uetrecht J (2008) Demonstration of the metabolic pathway responsible for nevirapine-induced skin rash. *Chem Res Toxicol* **21**:1862-1870.

Couri D and Milks M (1982) Toxicity and metabolism of the neurotoxic hexacarbons n-hexane, 2-hexanone, and 2,5-hexanedione. *Annu Rev Pharmacol Toxicol* **22**:145-166.

Couri D and Milks MM (1985) Hexacarbon neuropathy: tracking a toxin. *Neurotoxicology* **6**:65-71.

Dahl GA, Miller JA and Miller EC (1978) Vinyl carbamate as a promutagen and a more carcinogenic analog of ethyl carbamate. *Cancer Res* **38**:3793-3804.

Edgar B, Bailey D, Bergstrand R, Johnsson G and Regårdh CG (1992) Acute effects of drinking grapefruit juice on the pharmacokinetics and dynamics of felodipine--and its potential clinical relevance. *Eur J Clin Pharmacol* **42**:313-317.

Erdmann O and Marchand R (1842) Metabolism of cinnamic acid to hippuric acid in animals. *Ann Chem Pharm* **44**:344.

Erickson DA, Mather G, Trager WF, Levy RH and Keirns JJ (1999) Characterization of the in vitro biotransformation of the HIV-1 reverse transcriptase inhibitor nevirapine by human hepatic cytochromes P-450. *Drug Metab Dispos* **27**:1488-1495.

Estabrook R, Cooper D and Rosenthal O (1963) The light-reversible carbon monoxide inhibition of the steroid C-21 hydroxylation system of the adrenal cortex. *Biochem Z* **338**:741-755.

Fan-Havard P, Liu Z, Chou M, Ling Y, Barrail-Tran A, Haas DW, Taburet AM and Group AS (2013) Pharmacokinetics of phase I nevirapine metabolites following a single dose and at steady state. *Antimicrob Agents Chemother* **57**:2154-2160.

Fayet Mello A, Buclin T, Decosterd LA, Delhumeau C, di Iulio J, Fleurent A, Schneider MP, Cavassini M, Telenti A, Hirschel B and Calmy A (2011) Successful efavirenz dose reduction guided by therapeutic drug monitoring. *Antivir Ther* **16**:189-197.

Feeney ER and Mallon PW (2011) HIV and HAART-Associated Dyslipidemia. *Open Cardiovasc Med J* **5**:49-63.

Genter St Clair MB, Amarnath V, Moody MA, Anthony DC, Anderson CW and Graham DG (1988) Pyrrole oxidation and protein cross-linking as necessary steps in the development of gamma-diketone neuropathy. *Chem Res Toxicol* **1**:179-185.

Gilead Sciences (2018) ATRIPLA ® [Prescribing Information], in, Gilead Sciences, Inc., Foster City, CA.

Goebel F, Yakovlev A, Pozniak AL, Vinogradova E, Boogaerts G, Hoetelmans R, de Béthune MP, Peeters M and Woodfall B (2006) Short-term antiviral activity of TMC278--a novel NNRTI--in treatment-naive HIV-1-infected subjects. *AIDS* **20**:1721-1726.

Gonzalez FJ and Nebert DW (1990) Evolution of the P450 gene superfamily: animal-plant 'warfare', molecular drive and human genetic differences in drug oxidation. *Trends Genet* **6**:182-186.

Gounden V, van Niekerk C, Snyman T and George JA (2010) Presence of the CYP2B6 516G> T polymorphism, increased plasma Efavirenz concentrations and early neuropsychiatric side effects in South African HIV-infected patients. *AIDS Res Ther* **7**:32.

Grilo NM, Correia MJ, Sequeira C, Harjivan SG, Caixas U, Diogo LN, Marques MM, Monteiro EC, Antunes AM and Pereira SA (2016) Efavirenz biotransformation as an up-stream event of mood changes in HIV-infected patients. *Toxicol Lett* **260**:28-35.

Guengerich F (2015) Human Cytochrome P450 Enzymes, in *Cytochrome P450: Structure, Mechanism, and Biochemistry, Fourth Edition* (Ortiz de Montellano P ed) pp 523-785, Springer International Publishing.

Guengerich FP (2001) Common and uncommon cytochrome P450 reactions related to metabolism and chemical toxicity. *Chem Res Toxicol* **14**:611-650.

Guengerich FP (2007) Mechanisms of cytochrome P450 substrate oxidation: MiniReview. *J Biochem Mol Toxicol* **21**:163-168.

Hollenberg PF, Kent UM and Bumpus NN (2008) Mechanism-based inactivation of human cytochromes p450s: experimental characterization, reactive intermediates, and clinical implications. *Chem Res Toxicol* **21**:189-205.

James LP, Mayeux PR and Hinson JA (2003) Acetaminophen-induced hepatotoxicity. *Drug Metab Dispos* **31**:1499-1506.

Jao J, Sturdevant M, del Rio Martin J, Schiano T, Fiel MI and Huprikar S (2010) Nevirapine-induced stevens johnson-syndrome and fulminant hepatic failure requiring liver transplantation. *Am J Transplant* **10**:1713-1716.

Jollow DJ, Mitchell JR, Potter WZ, Davis DC, Gillette JR and Brodie BB (1973) Acetaminophen-induced hepatic necrosis. II. Role of covalent binding in vivo. *J Pharmacol Exp Ther* **187**:195-202.

Jones AW (2015) Profiles in drug metabolism and toxicology: Richard Tecwyn Williams (1909-1979). *Drug Metab Rev* **47**:401-405.

Keller W (1842) M. Keller on the Conversion of Benzoic into Hippuric Acid. *Prov Med J Retrosp Med Sci* **4**:256-257.

Klingenberg M (1958) Pigments of rat liver microsomes. *Arch Biochem Biophys* **75**:376-386.

Kontorinis N and Dieterich DT (2003) Toxicity of non-nucleoside analogue reverse transcriptase inhibitors. *Semin Liver Dis* **23**:173-182.

Lin HL, Kent UM and Hollenberg PF (2005) The grapefruit juice effect is not limited to cytochrome P450 (P450) 3A4: evidence for bergamottin-dependent inactivation, heme destruction, and covalent binding to protein in P450s 2B6 and 3A5. *J Pharmacol Exp Ther* **313**:154-164.

Mak A and Uetrecht J (2017) Immune mechanisms of idiosyncratic drug-induced liver injury. *J Clin Transl Res* **3**:145-156.

Marinho AT, Rodrigues PM, Caixas U, Antunes AM, Branco T, Harjivan SG, Marques MM, Monteiro EC and Pereira SA (2014) Differences in nevirapine biotransformation as a factor for its sex-dependent dimorphic profile of adverse drug reactions. *J Antimicrob Chemother* **69**:476-482.

Marzolini C, Telenti A, Decosterd LA, Greub G, Biollaz J and Buclin T (2001) Efavirenz plasma levels can predict treatment failure and central nervous system side effects in HIV-1-infected patients. *AIDS* **15**:71-75.

Mitchell JR, Jollow DJ, Potter WZ, Davis DC, Gillette JR and Brodie BB (1973a) Acetaminophen-induced hepatic necrosis. I. Role of drug metabolism. *J Pharmacol Exp Ther* **187**:185-194.

Mitchell JR, Jollow DJ, Potter WZ, Gillette JR and Brodie BB (1973b) Acetaminophen-induced hepatic necrosis. IV. Protective role of glutathione. *J Pharmacol Exp Ther* **187**:211-217.

Mueller GC and Miller JA (1949) The reductive cleavage of 4-dimethylaminoazobenzene by rat liver; the intracellular distribution of the enzyme system and its requirement for triphosphopyridine nucleotide. *J Biol Chem* **180**:1125-1136.

Murphy PJ (2001) Xenobiotic metabolism: a look from the past to the future. *Drug Metab Dispos* **29**:779-780.

Nebert DW, Wikvall K and Miller WL (2013) Human cytochromes P450 in health and disease. *Philos Trans R Soc Lond B Biol Sci* **368**:20120431.

Nelson DR (2006) Cytochrome P450 nomenclature, 2004. *Methods Mol Biol* **320**:1-10.

Ngaimisi E, Mugusi S, Minzi OM, Sasi P, Riedel KD, Suda A, Ueda N, Janabi M, Mugusi F, Haefeli WE, Burhenne J and Aklillu E (2010) Long-term efavirenz autoinduction and its effect on plasma exposure in HIV patients. *Clin Pharmacol Ther* **88**:676-684.

Omura T and Sato R (1962) A new cytochrome in liver microsomes. *J Biol Chem* **237**:1375-1376.

Oritz de Montellano PR and Correia MA (1983) Suicidal destruction of cytochrome P-450 during oxidative drug metabolism. *Annu Rev Pharmacol Toxicol* **23**:481-503.

Ortiz de Montellano P (2015) Substrate Oxidation by Cytochrome P450 Enzymes, in *Cytochrome P450: Structure, Mechanism, and Biochemistry, Fourth Edition* (Ortiz de Montellano P ed), Springer International Publishing.

Ortiz de Montellano PR and Kunze KL (1980) Self-catalyzed inactivation of hepatic cytochrome P-450 by ethynyl substrates. *J Biol Chem* **255**:5578-5585.

Pinheiro PF, Pereira SA, Harjivan SG, Martins IL, Marinho AT, Cipriano M, Jacob CC, Oliveira NG, Castro MF, Marques MM, Antunes AM and Miranda JP (2016) Hepatocyte spheroids as a competent in vitro system for drug biotransformation studies: nevirapine as a bioactivation case study. *Arch Toxicol*.

Pond SM and Tozer TN (1984) First-pass elimination. Basic concepts and clinical consequences. *Clin Pharmacokinet* **9**:1-25.

Popovic M, Shenton JM, Chen J, Baban A, Tharmanathan T, Mannargudi B, Abdulla D and Uetrecht JP (2010) Nevirapine hypersensitivity. *Handb Exp Pharmacol*:437-451.

Potter WZ, Davis DC, Mitchell JR, Jollow DJ, Gillette JR and Brodie BB (1973) Acetaminophen-induced hepatic necrosis. 3. Cytochrome P-450-mediated covalent binding in vitro. *J Pharmacol Exp Ther* **187**:203-210.

Rendic S and Guengerich FP (2015) Survey of Human Oxidoreductases and Cytochrome P450 Enzymes Involved in the Metabolism of Xenobiotic and Natural Chemicals. *Chem Res Toxicol* **28**:38-42.

Schultzen O and Naunyn B (1867) The behavior of benzene-derived hydrocarbons in the animal organism. *duBois-Reymond's Arch Anat Physiol*:349.

Sharma AM, Klarskov K and Uetrecht J (2013) Nevirapine bioactivation and covalent binding in the skin. *Chem Res Toxicol* **26**:410-421.

Sharma AM, Li Y, Novalen M, Hayes MA and Uetrecht J (2012) Bioactivation of nevirapine to a reactive quinone methide: implications for liver injury. *Chem Res Toxicol* **25**:1708-1719.

Shubber Z, Calmy A, Andrieux-Meyer I, Vitoria M, Renaud-Théry F, Shaffer N, Hargreaves S, Mills EJ and Ford N (2013) Adverse events associated with nevirapine and efavirenz-based first-line antiretroviral therapy: a systematic review and meta-analysis. *AIDS* **27**:1403-1412.

Tovar-y-Romo LB, Bumpus NN, Pomerantz D, Avery LB, Sacktor N, McArthur JC and Haughey NJ (2012) Dendritic spine injury induced by the 8-hydroxy metabolite of efavirenz. *J Pharmacol Exp Ther* **343**:696-703.

Urano F, Wang X, Bertolotti A, Zhang Y, Chung P, Harding HP and Ron D (2000) Coupling of stress in the ER to activation of JNK protein kinases by transmembrane protein kinase IRE1. *Science* **287**:664-666.

Ure A (1841) On gouty concretions, with a new method of treatment. *Med Chir Trans* **24**:30-35.

Usach I, Melis V and Peris JE (2013) Non-nucleoside reverse transcriptase inhibitors: a review on pharmacokinetics, pharmacodynamics, safety and tolerability. *J Int AIDS Soc* **16**:1-14.

Ward BA, Gorski JC, Jones DR, Hall SD, Flockhart DA and Desta Z (2003) The cytochrome P450 2B6 (CYP2B6) is the main catalyst of efavirenz primary and secondary metabolism: implication for HIV/AIDS therapy and utility of

efavirenz as a substrate marker of CYP2B6 catalytic activity. *J Pharmacol Exp Ther* **306**:287-300.

WHO (2017) WHO Model List of Essential Medicines- 20th Edition, in, World Health Organization, http://www.who.int/medicines/publications/essentialmedicines/en/.

Williams RT (1959) *Detoxication mechanisms*. John Wiley and Sons, London.

Wohler F and Frerichs F (1848) Concerning the modifications which particular organic materials undergo in their transition to the urine. *Ann Chem Pharm* **63**:335.

Yimer G, Amogne W, Habtewold A, Makonnen E, Ueda N, Suda A, Worku A, Haefeli WE, Burhenne J, Aderaye G, Lindquist L and Aklillu E (2012) High plasma efavirenz level and CYP2B6*6 are associated with efavirenz-based HAART-induced liver injury in the treatment of naïve HIV patients from Ethiopia: a prospective cohort study. *Pharmacogenomics J* **12**:499-506.

Zhang X, Sharma AM and Uetrecht J (2013) Identification of danger signals in nevirapine-induced skin rash. *Chem Res Toxicol* **26**:1378-1383.

## Chapter 2: Efavirenz and Efavirenz-like Compounds Activate Human, Murine, and Macaque Hepatic IRE1α-XBP1

### Abstract

Efavirenz (EFV), a widely used antiretroviral drug, is associated with idiosyncratic hepatotoxicity and dyslipidemia. Here we demonstrate that EFV stimulates the activation in primary hepatocytes of key cell stress regulators: inositol requiring 1α (IRE1α) and X-box binding protein 1 (XBP1). Following EFV exposure, XBP1 splicing (indicating activation) was increased 35.7-fold in primary human hepatocytes. Paralleling this, XBP1 splicing and IRE1α phosphorylation (p-IRE1α, active IRE1α) were elevated 36.4-fold and 4.9-fold, respectively, in primary mouse hepatocytes. Of note, with EFV treatment, 47.2% of mouse hepatocytes were apoptotic; which was decreased to 23.9% in the presence of STF083010, an inhibitor of XBP1 splicing. Experiments performed using pregnane X receptor (PXR)-null mouse hepatocytes revealed that EFV-mediated XBP1 splicing and hepatocyte death were not dependent on PXR, which is a nuclear receptor transcription factor that plays a crucial role in the cellular response to xenobiotics. Interestingly, incubation with the primary metabolite of EFV, 8-hydroxyEFV (8-OHEFV), only resulted in 10.3-, and 2.9-fold increased XBP1 splicing in human and mouse hepatocytes and no change in levels of p-IRE1α in mouse hepatocytes. To further probe the structure-activity relationship of IRE1α-XBP1 activation by EFV, 16 EFV analogs were employed. Of these, an analog in which the EFV alkyne is replaced with an alkene and an analog in which the oxazinone oxygen is replaced by a carbon stimulated XBP1

splicing in human, mouse, and macaque hepatocytes. These data demonstrate that EFV and compounds sharing the EFV scaffold can activate IRE1α-XBP1 across humans, mice, and macaques.

## Introduction

Efavirenz (EFV) is a non-nucleoside reverse transcriptase inhibitor widely used for treatment of HIV. Both EFV and EFV-containing multidrug regimens are classified as essential therapies by the World Health Organization (WHO, 2017a). However, EFV causes dyslipidemia (Feeney and Mallon, 2011) and hepatotoxicity (Shubber *et al.*, 2013) in some patients, and elevated plasma EFV concentrations have been linked to EFV-induced liver injury (Yimer *et al.*, 2012). Target therapeutic plasma concentration range for EFV is 3-12 μM, however concentrations can climb dramatically above this, requiring dose adjustment (Fayet Mello *et al.*, 2011). In some instances, plasma EFV concentrations have been reported to meet or exceed 50 μM (Marzolini *et al.*, 2001; Gounden *et al.*, 2010).

EFV is extensively metabolized in the liver by cytochrome P450 (CYP) mono-oxygenases (Avery *et al.*, 2013), with the primary mono-oxygenated metabolite being 8-hydroxyefavirenz (8-OHEFV) (Ward *et al.*, 2003). Concentrations of 8-OHEFV can become nearly equal to EFV in plasma during EFV dosing (Ngaimisi *et al.*, 2010; Grilo *et al.*, 2016). One study measured average plasma EFV and 8-OHEFV concentrations of 4.61 μM and 3.14 μM, respectively, in patients receiving 600 mg of EFV daily for at least one month (Grilo *et al.*, 2016). In addition, EFV induces its own metabolism via activation of

the pregnane X receptor (PXR) (Ngaimisi *et al.*, 2010; Swart *et al.*, 2012; Sharma *et al.*, 2013b; Narayanan *et al.*, 2018), which is a nuclear receptor transcription factor that modulates the cellular response to xenobiotics via altering expression of drug metabolizing enzymes (Hedrich *et al.*, 2016; Buchman *et al.*, 2018). Previously, we demonstrated that 8-OHEFV causes hepatocyte death in vitro, observing that incubation with either EFV or 8-OHEFV is able to activate cell death in a c-Jun N-terminal kinase (JNK)-dependent fashion in primary human hepatocytes (Bumpus, 2011).

One highly conserved signaling pathway that results in JNK- dependent cell death activation is the inositol-requiring enzyme 1α (IRE1α) arm of the endoplasmic reticulum (ER) stress response (Urano *et al.*, 2000). During ER stress, misfolded proteins accumulate in the ER, stimulating the release of deactivating chaperone binding immunoglobulin protein from IRE1α, allowing this membrane protein to dimerize and auto-phosphorylate, at which point IRE1α is considered to be activated (Bertolotti *et al.*, 2000; Lee *et al.*, 2008b; Korennykh *et al.*, 2009). When activated, IRE1α can recruit TNF receptor-associated factor 2 and subsequently activate JNK-dependent cell death (Urano *et al.*, 2000). In addition, dimerized IRE1α possess endoribonuclease activity allowing for targeted cleavage of the mRNA transcript of the transcription factor X-box-binding protein 1 (XBP1); resulting in the loss of an internal 26 nucleotide sequence, converting this transcript from its unspliced, inactive form (uXBP1), to its spliced, active form (sXBP1) (Lee *et al.*, 2002). As such, the levels of phosphorylated IRE1α and XBP1 splicing are routinely measured experimentally

as hallmarks of the activation of this pathway (Sha *et al.*, 2009; Ning *et al.*, 2011; Hur *et al.*, 2012).

It is generally assumed that sXBP1 transcriptional regulation serves a cytoprotective function, as many of its known gene targets consist membrane biogenesis and ER-associated protein degradation components, that work to reduce the build-up of potentially harmful misfolded proteins, as well as expand the capacity of the ER (Jiang D, 2015). However, in the instance of hepatotoxicity and hepatic dyslipidemia, sXBP1 has been shown to both prevent and promote these occurrences, depending upon the stimuli. Inhibition of XBP1 splicing diminished the negative effects of high-fat diet in mice, which exhibited decreased steatosis, decreased hepatic lipid droplet number, and decreased serum alanine and aspartate transaminases (Lebeaupin *et al.*, 2018). Conversely, hepatocyte specific IRE1α-null mice, which lack the ability to activate XBP1, show increased hepatic steatosis and lipid content over WT mice both basally and during ER stress activation. (Zhang *et al.*, 2011).

With this previous work in mind, we sought to gain a deeper understanding of the impact of EFV and 8-OHEFV on hepatocytes. In doing so, we tested whether EFV and 8-OHEFV activate IRE1α-XBP1 signaling, and on a broader level the relationship in EFV structure and its ability to activate IRE1α-XBP1. We observed the conservation of this response across sex and in humans versus model organisms. Because EFV causes patient hepatic dyslipidemia and XBP1 regulates lipid homeostasis, we probed for XBP1-dependency in EFV-mediated hepatic lipid accumulation. And finally, we investigated whether

activation of either IRE1α-XBP1 signaling plays a role in EFV- and 8-OHEFV-induced hepatotoxicity. Using EFV, 8-OHEFV, and structurally-related compounds to EFV we aim to contribute to the growing body of work on the stimuli-specific role of XBP1s in liver disease progression.

## Materials and Methods

### Chemical Reagents

Efavirenz (EFV) was obtained from the National Institutes of Health AIDS Research and Reference Reagent Program (Germantown, MD), and had a purity of 99.4% as assessed by the manufacturer using HPLC in comparison to a USP reference standard. EFV analogs and 8-OHEFV were synthesized by Toronto Research Chemicals (Toronto, Canada). Analogs used in this study were (S)-1-(2-Amino-5-chlorophenyl)-1-(trifluoromethyl)-3-cyclopropyl-2-propyn-1-ol (**1**), (R)-5-Chloro-α-(cyclopropylethynyl)-2-amino-α-(trifluoromethyl) benzenemethanol (**2**), (4S)-6-Chloro-4-[(1E)-2-cyclopropylethenyl]-1,4-dihydro-4-(trifluoromethyl)-2H-3,1-Benzoxazin-2-one (**3**), rac 6-Chloro-1,4-dihydro-4-(1-pentynyl)-4-(trifluoromethyl)-2H-3,1-benzoxazin-2-one (**4**), (R)-5-Chloro-α-(cyclopropylethynyl)-2-[[(4-methoxyphenyl)methyl]amino]-α-(trifluoromethyl)benzenemethanol (**5**), (S)-5-Chloro-α-(cyclopropylethynyl)-2-[[(4-methoxyphenyl)methyl]amino]-α-(trifluoromethyl)benzenemethanol (**6**), rac N-[4-Chloro-2-[3-cyclopropyl-1-hydroxy-1-(trifluoromethyl) -2-propynyl]phenyl]-4-methoxybenzamide (**7**), (4S)-6-Chloro-4-(2-cyclopropylethynyl)-1,4-dihydro-4-(trifluoromethyl)-2H-3,1- benzoxazine (**8**), (4S)-6-Chloro-4-(cyclopropylethynyl)-1,4-dihydro-2-(4-methoxyphenyl)-4-(trifluoromethyl)-2H-3,1-benzoxazine (**9**), 1-

(2-Amino-5-chloro-3-methoxyphenyl)-2,2,2-trifluoro Ethanone (**10**), 6-Chloro-4-(2-cyclopropylethynyl)-1,4-dihydro-2-methyl-4-(trifluoromethyl)-2H-3,1-benzoxazine (**11**), (4S)-6-Chloro-4-[(1E)-2-cyclopropylethenyl]-3,4-dihydro-4-(trifluoromethyl)-,2(1H)-quinazolinone (**12**), (4S)-6-chloro-4-(cyclopropylethynyl)-3,4-dihydro-4-(trifluoromethyl)-2(1H)-Quinazolinone (**13**), 6-Chloro-4-(cyclopropylethynyl)-3,4-dihydro-4-(trifluoromethyl)-2(1H)-quinolinone (**14**), 6-Chloro-4-(cyclopropylethynyl)-4-(trifluoromethyl)-4H-benzo[d][1,3]dioxin-2-one (**15**), and 7-Chloro-1-(cyclopropylethynyl)-1-(trifluoromethyl)isochroman-3-one (**16**). EFV analogs and 8-OHEFV had a purity of ≥ 97%, except analog **9** which had a purity of 95%, as assessed by the manufacturer (using 1H nuclear magnetic resonance and mass spectrometry). Tunicamycin (TM) was purchased from Sigma, STF083010 from Tocris Bioscience, staurosporine from Cell Signaling Technology, oleic acid from Sigma, and hydrogen peroxide from Sigma.

**Primary hepatocyte isolation and culture**

Experiments using mice were approved by the Johns Hopkins Animal Care and Use Committee and performed in accordance with Guide for the Care and Use of Laboratory Animals as adopted and promulgated by the U.S. National Institutes of Health. Primary mouse hepatocytes were isolated from C57BL/6J male and female wild-type mice, aged 8-12 weeks (The Jackson Laboratory), and from male and female PXR-null mice, aged 8-12 weeks (Taconic Biosciences, Inc). Hepatocytes were isolated as previously described (Lee *et al.*, 2004). All hepatocyte preparations used for experiments were ≥ 80% viable upon plating. For mRNA isolation, cells were plated onto 12-well collagen coated

plates (Corning) at a density of 100,000 viable cells/well. For protein isolation, cells were plated onto 6-well collagen coated plates (Corning) at density of 240,000 viable cells/well. For cell staining experiments, cells were plated on rat tail collagen-1 (ThermoFisher) coated 18 mm coverslips and placed in non-coated 12-well plates (Falcon), at a density of 100,000 cells/well. Cells were allowed to adhere overnight following isolation, and new medium was added prior to treatment.

Primary human (male and female) and cynomolgus macaque (male) hepatocytes were purchased from BioIVT (Baltimore, MD). Cells were plated at a density of 700,000 viable cells/well for EFV versus analog incubations and at 100,000 viable cells/well for EFV versus 8-OHEFV with a viability of ≥ 90%. Cells were plated in 12-well collagen coated plates. Upon receipt of the cells, the medium was changed to the above described and cells were allowed to acclimate to medium for 4 hours prior to addition of drug. Hepatocytes from all species were cultured in Williams' E Medium (Gibco) supplemented with 5% fetal bovine serum (Gibco) 2 mM L-Glutamine (Gibco) 100 units/mL penicillin and 100 µg/mL streptomycin (Gibco).

**RT-PCR measurement of XBP1 splicing**

EFV, 8-OHEFV and analogs dissolved in 100% DMSO were added directly to culture wells (containing 1 mL of medium) for final concentrations of 10, 20, 30, 40, or 50 µM and 0.1% DMSO. For comparison of EFV and 8-OHEFV, cells were incubated with 10 or 50 µM of EFV or 8-OHEFV for 4 hours. For time and concentration dependency experiments, cells were exposed to

concentrations ranging from 10-50 μM EFV for 4 hours or 50 μM EFV for 5 minutes, 15 minutes, 30 minutes, 1 hour, 2 hours, or 4 hours. For comparison of analogs, a final concentration of 50 μM EFV or analogs of EFV was tested for 4 hours. For PXR dependency experiments, WT and PXR-null cells were treated with 50 μM EFV for 4 hours. For co-treatments with STF083010, STF083010 was added at the same time as EFV for final concentrations of: 100 μM inhibitor, 50 μM EFV or analogs, and 0.2% DMSO, with which cells were incubated for 8 hours. Positive control incubations with tunicamycin (TM) at 1 μg/mL were performed. After incubations, medium was aspirated,and cells were harvested in 0.5 mL TRIzol reagent (Life Technologies). RNA was isolated following the manufacturer's protocol for TRIzol reagent. RNA was then quantified (A260) and reverse transcribed (RT) at 50 ng/μL into cDNA (Maxima enzyme, ThermoFisher). Polymerase chain reaction (PCR) (Phusion HF enzyme, New England Biolabs) was then performed using primers (purchased from IDT) that simultaneously amplify both sXBP1 and uXBP1, which was confirmed by Sanger sequencing. The primer sequences used were: 5'-TACGGGAGAAAACTCACGG-3' (Mouse XBP1 forward), 5'-TTCCAGCTTGGCTGATGAGG-3' (Mouse XBP1 reverse), 5'-GCTCGAATGAGTGAGCTGGA-3' (Human and Cynomolgus macaque XBP1 forward), and 5'-GGTGGTAAGGAACTGGGTC-3' (Human and Cynomolgus macaque XBP1 reverse). PCR products were resolved using 7.5% polyacrylamide (Biorad) tris-borate EDTA (Quality Biologicals) gel electrophoresis. Gels were stained with SYBR safe DNA stain (Invitrogen) and visualized using UV light with a Bio-Rad ChemiDoc gel imager. Image Lab

software by Bio-Rad (Version 5.2.1) was used for densitometric PCR band quantitation. Densitometric signal for sXBP1 was divided by that for uXBP1 to obtain a semi-quantitative measure of XBP1 splicing activation.

**Immunoblotting**

For comparison of IRE1α phosphorylation activation by EFV and 8-OHEFV, cells were incubated with EFV at 10, 20, 30, 40, or 50 μM, or 8-OHEFV at 50 μM for 2 hours. For PXR-dependency of IRE1α phosphorylation experiments, cells were treated with EFV at 50 μM for 2 hours. For 4-hydroxynonenal measurements, cell were treated with EFV at 20 μM for 8 hours. DMSO (0.1%) was used for vehicle. Hepatocytes were washed and harvested in PBS (Gibco), lysed in 1X cell lysis buffer (Cell Signaling Technology) with 0.5 mM phenylmethylsulfonyl fluoride (Sigma) and 1X Halt™ protease and phosphatase inhibitor cocktail (ThermoFisher) by passage through a 27-gauge syringe tip 30 times. Insoluble debris was removed by centrifugation at 3000 x *g* for 10 minutes at 4 °C. Protein concentration was quantified using a bicinchoninic acid assay (Pierce), 50 μg of protein per sample was resolved using 10% sodium dodecyl sulfate polyacrylamide gel electrophoresis (Biorad) and then transferred to a nitrocellulose membrane (Life Technologies). Blots were then probed using antibodies specific to the following target proteins: phospho-S724-IRE1α (Abcam, ab48187), IRE1α (Cell Signaling Technology, 14C10), 4-hydroxynonenal (Abcam, ab46545) and β-actin (Cell Signaling Technology, 13E5), and probe binding detected with horseradish peroxidase-conjugated goat anti-rabbit IgG secondary antibody (Cell Signaling Technology) followed by development with

SuperSignal® West Femto Maximum Sensitivity Substrate (p-IRE1α, and IRE1α) or SuperSignal® West Dura Extended Duration Substrate (β-actin). Light release was imaged using a Bio-Rad ChemiDoc gel imager. Densitometry quantitation was performed as described above and p-IRE1α signal intensity divided by IRE1α signal intensity.

**Lipid Droplet Staining**

Hepatocytes were incubated for 8 hours with EFV at 20 μM (with 0.1% DMSO as a final vehicle concentration) or with EFV at 20 μM in the presence or absence of 100 μM STF083010 (with 0.2% DMSO as a final vehicle concentration). Positive control incubations were with oleic acid at 500 μM. Cells were washed in PBS, fixed in 4% paraformaldehyde in PBS (Affymetrix) for 7 minutes, permeabilized in 60% isopropanol (Fisher Chemical) for 5 minutes, stained with 0.3% Oil Red O (Sigma) in 60% isopropanol, and counterstained with hematoxylin (Cell Signaling Technology). Coverslips were then attached to slides with SignalStain mounting media (Cell Signaling Technology) and allowed to dry overnight. Images were taken using Olympus BX51TF bright field microscope equipped with a DP70 color camera, maintained by the Johns Hopkins Medicine Institute for Basic Biomedical Sciences Microscope Facility. Oil Red O stain was quantified using Nikon NIS- Elements, Advanced Research Version 3.22.00, and normalized to cell count for each image.

**8-hydroxydeoxyguanosine staining**

Following 4 hour exposure to 20 μM EFV, 50 μM EFV, or 200 μM of the positive control hydrogen peroxide (all treatments were in a final vehicle

concentration of 0.1% DMSO) cells were washed in PBS, then fixed and permeabilized by incubation at room temperature in pre-chilled 100% methanol (Fisher Chemical) for 5 minutes. Coverslips were blocked using 1% bovine serum albumin (Sigma), 300 mM glycine (Affymetrix) and 0.1% Triton™ Xte-100 (Sigma) in PBS, probed with an antibody specific to 8-hydroxydeoxyguanosine (8-OHdG, ThermoFisher, PA1-84172), and probe binding detected with an Alexa Fluor 488 conjugated rabbit anti-goat IgG Superclonal™ secondary antibody (ThermoFisher). Nuclei were counterstained with 4',6-Diamidino-2-Phenylindole, Dihydrochloride (DAPI, Cell Signaling Technology). Coverslips were mounted as described above and images were obtained using an Olympus BX51 fluorescent equipped with a Roper Photometrics Coolsnap HQ CCD camera, maintained by the Johns Hopkins Medicine Institute for Basic Biomedical Sciences Microscope Facility. DAPI was detected using a dichroic 400 nm filter, and for Alexa Fluor 488 a dichroic filter of 495 nm for excitation and a 525/50 nm filter for emission. Images were processed using ImageJ software. Staining was assessed by cell counting, with cell nuclei co-staining for both DAPI and 8-hydroxydeoxyguanosine identified as positive.

**Cell viability staining**

Cells were treated for 8 hours with EFV, analog 3, or analog 14 at 20 μM in the presence or absence of 100 μM STF083010, or staurosporine alone at 10 μM (all treatments were in a final vehicle concentration of 0.2% DMSO). Cells were then washed in PBS, and incubated in 100 μg/mL ethidium bromide (EtBr, Sigma) and 100 μg/mL acridine orange (AcrO, Life Technologies) diluted in PBS

for 15 minutes at room temperature. Coverslips were mounted, fluorescently imaged, and images processed in ImageJ. EtBr was detected using dichroic filter of 593 nm for excitation and a 642/40 nm filter for emission, and for AcrO a dichroic filter of 495 nm for excitation and a 525/50 nm filter for emission. Viability was assessed by cell counting, with cell nuclei co-staining with both AcrO and EtBr identified as apoptotic.

**qPCR measurement of DNJB9 and CYP2B10 gene expression**

Hepatocytes were incubated for 8 hours with 20 μM EFV, 20 μM analog 3, 20 μM analog 14, or 1 μg/mL TM for DnaJ heat-shock protein family member 9 (DNAJB9) expression analysis or with 50 μM EFV for 4 hours for CYP2B10 expression analysis (treatments were performed with final vehicle concentrations of 0.1% DMSO). RNA was isolated and reverse transcribed as described above. Quantitative PCR was performed for DNAJB9 and GAPDH using Maxima SYBR Green qPCR Master Mix (ThermoFisher). The primers used during quantitative real-time PCR analyses of mouse DNAJB9, CYP2B10, and GAPDH were as follows: DNJB9 forward 5'-GGGCGCACAGGTTATTAGAA-3', DNAJB9 reverse 5'-ACGCTTCTGCAATCTCTCTGA-3', CYP2B10 Forward 5'-GCCCAATGTTTAGTGGAGGA-3', CYP2B10 Reverse 5'-GACTTCTCCTTCTCCATGCG-3' GAPDH forward 5'-GAAGGCCGGGGCCCACTTGA-3', and GAPDH reverse 5'-TCTCCAGGCGGCACGTCAGA-3'. The GAPDH PCR product from mouse cDNA was isolated and ligated into a pJET1.2 plasmid using a CloneJET PCR cloning kit (ThermoFisher). This plasmid was transformed into and purified from DH5α

competent cells (Invitrogen). Purified plasmid was used to generate a gene copy number standard curve used in qPCR analyses. Normalized DNAJB9 expression levels were calculated by dividing DNAJB9 copy number by GAPDH copy number.

**Data Analysis**

Statistical analysis was performed in GraphPad Prism 7. For any measures involving ratios (sXBP1/uXBP1, p-IRE1α/ IRE1α, qPCR gene expression analysis, and fold change in Oil Red O staining), data was log-transformed, and the data analysis performed on the log transformed data. For these data sets, fold-changes throughout the text are reported as ratios of geometric means. For XBP1 splicing, western blotting, qPCR, and Oil Red O staining data, statistical significance was determined using an unpaired t-test (without assuming consistent SD, without corrections for multiple comparisons, generating two-tailed P values). For comparison of XBP1 splicing levels across sex, statistical significance from vehicle was determined for treatments in both male and female mouse primary hepatocytes, and for any compounds that showed statistically significant splicing in either group, statistical significance of splicing differences between male and female mouse hepatocytes was assessed. For cell imaging with EtBr/AcrO and 8-OHdG staining a paired-ratio t-test was performed to assess statistical significance of fold-changes between control and treated values, generating two-tailed P values. P-values are shown as: * or # $P<0.05$, ** or ## $P<0.01$, *** or ### $P<0.001$, and n.s. highlighting select non-statistically significant differences. For values reported in the text,

95% confidence intervals have been provided, and were calculated assuming normal distribution.

## Results

### Stimulation of IRE1α-XBP1 Activation by EFV in Human and Mouse Primary Hepatocytes

In order to investigate whether IRE1α -XBP1 is activated by EFV and 8-OHEFV, XBP1 splicing was quantified following incubation of primary hepatocytes with these two compounds. In primary human hepatocytes, a 35.7-fold (95% CI [10.6,120.3]) increase in the ratio of unspliced to spliced XBP1 was measured following 4 hour exposure of cells to 50 μM EFV as compared to vehicle control, while parallel treatments performed using 8-OHEFV only rendered a 10.3-fold increase (95% CI [4.9,21.7]). Neither compound stimulated splicing at 10 μM in primary human hepatocytes. In order to test whether the impact of EFV and 8-OHEFV on hepatic XBP1 splicing is conserved in mice, mouse primary hepatocytes were employed. Commensurate with what was observed using human hepatocytes, XBP1 splicing was increased 36.4-fold (95% CI [21.0, 63.3]) in mouse hepatocytes in response to 50 μM EFV. In addition, primary mouse hepatocytes incubated with 10 μM EFV showed a 1.9-fold (95% CI [1.3, 2.9]) increase in XBP1 splicing. In contrast to what was observed using primary human hepatocytes, the presence of 50 μM 8-OHEFV only resulted in a 2.9-fold increase (95% CI [1.5, 6.0]) in spliced XBP1 in mouse hepatocytes. Tunicamycin (TM), a known activator of IRE1α -XBP1 signaling (Yoshida *et al.*, 2001), was used as a positive control in this study, exhibiting an increase in

splicing in both human and mouse primary hepatocytes (Figure 1). To further characterize this response in primary mouse hepatocytes, we examined time-and dose-dependence of EFV activation of XBP1 splicing. When primary mouse hepatocytes were incubated for 4 hours with a range of concentrations of EFV (10-50 μM) XBP1 splicing was elevated in the presence of 30, 40 and 50 μM EFV (Figure 2A). Following primary mouse hepatocyte treatment with 50 μM EFV for a range of time points (5 min to 4 hours), XBP1 splicing was first elevated at 1 hour and this was sustained through 4 hours. The time profile determined for EFV paralleled that of TM (Figure 2B).

Since IRE1α is the endoribonuclease responsible for splicing XBP1 mRNA, and phosphorylation of IRE1α is a marker for activation of this enzyme (Lee *et al.*, 2008b), we tested whether IRE1alpha is phosphorylated in response to EFV or 8-OHEFV. Following 2 hours of treatment, the levels of phosphorylated IRE1α were increased in a dose responsive manner from 1.5-fold (95% CI [1.2, 1.9]) with 20 μM EFV to 4.9-fold (95% CI [4.1, 5.8]) with 50 μM EFV, as compared to vehicle control. Phosphorylation of IRE1α was not elevated above vehicle controls in the presence of 10 μM EFV or 50 μM 8-OHEFV (Figure 2C).

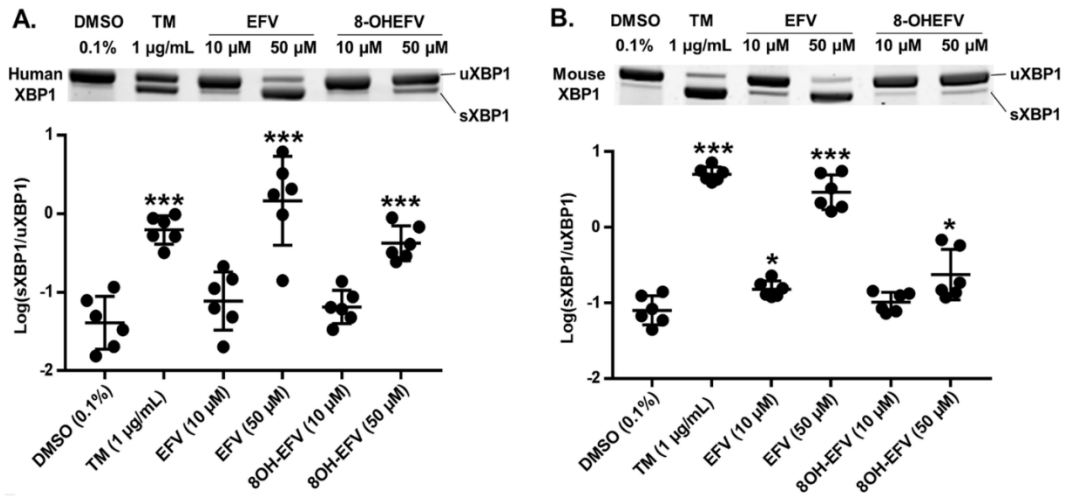


**Figure 1. XBP1 splicing during incubation of primary human and mouse hepatocytes with EFV and 8-OHEFV.** Representative gel images and sXBP1/uXBP1 densitometry quantification ratios of XBP1 mRNA splicing from semi-quantitative RT-PCR in A. human primary hepatocytes (n=6) and B. male mouse primary hepatocytes (n=6) in the presence of EFV or 8OH-EFV at 10 µM or 50 µM for 4 hours. Data are the mean ± SD. Ratios of sXBP1/uXBP1 densitometry were log-transformed and the statistical significance of TM, EFV, or 8-OHEFV treatments from DMSO (0.1%) control was determined using an unpaired t-test on the transformed data, generating two-tailed P-values (* $P<0.05$ and *** $P<0.001$).

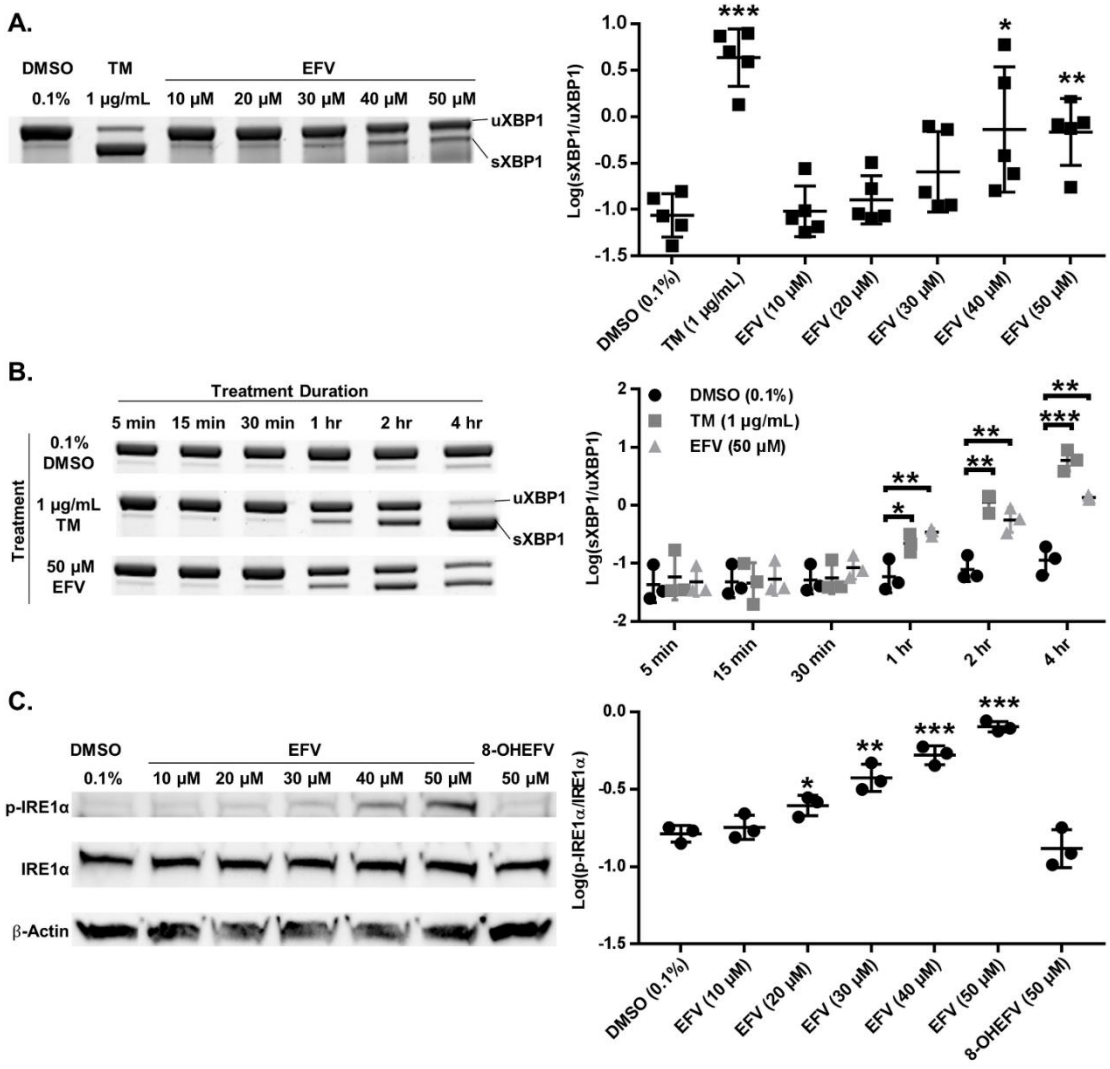


**Figure 2. IRE1α-XBP1 signaling during exposure of primary mouse hepatocytes to EFV or 8-OHEFV.** Representative gel images and sXBP1/uXBP1 densitometry quantification ratios of XBP1 mRNA splicing from semi-quantitative RT-PCR in A. male mouse primary hepatocytes incubated with 10, 20, 30, 40, or 50 μM EFV for 4 hours (mean ± SD, n=5), and B. male mouse primary hepatocytes with 50 μM EFV for 5 min, 15 min, 30 min, 1 hr, 2 hr, or 4 hr (mean ± SD, n=4). C. Representative images for western blotting of p-IRE1α, total IRE1α, and β-Actin and densitometry quantification ratios of p-IRE1α/total

IRE1α for male mouse primary hepatocytes treated with 10, 20, 30, 40, 50 μM EFV or 50 μM 8-OH EFV for 2 hours (mean ± SD, n=3). Ratios of sXBP1/uXBP1 and p-IRE1α/total IRE1α densitometry were log-transformed and the statistical significance of TM, EFV, or 8-OHEFV treatments from DMSO (0.1%) control was determined using an unpaired t-test on the transformed data. For B. treatments were compared to the DMSO control from the same time point. Two-tailed P-values were generated for all analyses (* $P<0.05$, ** $P<0.01$, *** $P<0.001$).

**Impact of EFV Structure on XBP1 Splicing Activation in Primary Mouse Hepatocytes**

Single oxygen insertion, changing EFV to 8-OHEFV, markedly decreased IRE1α-XBP1 activation. Because of this, we were interested in investigating how other structural changes to EFV impact its ability to activate this signaling event, and whether the structure-activity relationship between EFV and IRE1α-XBP1 activation is conserved across species. A panel of sixteen EFV analogs was employed (Figure 3). The structural changes in these analogs have been previously observed by our group to impact both PXR activation (Narayanan *et al.*, 2018) and metabolism by CYP2B6 (Cox and Bumpus, 2014; Cox and Bumpus, 2016). They have been designed to probe specific sections and features of the EFV molecule: the integrity of the oxazinone ring (analogs 1 and 2), the alkyne-cyclopropyl arm (analogs 3 and 4), increases in EFV size (analogs 5-7, and 9), decrease in size (analog 10), and discreet changes to the constituents of the oxazinone ring (analogs 8 and 11-16).

In addition to EFV, treatment with several of the sixteen analogs tested consistently resulted XBP1 splicing activation across species (Figure 4): analog **3**, in which the EFV alkyne is changed to a trans-alkene; analog **14**, in which the oxazinone ring oxygen has been replaced with a carbon atom; and analogs **12, 13, 14** and **15**. Macaque hepatocytes were least sensitive to XBP1 splicing activation in response to both EFV and analogs of EFV (Figure 4A and 4D).

To investigate potential sexual dimorphisms in the activation of IRE1α-XBP1 by EFV and EFV analogs, XBP1 splicing was quantified in male and

female primary mouse hepatocytes separately (Figure 4B). XBP1 splicing in vehicle control treated hepatocytes was not statistically different between the two groups. In the presence of EFV, as well as analogs **3**, **5, 6, 7**, **12**, **14**, and **15**, similar magnitudes of XBP1 splicing were observed in male and female primary mouse hepatocytes. Of note, analogs **3** and **14** exhibited higher levels of XBP1 splicing than that of EFV in both groups. Using analog **3,** XBP1 splicing was 2.4-fold (male) and 1.8-fold (female) higher (95% CI are [0.8, 7.0] and [0.67, 4.9], respectively) than splicing in EFV cells, and using analog **14**, splicing was 3.7-fold (male) and 2.7-fold (female) greater (95% CI are [1.2, 11.5] and [1.0, 6.9], respectively) than that measured following treatment with EFV. Analog **11** stimulated splicing to a level that reached statistical significance only in male mouse hepatocytes, although XBP1 splicing was also elevated, albeit not to a statistically significant degree, by this compound in female mouse hepatocytes as well. XBP1 splicing in the presence of analog **13** was measured in both male and female primary hepatocytes, but was higher in female (4.1-fold above that in male, 95% CI [2.1, 8.2]). Following incubation with analog **1** or **2**, both of which have broken oxazinone rings with missing carbonyl moieties, splicing was detectable over vehicle, demonstrating a 3.5-fold increase for analog **1** and 3.2-fold with analog **2** (95% CI are [2.0, 6.2] and [1.7, 5.9], respectively) in female mouse hepatocytes only (Figure 4B).

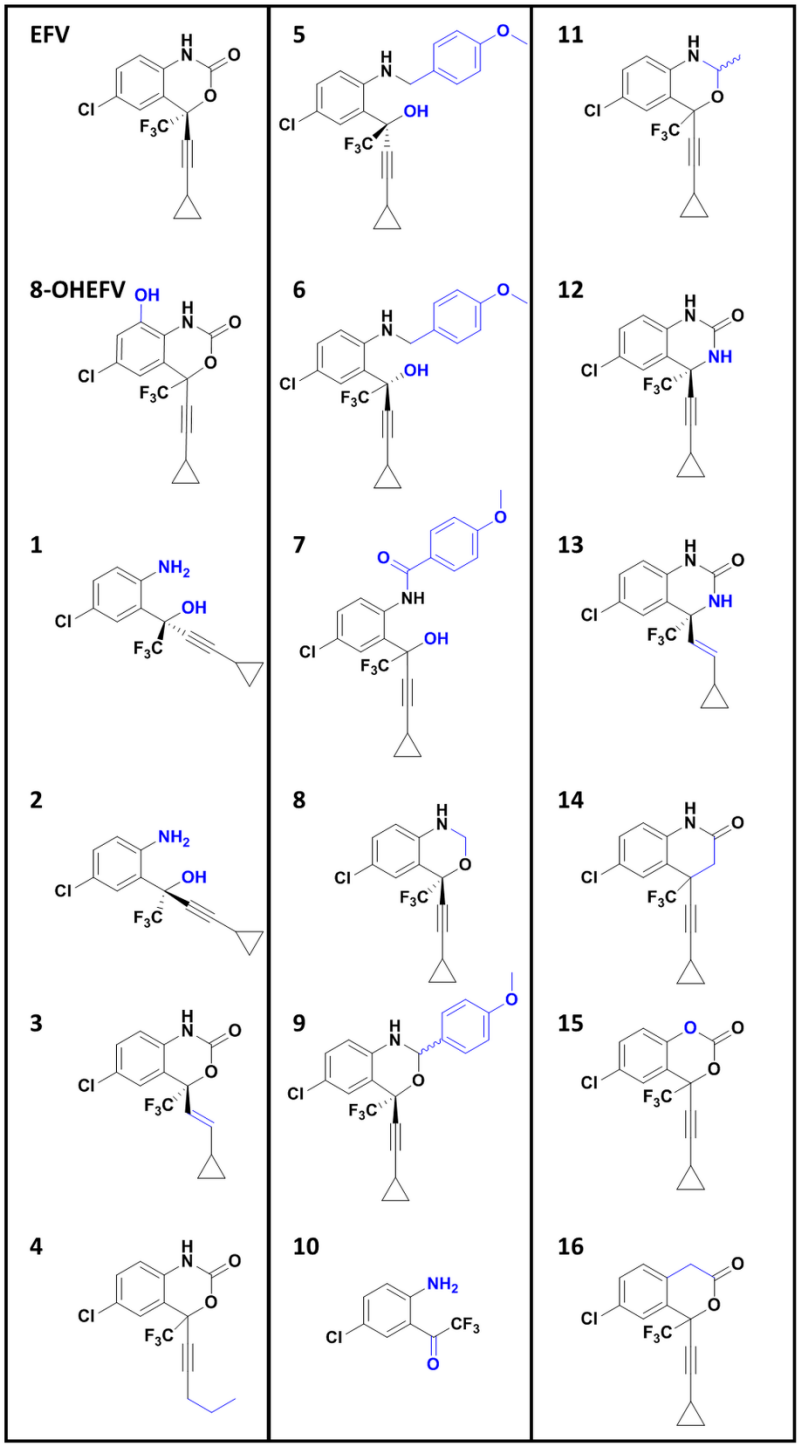


**Figure 3. EFV, 8-OHEFV, and the structural analogs of EFV used in this study, with differences from EFV highlighted in blue.**

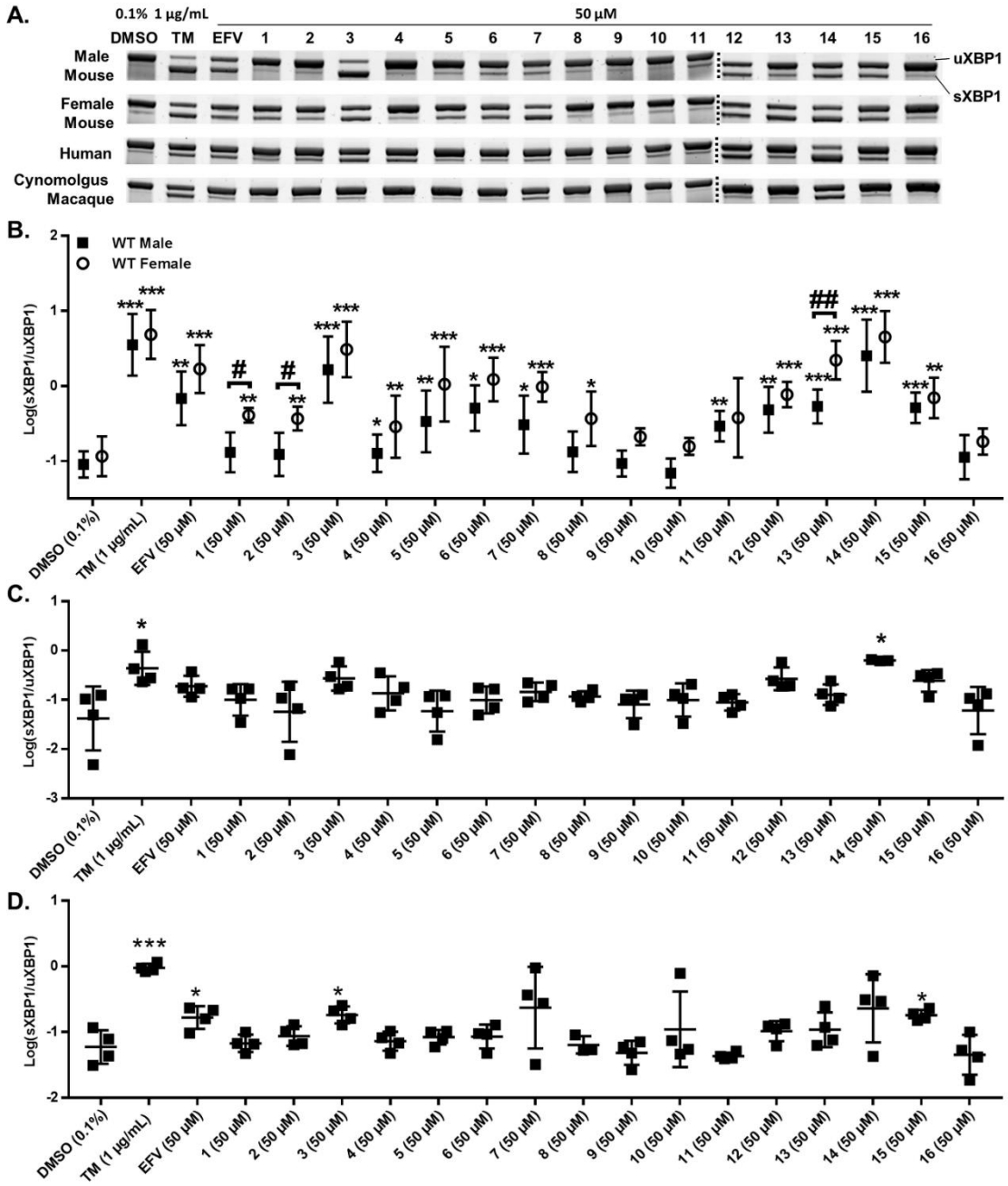


**Figure 4. XBP1 splicing activation in primary hepatocytes in the presence of EFV and structural analogs of EFV.** A. Representative XBP1 mRNA splicing PAGE gel images for male mouse (n=5 for all but 3 and 14, for which n=8), female mouse (n=4), human (n=4, for all but 14, in which n=3), and cynomolgus macaque (n=4 for all but 8, in which n=3) primary hepatocytes incubated with

EFV and analogs of EFV at 50 μM for 4 hours. B. sXBP1/uXBP1 densitometry quantification ratios of XBP1 mRNA splicing for the above described treatments in male and female mouse primary hepatocytes, C.in human hepatocytes, and D. in primary cynomolgus macaque hepatocytes. In male primary mouse hepatocytes, a DMSO (0.1%) control and TM positive control was run for all replicates, including additional replicates measuring splicing with only analog 3 and analog 14. For statistical analysis of this data from male mouse hepatocytes, each treatment was compared to the DMSO controls that were run in the same preparations of primary hepatocytes. For all data sets, ratios of sXBP1/uXBP1 densitometry were log-transformed and the statistical significance of TM, EFV, or analog treatments from DMSO (0.1%) control was determined using an unpaired t-test on the transformed data, generating two-tailed P-values (* $P<0.05$, ** $P<0.01$, *** $P<0.001$). Ratios were compared between male and female hepatocytes for any treatment that showed significant splicing in either group using an unpaired t-test, generating two-tailed P- values (# $P<0.05$ and ## $P<0.01$).

**IRE1α-XBP1 activation with EFV in PXR-null Mouse Primary Hepatocytes**

EFV is a well-known activator of the xenobiotic sensing nuclear receptor PXR (Sharma *et al.*, 2013b). We therefore sought to determine whether PXR might play a role in the activation of IRE1α-XBP1 in response to EFV. Of note, EFV activation of XBP1 splicing was not dependent upon PXR, since in fact there was a trend towards increased XBP1 splicing in hepatocytes isolated from PXR-null mice versus WT mice, demonstrating 4.2-fold (95% CI [1.1, 18.7]) greater splicing in male PXR-null mouse hepatocytes as compared to male WT, and 2.0-fold greater (95% CI [0.64, 6.3]) in female mouse PXR-null as compared to female WT, although this difference did not rise to the level of statistical significance (Figure 5A). Still, in consideration of this increase, we moved forward by probing for differences in the levels of IRE1α phosphorylation between WT and male PXR-null mouse hepatocytes in response to EFV. In line with the above XBP1 splicing data, the levels of phosphorylated IRE1α in PXR-null mouse hepatocytes were commensurate with those of WT mice (Figure 5B).

Given that EFV activates PXR, resulting in the increased expression of P450 drug-metabolizing enzymes, we wanted to investigate whether a change in the expression of EFV-metabolizing P450 enzymes occurs during EFV treatment in these hepatocytes. Though it is unknown which P450 metabolize EFV in mouse, EFV is primarily metabolized by CYP2B6 in humans (Ward *et al.*, 2003), and because of this we measured expression of mouse CYP2B10, which shares 74% amino acid sequence identity with human CYP2B6(Davies *et al.*, 2005). The normalized expression of CYP2B10 did not change with EFV treatment (50 μM, 4

hours) as compared to the DMSO control in both WT and PXR-null primary mouse hepatocytes. However, the overall expression of CYP2B10 was on average 2.9-fold (n=3, 95% CI [2.1, 4.0], $P<0.0001$, unpaired t-test) higher in WT cells as compared to PXR-null cells.

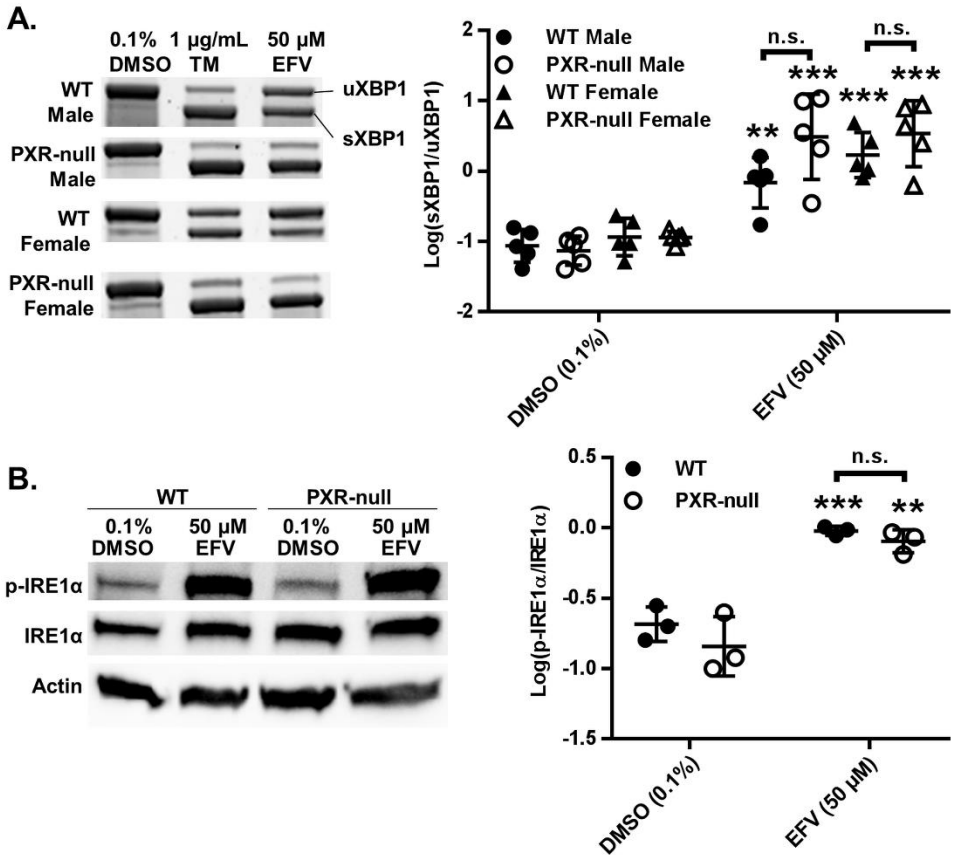


**Figure 5. IRE1α-XBP1 signaling in WT and PXR-null primary hepatocytes during exposure to EFV.** A. Representative XBP1 mRNA splicing PAGE gel images and densitometry quantification (mean ± SD) of XBP1 mRNA splicing from semi-quantitative RT-PCR for sXBP1 and uXBP1 in WT (n=5) and PXR-null male (n=5) mouse primary hepatocytes, as well as WT (n=5) and PXR-null (n=5) female hepatocytes treated with EFV and analogs of EFV at 50 µM for 4 hours. B. Representative images for western blotting of p-IRE1α, total IRE1α, and β-Actin and densitometry quantification ratios of p-IRE1α/total IRE1α for WT (n=3) and PXR-null (n=3) male mouse primary hepatocytes incubated with 50 µM EFV for 2 hours (mean ± SD). Ratios of sXBP1/uXBP1 and p-IRE1α/total IRE1α densitometry were log-transformed and the statistical significance of EFV

treatments from DMSO (0.1%) control determined using an unpaired t-test on transformed data, generating two-tailed P-values (** P<0.01, *** P<0.001).

**Effects of inhibition of XBP1 splicing on lipid droplet formation with EFV**

Because XBP1 has been previously demonstrated to be involved in lipid biogenesis (Sriburi *et al.*, 2004), and hepatic dyslipidemia is commonly indicated clinically along with EFV toxicity (Feeney and Mallon, 2011), we tested whether we could detect lipid accumulation in mouse hepatocytes following treatment with EFV and subsequently, if this accumulation was XBP1 dependent. Following 8 hours in the presence of 20 μM EFV, an approximate 7.7-fold (95% CI [3.6, 16.4] increase in lipid droplet formation was measured as compared to vehicle in primary mouse hepatocytes (Figure 6). Since lipid homeostasis has been previously shown to be differentially regulated in WT versus PXR-null mice (He *et al.*, 2013; Choi *et al.*, 2018) we also performed experiments to probe the impact of PXR on EFV-mediated lipid droplet formation. We observed no difference in lipid droplet formation in response to EFV between PXR-null and WT mouse hepatocytes (Figure 6).

To investigate whether EFV increases lipid droplet formation in an XBP1-dependent manner, STF083010, a chemical inhibitor of IRE1α endoribonuclease activity (Papandreou *et al.*, 2011) was employed. Following 8 hours with 20 μM EFV ± 100 μM STF083010, there was no observed impact of XBP1 splicing inhibition on EFV-mediated lipid droplet accumulation in primary mouse hepatocytes (Figure 7A). We did however confirm that co-treatment with STF083010 at 100 μM decreased the activation of XBP1 splicing by both EFV at 50 μM and TM after 8 hours (Figure 7B): though splicing levels were still higher

than vehicle with both compounds, XBP1 splicing with EFV was 9.9-fold lower (95% CI [6.1, 16.0]) in the presence of STF083010.

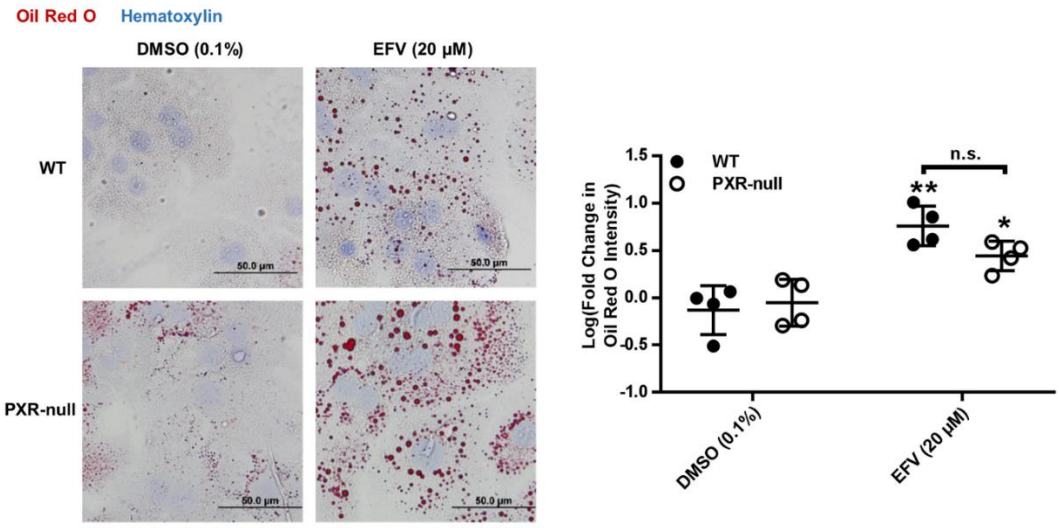


**Figure 6. Lipid droplet formation in WT and PXR-null primary hepatocytes treated with EFV.** Representative images (40X) of Oil Red O (red) and hematoxylin (blue) stained primary mouse hepatocytes and quantitation of Oil Red O signal intensity in WT (n=4) and PXR-null (n=4) primary mouse hepatocytes incubated with 20 µM EFV for 8 hours (mean ± SD).. Fold change was calculated with respect to the mean of the DMSO (0.1%) control within each group, and fold changes were log-transformed. The statistical significance of EFV treatments from DMSO (0.1%) control was determined using an unpaired t-test on transformed data, generating two-tailed P-values (* P<0.05, ** P<0.01).

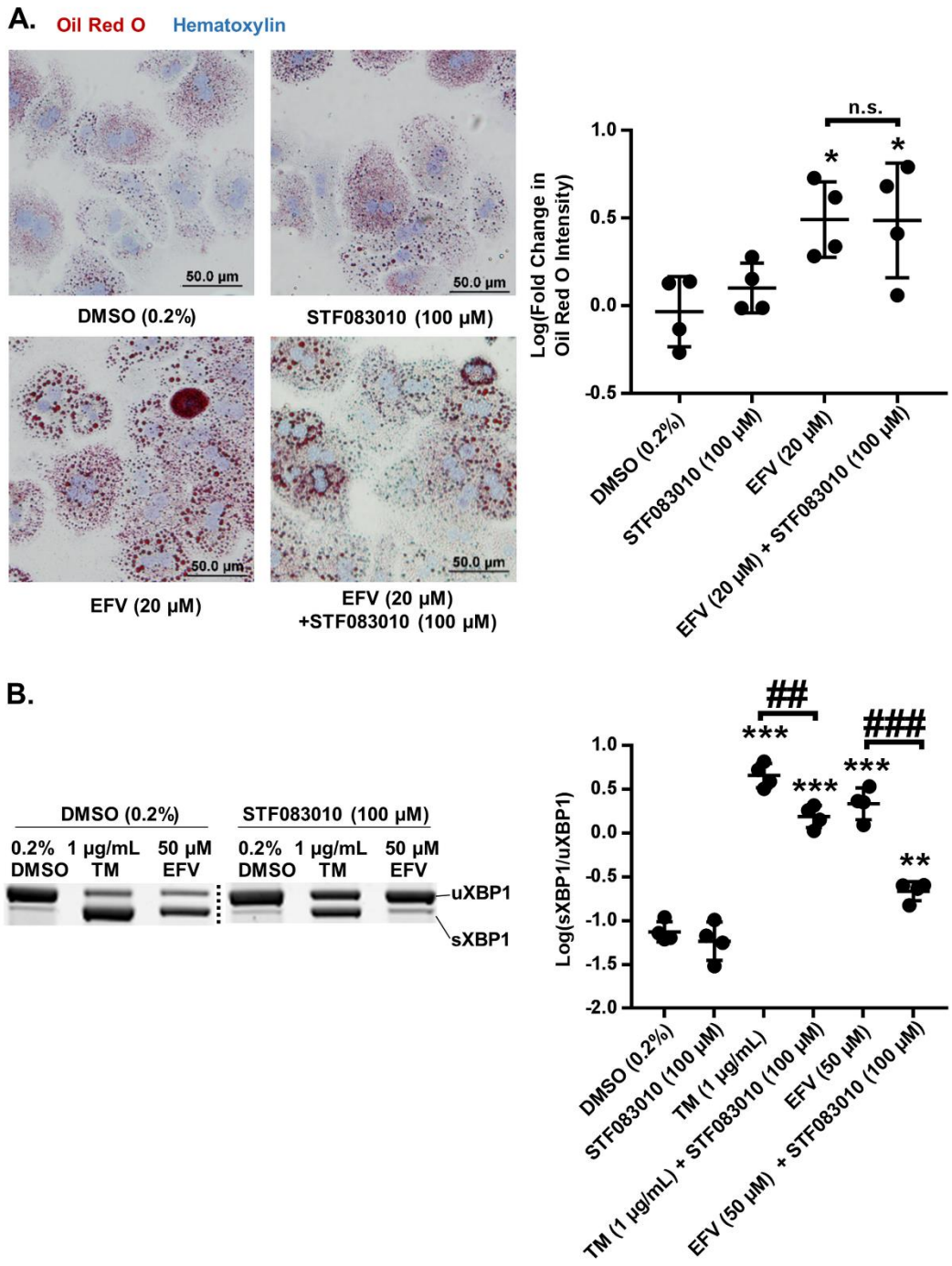


**Figure 7. XBP1 splicing and lipid droplet formation in male mouse primary hepatocytes during EFV exposure.** A. Representative images (20X) of Oil Red O (red) and hematoxylin (blue) stained primary mouse hepatocytes and quantitation of Oil Red O signal intensity in WT (n=4) primary mouse hepatocytes

in presence of 20 μM EFV for 8 hours ± STF083010 at 100 μM (mean ± SD). Fold change in Oil Red O intensity was calculated with respect to the mean of the DMSO (0.1%) control and fold changes were log-transformed. B. Representative XBP1 mRNA splicing PAGE gel images and densitometry quantification (mean ± SD) of XBP1 mRNA splicing from semi-quantitative RT-PCR for sXBP1 and uXBP1 in male mouse primary hepatocytes (n=4) treated with EFV and analogs of EFV at 50 μM for 8 hours +/- STF083010 at 100 μM. Ratios of sXBP1/uXBP1 and p-IRE1α/total IRE1α densitometry were log-transformed. The statistical significance in both A. and B. was determined for all treatments with respect to DMSO (0.2%) control using an unpaired t-test on transformed data, generating two-tailed P-values (* $P<0.05$, ** $P<0.01$, *** $P<0.001$). Additional un-paired t-tests were performed to compare treatments indicated by brackets generating two-tailed P- values (## $P<0.01$ and ### $P<0.001$).

**Primary hepatocyte death in response to EFV and the role of XBP1 splicing**

Reactive oxygen species accumulation is one example of a cellular stressor that can result in IRE1α-XBP1 activation (Hanada *et al.*, 2007). We measured formation of 8-hydroxydeoxyguanosine (8-OHdG) DNA adducts, which are formed when reactive oxygen species build up in the cell (Kasai *et al.*, 1986), during incubation with EFV. In primary mouse hepatocytes treated for 4 hours, positive 8-OHdG staining increased in from 25.3 % (95% CI [13.2, 37.3]) with vehicle to 52.2% (95% CI [41.1, 73.9]) with 20 μM EFV, and increased from 20.9 % (95% CI [7.7, 34.1]) with vehicle to 52.2% (95% CI [39.9, 64.5]) in the presence of 50 μM EFV (Figure 8A). Given this observed increase in 8-OHdG with EFV, as well as the increase in lipid droplet formation with EFV, we also probed for formation of 4-hydroxynonenal protein adducts, a result of increased lipid oxidation during cellular oxidative stress (Comporti, 1998). After an 8 hour incubation with EFV at 20 μM, no 4-hydroxynonenal protein adducts were observed (data not shown).

To assay the impact of EFV exposure on primary hepatocyte viability, AcrO/EtBr co-staining was used in primary male mouse hepatocytes treated with 20 μM EFV for 8 hours (Figure 8B). In the presence of EFV, a marked increase in EtBr positive cells was observed, with 47.2 % (95% CI [32.3, 62.0]) of cells positive, as compared to 10.8 % (95% CI [1.59, 20.0]) for vehicle. Because we saw higher levels of XBP1 splicing with analog **3** and analog **14**, we also performed EtBr/AcrO viability measurements during incubation with these compounds at 20 μM for 8 hours. Interestingly, analog **3** also resulted in an

increase in EtBr positive cells, with 49.7% (95% CI [30.8, 68.6]) positive, as compared to 7.3% (95% CI [4.0, 10.5]) for vehicle. Analog **14** showed no increase in positive EtBr/AcrO staining (Figure 8B). To assay whether this cell death was dependent upon IRE1α endoribonuclease activity, we also performed EtBr/AcrO staining on cells co-treated with 100 μM of the splicing inhibitor STF083010 and either EFV, analog **3**, or analog **14**. Co-treatment with this XBP1 splicing inhibitor decreased EFV-mediated hepatocyte death to 23.9% (95% CI [15.9, 32.0])of cells positive for apoptosis, but did not decrease cell death with analog **3** and had no impact on cell death with analog **14** (Figure 8B).

Because the cell death levels with EFV, analog 3, and analog 14 showed differential dependence on IRE1α-XBP1 signaling, we hypothesized that the activity of XBP1 as a transcription factor may differ across these stimuli. Because of this, we measured the expression of the XBP1 target gene DNAJ heat shock protein family member 9 (DNAJB9) (Lee *et al.*, 2003). During incubations with EFV, analog **3**, and analog **14**, 2.4- (n=4, 95% CI [1.7, 3.4], P<0.01), 1.9- (n=4, 95% CI [1.2, 2.9], P<0.05), and 1.9-fold (n=4, 95% CI [1.2, 3.2], P<0.05) increases were measured (respectively) in DNAJB9 expression (P-values generated using an un-paired t-test).

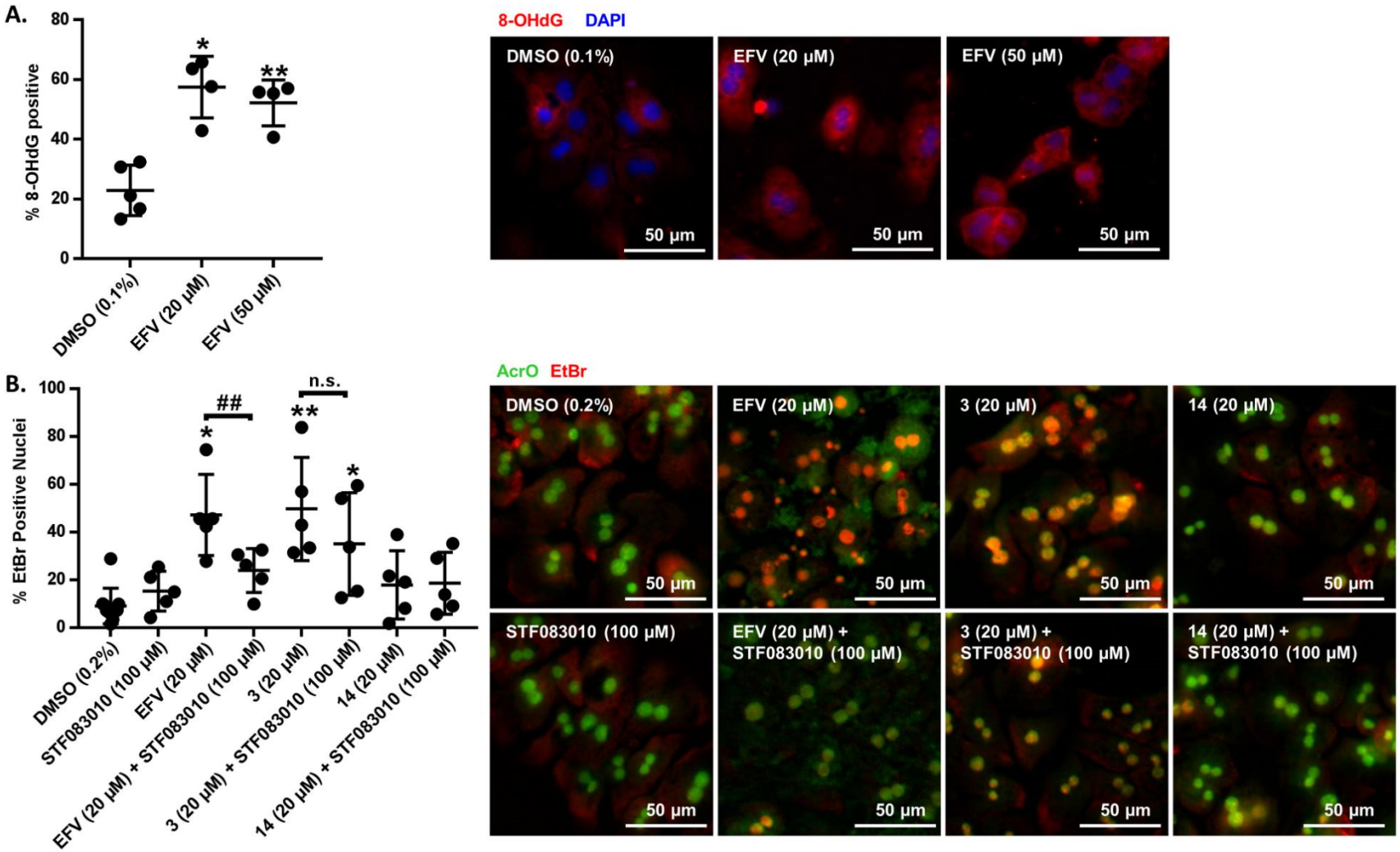
A.
% 8-OHdG positive
80
60
40
20
0
*
**
DMSO (0.1%)
EFV (20 μM)
EFV (50 μM)
8-OHdG DAPI
DMSO (0.1%)
EFV (20 μM)
EFV (50 μM)
50 μm
B.
% EtBr Positive Nuclei
100
80
60
40
20
0
##
n.s.
*
**
*
DMSO (0.2%)
STF083010 (100 μM)
EFV (20 μM)
EFV (20 μM) + STF083010 (100 μM)
3 (20 μM)
3 (20 μM) + STF083010 (100 μM)
14 (20 μM)
14 (20 μM) + STF083010 (100 μM)
AcrO EtBr
DMSO (0.2%)
EFV (20 μM)
3 (20 μM)
14 (20 μM)
STF083010 (100 μM)
EFV (20 μM) + STF083010 (100 μM)
3 (20 μM) + STF083010 (100 μM)
14 (20 μM) + STF083010 (100 μM)
50 μm

**Figure 8. 8-OHdG and EtBr/AcrO viability staining in primary mouse hepatocytes during EFV incubations.** A. Representative images (20X) of 8-OHdG (red) and DAPI (blue) stained primary mouse hepatocytes and quantitation (mean ± SD, n=4) of 8-OHdG stained cells after incubations with EFV at either 20 or 50 μM for 4 hours. Positively stained 8-OHdG nuclei are purple. B. Representative images (20X) of EtBr (red) and AcrO (green) stained primary mouse hepatocytes and quantitation (mean ± SD, n=5) after treatment with EFV, analog 3 or analog 14 for 8 hours ± co-treatment with STF083010 at 100 μM. Hepatocytes positive for cell death have yellow/orange nuclei. Ratio-paired t-tests were performed to determine significance from DMSO controls or for bracketed comparisons. For A. five separate isolations of mouse hepatocytes were used to generate these results, and each treatment EFV (20 μM) and EFV (50 μM) was performed four times among these five batches of cells. For B. STF083010 (100 μM), EFV (20 μM), and EFV (20 μM) + STF083010 (100 μM) were performed in the same group of five hepatocyte isolations, while treatments with 3 (20 μM), 3 (20 μM) + STF083010 (100 μM), 14 (20 μM), and14 (20 μM) + STF083010 (100 μM), were performed in a separate set of five isolations. A ratio paired t-test was used to test for significance from DMSO controls or for bracketed comparisons in both A. and B, generating two-tailed P-values (* $P<0.05$, ** $P<0.01$ for significance from DMSO control and ## $P<0.01$ for indicated comparisons.)

## Discussion

In this work, we demonstrate that EFV and 8-OHEFV, despite being very structurally similar compounds, differ in their activation of IRE1α-XBP1signalling. EFV treatment resulted in greater XBP1 splicing in human and mouse primary hepatocytes than 8-OHEFV. Previously, our group has shown that both compounds activate cell death in a JNK- and BimEL- dependent mechanism, with 8-OHEFV exposure resulting in greater activation than EFV (Bumpus, 2011). Taken together, these results indicate that EFV and 8-OHEFV have diverging pharmacological effects, via activating different cell signaling events. It is especially important to consider the effects of 8-OHEFV because the levels of this metabolite in the blood stream can reach levels nearly equal to EFV (Ngaimisi *et al.*, 2010; Grilo *et al.*, 2016).

While it has been previously shown that EFV activates XBP1 splicing in HEP3B cells and increases XBP1 expression in both Hep3B cells and primary human hepatocytes (Apostolova *et al.*, 2013), the role of XBP1 splicing activation in EFV-mediated hepatocyte death has not been explored. In addition, we have expanded on this by directly monitoring EFV activation of XBP1 splicing in primary human, male and female mouse, and cynomolgus macaque primary hepatocytes. Importantly, we have examined the impact of structural changes to EFV on IRE1α-XPB1 activation and to the best of our knowledge this is the first study to perform this structure-activity analysis. As such, these data can be leveraged in understanding the activation of these signaling molecules more broadly. Several changes to the structure of EFV, including breaking of the

oxazinone ring (analogs **1** and **2**), the cyclopropyl group (analog **4**), removal of the oxazinone carbonyl (analog **8**), or replacement of the oxazinone ring oxygen with carbon (analog **16**) all decreased or abrogate activation of XBP1 splicing. Conversely, changing the EFV alkyne to an alkene (analog **3**), and replacement of the oxazinone ring nitrogen with carbon (analog **14**) resulted in augmented XBP1 splicing. These structural changes to EFV could modulate IRE1α-XBP1 activation in several ways: through impacting compound reactivity and therefore stimulation of reactive oxygen species formation, or by changing certain physiochemical properties (such as Log P and protein binding) that affect free intracellular concentration of the compound. Future work to directly monitor ROS formation with these compounds and the free intracellular concentration would help to elucidate how each structural change impacts IRE1α-XBP1 activation. Though few of the analogs in this study have been tested for anti-retroviral activity, two compounds, analog **12** and **13** have previously demonstrated nearly identical IC90s against viral replication to that of EFV (Corbett *et al.*, 2000). Here we observed that like EFV, both of these compounds activate IRE1α-XBP1.

Here we observed a trend toward increased activation of XBP1 splicing in primary hepatocytes from female mice, as compared to those from male mice, though for most compounds tested this change was not statistically significant. This difference could be suggestive of increased sensitivity to IRE1α-XBP1 activation in females, which could be cytoprotective or cytotoxic. It would also be interesting to test whether all ER stress machinery is more readily activated in

females. Further research is necessary to investigate this sex difference and its potential biological implications.

We show similar impacts of EFV structure on activation of XBP1 splicing across model organisms. Of note, while IRE1α-XBP1 activation has been previously measured in rhesus macaque primary retinal pigment epithelium cells (Ma *et al.*, 2016), it has not to our knowledge been measured before in cynomolgus macaque. In fact, previous studies regarding ER stress in this biological model are limited to one regarding in a cynomolgus macaque glaucoma model (Ito *et al.*, 2011). Considering the growing knowledge of this pathway's role in drug toxicities, (Cao *et al.*, 2010; Van Summeren *et al.*, 2011; Hur *et al.*, 2012; Uzi *et al.*, 2013; McConkey, 2017) and the fact that cynomolgus macaques are often used as models in drug development studies, during which early indications of toxicities may be observed, we feel our comparison is especially important. Here we demonstrate that for EFV and this panel of structures that similar XBP1 splicing activation results can be seen across nonhuman models (cynomolgus macaque and mouse) that are used in various stages of clinical development. In addition, we have expanded upon the characterization of EFV hepatotoxicity in vitro by demonstrating lipid droplet formation, 8-OHdG formation, and positive EtBr/AcrO staining in primary mouse hepatocytes treated with EFV.

PXR ablation has been shown to reduce high fat diet induced JNK-dependent cell-death and lower levels of hepatic lipid accumulation in mice receiving a high fat diet (He *et al.*, 2013). On the other hand, PXR-ablation shows

no protective effect against ethanol-induced triglyceride formation and lipid droplet staining in mice, and higher basal levels of the lipid biosynthesis-activating transcription factor sterol regulatory element binding protein 1c (Srebp1c) (Choi *et al.*, 2018). From this, it seems that PXR's involvement in lipid homeostasis and hepatotoxicity varies across stimuli. With this work we showed that there is no measurable effect of PXR-ablation on EFV-mediated lipid droplet formation or IRE1α- XBP1 activation.

Though the targets of XBP1, such as protein degradation and membrane biogenesis machinery, are often considered to be cytoprotective (Iurlaro and Muñoz-Pinedo, 2016)**,** the role of XBP1 in hepatocyte cell death and dyslipidemia is not well understood. Increased sXBP1 levels have been shown to decrease triglyceride levels and lipogenic gene expression in diet-induced obesity mouse models (Herrema *et al.*, 2016), and hepatocyte specific IRE1α-null mice have increased steatosis over WT mice (Zhang *et al.*, 2011). On the other hand, XBP1 ablation has shown to decrease hepatic lipogenesis associated with high-carbohydrate diet in mice (Lee *et al.*, 2008a). In addition, co-treatment with the IRE1α inhibitor STF083010 has been demonstrated to decrease serum transaminase levels, hepatic lipid accumulation, steatosis, and apoptosis associated with high fat diet in mice (Lebeaupin *et al.*, 2018). As with PXR, the contribution of XBP1 splicing to hepatocyte cell death and lipid formation appears to be stimuli dependent.

In this study we determined that co-treatment of cells with the IRE1α endoribonuclease inhibitor STF083010, which inhibited XBP1 splicing activated

by EFV in primary mouse hepatocytes, lessened EFV-induced primary hepatocyte death, but not lipid droplet formation. These results suggest that for EFV, IRE1α-XBP1 signaling promotes cell death in response to EFV (Figure 9), but does not play a role in EFV-mediated hepatocyte lipid accumulation. Interestingly, STF083010 did not block primary hepatocyte cell death caused by the EFV analog **3**, which stimulated a splicing to a greater extent than that of EFV. Further, analog **14**, despite resulting in the highest levels of XBP1 splicing activation, caused no measureable primary hepatocyte cell death. Yet, we found that EFV, analog **3**, and analog **14** were all able increase the mRNA abundance of DNAJB9, an XBP1 target gene, to a similar extent. Taken together, these data reveal that the consequences of IRE1α-XBP1 are stimuli dependent, and while beyond the scope of the present study, this warrants future investigation.

In summary, our results demonstrate that EFV and several EFV-like compounds activate XBP1, and this is conserved among humans, mice and macaques. Further, activation of XBP1 by EFV may contribute to EFV-mediated hepatocyte death. Of broader interest, our data indicate that even within a class of structurally similar compounds discreet changes in structure can impact the magnitude and outcome of XBP1 splicing. These findings provide insight into the impact of EFV on cellular signaling within hepatocytes while also identifying structural features that may contribute to IRE1α-XBP1 activation.

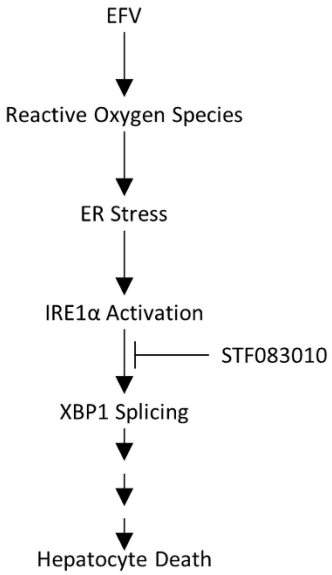


**Figure 9. EFV activation of IRE1α-XBP1.** Treatment with EFV results in the activation of IRE1α and subsequently IRE1α-catalyzed mRNA splicing of XBP1. In addition, EFV exposure causes formation of reactive oxygen species, an event that can lead to the activation of ER stress response, including the IRE1α-XBP1 signaling axis (Hanada *et al.*, 2007). Reactive oxygen species production may drive the activation IRE1α-XBP1 by EFV, though a direct link between these two events remains to be established. STF083010 inhibition of XBP1 splicing by IRE1α during incubation with EFV results in decreased EFV-mediated hepatocyte death

## References


Apostolova N, Gomez-Sucerquia LJ, Alegre F, Funes HA, Victor VM, Barrachina MD, Blas-Garcia A and Esplugues JV (2013) ER stress in human hepatic cells treated with Efavirenz: Mitochondria again. *Journal of Hepatology* **59**:780-789.

Avery LB, VanAusdall JL, Hendrix CW and Bumpus NN (2013) Compartmentalization and antiviral effect of efavirenz metabolites in blood plasma, seminal plasma, and cerebrospinal fluid. *Drug Metab Dispos* **41**:422-429.

Bertolotti A, Zhang Y, Hendershot LM, Harding HP and Ron D (2000) Dynamic interaction of BiP and ER stress transducers in the unfolded-protein response. *Nat Cell Biol* **2**:326-332.

Buchman CD, Chai SC and Chen T (2018) A current structural perspective on PXR and CAR in drug metabolism. *Expert Opin Drug Metab Toxicol* **14**:635-647.

Bumpus NN (2011) Efavirenz and 8-hydroxyefavirenz induce cell death via a JNK- and BimEL-dependent mechanism in primary human hepatocytes. *Toxicol Appl Pharmacol* **257**:227-234.

Cao R, Hu Y, Wang Y, Gurley EC, Studer EJ, Wang X, Hylemon PB, Pandak WM, Sanyal AJ, Zhang L and Zhou H (2010) Prevention of HIV protease inhibitor-induced dysregulation of hepatic lipid metabolism by raltegravir via endoplasmic reticulum stress signaling pathways. *J Pharmacol Exp Ther* **334**:530-539.

Choi S, Gyamfi AA, Neequaye P, Addo S, Gonzalez FJ and Gyamfi MA (2018) Role of the pregnane X receptor in binge ethanol-induced steatosis and hepatotoxicity. *Journal of Pharmacology and Experimental Therapeutics*.

Comporti M (1998) Lipid peroxidation and biogenic aldehydes: from the identification of 4-hydroxynonenal to further achievements in biopathology. *Free Radic Res* **28**:623-635.

Corbett JW, Ko SS, Rodgers JD, Gearhart LA, Magnus NA, Bacheler LT, Diamond S, Jeffrey S, Klabe RM, Cordova BC, Garber S, Logue K, Trainor GL, Anderson PS and Erickson-Viitanen SK (2000) Inhibition of clinically relevant mutant variants of HIV-1 by quinazolinone non-nucleoside reverse transcriptase inhibitors. *J Med Chem* **43**:2019-2030.

Cox PM and Bumpus NN (2014) Structure-Activity Studies Reveal the Oxazinone Ring Is a Determinant of Cytochrome P450 2B6 Activity Toward Efavirenz. *ACS Med Chem Lett* **5**:1156-1161.

Cox PM and Bumpus NN (2016) Single Heteroatom Substitutions in the Efavirenz Oxazinone Ring Impact Metabolism by CYP2B6. *ChemMedChem* **11**:2630-2637.

Davies R, Schuurman A, Barker CR, Clothier B, Chernova T, Higginson FM, Judah DJ, Dinsdale D, Edwards RE, Greaves P, Gant TW and Smith AG (2005) Hepatic gene expression in protoporphyic Fech mice is associated with cholestatic injury but not a marked depletion of the heme regulatory pool. *Am J Pathol* **166**:1041-1053.

Fayet Mello A, Buclin T, Decosterd LA, Delhumeau C, di Iulio J, Fleurent A, Schneider MP, Cavassini M, Telenti A, Hirschel B and Calmy A (2011) Successful efavirenz dose reduction guided by therapeutic drug monitoring. *Antivir Ther* **16**:189-197.

Feeney ER and Mallon PW (2011) HIV and HAART-Associated Dyslipidemia. *Open Cardiovasc Med J* **5**:49-63.

Gounden V, van Niekerk C, Snyman T and George JA (2010) Presence of the CYP2B6 516G> T polymorphism, increased plasma Efavirenz concentrations and early neuropsychiatric side effects in South African HIV-infected patients. *AIDS Res Ther* **7**:32.

Grilo NM, Correia MJ, Sequeira C, Harjivan SG, Caixas U, Diogo LN, Marques MM, Monteiro EC, Antunes AM and Pereira SA (2016) Efavirenz biotransformation as an up-stream event of mood changes in HIV-infected patients. *Toxicol Lett* **260**:28-35.

Hanada S, Harada M, Kumemura H, Bishr Omary M, Koga H, Kawaguchi T, Taniguchi E, Yoshida T, Hisamoto T, Yanagimoto C, Maeyama M, Ueno T and Sata M (2007) Oxidative stress induces the endoplasmic reticulum stress and facilitates inclusion formation in cultured cells. *J Hepatol* **47**:93-102.

He J, Gao J, Xu M, Ren S, Stefanovic-Racic M, O'Doherty RM and Xie W (2013) PXR ablation alleviates diet-induced and genetic obesity and insulin resistance in mice. *Diabetes* **62**:1876-1887.

Hedrich WD, Hassan HE and Wang H (2016) Insights into CYP2B6-mediated drug-drug interactions. *Acta Pharm Sin B* **6**:413-425.

Herrema H, Zhou Y, Zhang D, Lee J, Salazar Hernandez MA, Shulman GI and Ozcan U (2016) XBP1s Is an Anti-lipogenic Protein. *J Biol Chem* **291**:17394-17404.

Hur KY, So JS, Ruda V, Frank-Kamenetsky M, Fitzgerald K, Koteliansky V, Iwawaki T, Glimcher LH and Lee AH (2012) IRE1α activation protects mice against acetaminophen-induced hepatotoxicity. *J Exp Med* **209**:307-318.

Ito Y, Shimazawa M, Inokuchi Y, Yamanaka H, Tsuruma K, Imamura K, Onoe H, Watanabe Y, Aihara M, Araie M and Hara H (2011) Involvement of endoplasmic reticulum stress on neuronal cell death in the lateral geniculate nucleus in the monkey glaucoma model. *Eur J Neurosci* **33**:843-855.

Iurlaro R and Muñoz-Pinedo C (2016) Cell death induced by endoplasmic reticulum stress. *FEBS J* **283**:2640-2652.

Jiang D NM, Koon AC. (2015) Targeting the IRE1α-XBP1 branch of the unfolded protein response in human diseases. *Semin Cancer Biol* **33**:48-56.

Kasai H, Crain PF, Kuchino Y, Nishimura S, Ootsuyama A and Tanooka H (1986) Formation of 8-hydroxyguanine moiety in cellular DNA by agents producing oxygen radicals and evidence for its repair. *Carcinogenesis* **7**:1849-1851.

Korennykh AV, Egea PF, Korostelev AA, Finer-Moore J, Zhang C, Shokat KM, Stroud RM and Walter P (2009) The unfolded protein response signals through high-order assembly of Ire1. *Nature* **457**:687-693.

Lebeaupin C, Vallée D, Rousseau D, Patouraux S, Bonnafous S, Adam G, Luciano F, Luci C, Anty R, Iannelli A, Marchetti S, Kroemer G, Lacas-Gervais S, Tran A, Gual P and Bailly-Maitre B (2018) Bax Inhibitor-1 protects from Non-Alcoholic Steatohepatitis by limiting IRE1α signaling. *Hepatology* **68**:515-532.

Lee AH, Iwakoshi NN and Glimcher LH (2003) XBP-1 regulates a subset of endoplasmic reticulum resident chaperone genes in the unfolded protein response. *Mol Cell Biol* **23**:7448-7459.

Lee AH, Scapa EF, Cohen DE and Glimcher LH (2008a) Regulation of hepatic lipogenesis by the transcription factor XBP1. *Science* **320**:1492-1496.

Lee K, Tirasophon W, Shen X, Michalak M, Prywes R, Okada T, Yoshida H, Mori K and Kaufman RJ (2002) IRE1-mediated unconventional mRNA splicing and S2P-mediated ATF6 cleavage merge to regulate XBP1 in signaling the unfolded protein response. *Genes Dev* **16**:452-466.

Lee KP, Dey M, Neculai D, Cao C, Dever TE and Sicheri F (2008b) Structure of the dual enzyme Ire1 reveals the basis for catalysis and regulation in nonconventional RNA splicing. *Cell* **132**:89-100.

Lee P, Peng H, Gelbart T and Beutler E (2004) The IL-6- and lipopolysaccharide-induced transcription of hepcidin in HFE-, transferrin receptor 2-, and beta

2-microglobulin-deficient hepatocytes. *Proc Natl Acad Sci U S A* **101**:9263-9265.

Ma JH, Wang JJ, Li J, Pfeffer BA, Zhong Y and Zhang SX (2016) The Role of IRE-XBP1 Pathway in Regulation of Retinal Pigment Epithelium Tight Junctions. *Invest Ophthalmol Vis Sci* **57**:5244-5252.

Marzolini C, Telenti A, Decosterd LA, Greub G, Biollaz J and Buclin T (2001) Efavirenz plasma levels can predict treatment failure and central nervous system side effects in HIV-1-infected patients. *AIDS* **15**:71-75.

McConkey DJ (2017) The integrated stress response and proteotoxicity in cancer therapy. *Biochem Biophys Res Commun* **482**:450-453.

Narayanan B, Lade JM, Heck CJS, Dietz KD, Wade H and Bumpus NN (2018) Probing Ligand Structure-Activity Relationships in Pregnane X Receptor (PXR): Efavirenz and 8-Hydroxyefavirenz Exhibit Divergence in Activation. *ChemMedChem* **13**:736-747.

Ngaimisi E, Mugusi S, Minzi OM, Sasi P, Riedel KD, Suda A, Ueda N, Janabi M, Mugusi F, Haefeli WE, Burhenne J and Aklillu E (2010) Long-term efavirenz autoinduction and its effect on plasma exposure in HIV patients. *Clin Pharmacol Ther* **88**:676-684.

Ning J, Hong T, Ward A, Pi J, Liu Z, Liu HY and Cao W (2011) Constitutive role for IRE1α-XBP1 signaling pathway in the insulin-mediated hepatic lipogenic program. *Endocrinology* **152**:2247-2255.

Papandreou I, Denko NC, Olson M, Van Melckebeke H, Lust S, Tam A, Solow-Cordero DE, Bouley DM, Offner F, Niwa M and Koong AC (2011)

Identification of an Ire1alpha endonuclease specific inhibitor with cytotoxic activity against human multiple myeloma. *Blood* **117**:1311-1314.

Sha H, He Y, Chen H, Wang C, Zenno A, Shi H, Yang X, Zhang X and Qi L (2009) The IRE1alpha-XBP1 pathway of the unfolded protein response is required for adipogenesis. *Cell Metab* **9**:556-564.

Sharma D, Lau AJ, Sherman MA and Chang TK (2013) Agonism of human pregnane X receptor by rilpivirine and etravirine: comparison with first generation non-nucleoside reverse transcriptase inhibitors. *Biochem Pharmacol* **85**:1700-1711.

Shubber Z, Calmy A, Andrieux-Meyer I, Vitoria M, Renaud-Théry F, Shaffer N, Hargreaves S, Mills EJ and Ford N (2013) Adverse events associated with nevirapine and efavirenz-based first-line antiretroviral therapy: a systematic review and meta-analysis. *AIDS* **27**:1403-1412.

Sriburi R, Jackowski S, Mori K and Brewer JW (2004) XBP1: a link between the unfolded protein response, lipid biosynthesis, and biogenesis of the endoplasmic reticulum. *J Cell Biol* **167**:35-41.

Swart M, Whitehorn H, Ren Y, Smith P, Ramesar RS and Dandara C (2012) PXR and CAR single nucleotide polymorphisms influence plasma efavirenz levels in South African HIV/AIDS patients. *BMC Med Genet* **13**:112.

Urano F, Wang X, Bertolotti A, Zhang Y, Chung P, Harding HP and Ron D (2000) Coupling of stress in the ER to activation of JNK protein kinases by transmembrane protein kinase IRE1. *Science* **287**:664-666.

Uzi D, Barda L, Scaiewicz V, Mills M, Mueller T, Gonzalez-Rodriguez A, Valverde AM, Iwawaki T, Nahmias Y, Xavier R, Chung RT, Tirosh B and Shibolet O (2013) CHOP is a critical regulator of acetaminophen-induced hepatotoxicity. *J Hepatol* **59**:495-503.

Van Summeren A, Renes J, Bouwman FG, Noben JP, van Delft JH, Kleinjans JC and Mariman EC (2011) Proteomics investigations of drug-induced hepatotoxicity in HepG2 cells. *Toxicol Sci* **120**:109-122.

Ward BA, Gorski JC, Jones DR, Hall SD, Flockhart DA and Desta Z (2003) The cytochrome P450 2B6 (CYP2B6) is the main catalyst of efavirenz primary and secondary metabolism: implication for HIV/AIDS therapy and utility of efavirenz as a substrate marker of CYP2B6 catalytic activity. *J Pharmacol Exp Ther* **306**:287-300.

WHO (2017) WHO Model List of Essential Medicines- 20th Edition, in p 58, World Health Organization, http://www.who.int/medicines/publications/essentialmedicines/en/.

Yimer G, Amogne W, Habtewold A, Makonnen E, Ueda N, Suda A, Worku A, Haefeli WE, Burhenne J, Aderaye G, Lindquist L and Aklillu E (2012) High plasma efavirenz level and CYP2B6*6 are associated with efavirenz-based HAART-induced liver injury in the treatment of naïve HIV patients from Ethiopia: a prospective cohort study. *Pharmacogenomics J* **12**:499-506.

Yoshida H, Matsui T, Yamamoto A, Okada T and Mori K (2001) XBP1 mRNA is induced by ATF6 and spliced by IRE1 in response to ER stress to produce a highly active transcription factor. *Cell* **107**:881-891.

Zhang K, Wang S, Malhotra J, Hassler JR, Back SH, Wang G, Chang L, Xu W, Miao H, Leonardi R, Chen YE, Jackowski S and Kaufman RJ (2011) The unfolded protein response transducer IRE1alpha prevents ER stress-induced hepatic steatosis. *Embo j* **30**:1357-1375.

## Chapter 3: Impact of Twelfth Position Deuterium Substitution on Hepatic Metabolism and Cytotoxicity of Nevirapine


### Abstract

Nevirapine (NVP) is an antiretroviral drug used in the treatment of HIV, despite causing potentially fatal hepatotoxicity. Previous work has implicated the cytochrome P450 metabolism of NVP to 12-hydroxy-NVP (12-OHNVP) in the development of NVP toxicities. With this, we investigated the impact of twelfth-position deuterium substitution (12-$D_3$NVP) on the hepatic metabolism of NVP. A 10.6- and 4.6-fold reduction was measured in the formation of 12-OHNVP with 12-$D_3$NVP vs. NVP (10 μM, 24h), in primary human and mouse hepatocytes, respectively. No increases in other P450 metabolites, 2- and 3-OHNVP, were observed. We profiled the contributions of human P450 isoforms to the formation of 12-OHNVP and concluded that multiple P450s contribute to the production of this metabolite. We quantified the kinetic isotope effect (KIE) in liver microsomal incubations with NVP and 12-$D_3$NVP, and measured an observed KIE of 10.1 and demonstrated a 9.1-fold decrease in the catalytic efficiency of 12-OHNVP production by P450s. During treatments of primary mouse hepatocytes with 400 μM NVP or 12-$D_3$NVP, only a modest reduction of cell death was observed (52.6% dead/dying cells with NVP vs. 36.8% with 12-$D_3$NVP). In addition, at these high treatment concentrations we saw evidence of metabolic switching. With this, we also profiled the changes in protein expression during treatment with NVP or 12-$D_3$NVP in primary human and mouse hepatocytes using relative quantitation proteomic analysis. Changes in the expression of several proteins

were observed uniquely with treatment with 12-$D_3$NVP, one of note being the hepatic stress marker IGFBP-1. These results demonstrate that while this trideuteration is an effective strategy to reduce P450 formation of 12-OHNVP, differential hepatocyte response specifically to 12-$D_3$NVP must be considered in the use of this tool to study P450 metabolite-related hepatotoxicity.

**Introduction**

Nevirapine (NVP) is a first generation non-nucleoside reverse transcriptase inhibitor currently used for the treatment of human immunodeficiency virus (HIV) infections, for HIV post-exposure prophylaxis, and for prevention of mother to child transmission of HIV during childbirth (Usach *et al.*, 2013; WHO, 2017). The World Health Organization includes both NVP and NVP-containing combination therapy on its most recent List of Essential Medicines (WHO, 2017). Unfortunately, NVP has been shown to cause life-threatening hepatotoxicity in patients (Pollard *et al.*, 1998; (CDC), 2001; Sanne *et al.*, 2005; Zhang *et al.*, 2013).

There have been many clinical studies that have reported on liver function with this standard NVP regimen, generally in combination with other antiretrovirals, with varying results. One review of prospective international clinical trial data from 906 adult patients taking NVP reported an incidence of abnormal liver function of 6.0% (Pollard *et al.*, 1998). In Sanne *et al.*, 2005, 17% of South African patients receiving NVP-containing combination therapies developed hepatotoxicity, while in another study of patients in China, the overall incidence of hepatotoxicity was 36.1%, with 7.7% of patients experiencing severe

hepatotoxicity. (Zhang *et al.*, 2013). In very rare cases, patients taking NVP have experienced fulminant hepatitis, sometimes resulting in liver transplantation or even death (CDC, 2001; Sanne *et al.*, 2005; Buyse *et al.*, 2006; Maniar *et al.*, 2006; Jao *et al.*, 2010).

NVP is metabolized by human cytochrome P450 phase-I drug metabolizing enzymes (P450s), resulting the in formation of four mono-oxygenated metabolites: 2-hydroxy- (2-OH), 3-hydroxy- (3-OH), 8-hydroxy- (8-OH), and 12-hydroxy- (12-OH) NVP (Erickson *et al.*, 1999; Riska *et al.*, 1999). The average plasma concentration of NVP during regular dosing has previously been observed to be 16.0 μM (95% CI [10.0, 19.2]), with 12-OHNVP at 1.3 μM (95% CI [0.9, 1.9]), followed by 2-OHNVP at 0.2 μM (95% CI [0.1, 0.4]), 3-OHNVP at 0.2 μM (95% CI [0.9, 1.9]), and unquantifiable levels of 8-OHNVP (Marinho *et al.*, 2014). These P450 metabolites are precursors to other NVP metabolites, including glucuronidation by uridine 5'-diphospho-glucuronosyltransferases (Riska *et al.*, 1999), sulfation by sulfotransferases (Sharma *et al.*, 2013), and glutathione conjugation by glutathione S-transferases (Wen *et al.*, 2009; Dekker *et al.*, 2016).

NVP toxicities have been characterized as immune hypersensitivity reactions (Carr *et al.*, 1996; Wit *et al.*, 2008), that may be a response to the formation of immunogenic NVP metabolite adducts with large biomolecules (Antunes *et al.*, 2010; Srivastava *et al.*, 2010; Caixas *et al.*, 2012). Formation of 12-OHNVP by P450s has been previously implicated the hepatotoxicity of NVP, as well as in skin toxicity, another severe side effect of NVP (Chen *et al.*, 2008;

Sharma *et al.*, 2012; Sharma *et al.*, 2013). Previous research suggests that NVP metabolism to 12-OHNVP may result in the formation of bio-reactive intermediates, either during the formation of 12-OHNVP itself (Sharma *et al.*, 2012) or through subsequent sulfation at the twelfth position (Chen *et al.*, 2008; Sharma *et al.*, 2013). To probe this, Chen *et al.* (2008) treated rats with NVP and a version of NVP in which the twelfth-position had been trideuterated (12-$D_3$NVP). This trideuteration was intended to reduce P450 oxygen insertion at the twelfth position and was demonstrated to reduce both circulating concentrations of 12-OHNVP and the incidence of skin rash in rats treated with 12-$D_3$NVP versus those treated with NVP (Chen *et al.*, 2008). Other work has demonstrated a reduction 12-OHNVP-protein adducts in the livers of mice and rats treated with 12-$D_3$NVP as compared to NVP (Sharma *et al.*, 2012). Substitution of hydrogens at the site of P450 metabolism with the heavier deuterium isotope of hydrogen has long been leveraged to study P450 reaction mechanisms. The impact of deuteration on P450 activity has been reported to vary significantly: a change of 1-20 fold in the rate of P450 bond breaking, which is a necessary step in cytochrome P450 product formation (also called the intrinsic kinetic isotope effect), has been observed. (Guengerich, 2017).

With this work, we probed the difference in P450-dependent metabolism of NVP versus 12-$D_3$NVP in primary human and mouse hepatocytes. Not only did we want to understand the impact on 12-OHNVP production, but also on the formation of other P450-dependent metabolites of NVP. In addition, we characterized the contribution of various human P450s in NVP metabolism and

quantified the observed kinetic isotope effect of this trideuteration on 12-OHNVP production by human liver microsomes. From here, we probed the difference in hepatocyte cell-death levels with either NVP or 12-$D_3$NVP, and performed relative-quantitation proteomics analysis of hepatocytes treated with NVP- and 12-$D_3$NVP in an effort to not only characterize novel signaling pathways involved in the hepatotoxicity of NVP, but also in differential response to this trideuterated compound.

## Materials and Methods

### Reagents

NVP (with a purity of > 99.9%, assessed by the manufacturer using HPLC compared to a USP standard) was provided National Institutes of Health AIDS Research and Reference Reagent Program. 12-$D_3$NVP (98% purity, 99% isotopic purity), 2-OHNVP (98% purity), 3-OHNVP (98% purity), and 12-OHNVP (96% purity) standards were synthesized by Toronto Research Chemicals. Purity of these compounds was assessed by the manufacturer using 1H nuclear magnetic resonance and mass spectrometry. Staurosporine was purchased from Cell Signaling Technology. Furafylline, tranylcypromine, sulfaphenozole, (+)-N-3-benzyl-nirvanol, quinidine, and ketoconazole were all purchased from Sigma. 2-phenyl-2-(1-piperidinyl)propane (PPP) was purchased from Santa Cruz. LC-MS grade water, acetonitrile, methanol, acetone and formic acid were all purchased from Fisher. Bovine pancreas trypsin was purchased from Sigma. Dithiothreitol, and iodoacetamide were purchased from Pierce.

**Primary mouse hepatocyte isolation and culture**

The Johns Hopkins Animal Care and Use Committee approved all experiments with mice, and all procedures were in accordance with Guide for the Care and Use of Laboratory Animals as adopted and promulgated by the US National Institutes of Health. Hepatocytes were isolated from male C57BL/6J mice, aged 8-12 weeks (The Jackson Laboratory). Primary hepatocytes were isolated as previously described (Lee *et al.*, 2004). Cells were ≥ 85% viable upon plating and were cultured as previously described (Heck *et al.*, 2019). Following adherence overnight, fresh treatment-containing medium was added.

**Cryoplateable human hepatocyte culture**

LIVERPOOL cryoplateable human hepatocytes (three lots of pools from 10 different human, mixed sex, donors) were obtained from BioIVT. Cells were thawed and plated as according to the manufacturer's protocol into 12-well collagen coated plates (Corning), with a viability of ≥ 90% upon plating. Cells were allowed to adhere overnight, after which they received fresh treatment-containing InVitroGRO CP medium supplemented with Torpedo Antibiotic Mix (BioIVT).

**Extraction of monooxygenated and O-glucuronidated metabolites of NVP and 12-$D_3$NVP from the culture medium of primary human and mouse hepatocytes**

Fresh mouse hepatocytes and cryoplateable human hepatocytes were treated in a 12-well format with vehicle (0.1% DMSO), 10 μM NVP, or 10 μM 12-$D_3$NVP for 24 or 48 hours. Fresh mouse hepatocytes were also treated with

vehicle (0.2% DMSO), 400 μM NVP, or 400 μM 12-$D_3$NVP for 8 hours. Following these treatments, 100 μL of culture medium was obtained and metabolites extracted via protein precipitation with the addition of acetonitrile to a final concentration of 50%. Samples were vortexed and centrifuged (3 minutes, 10,000*g*, 4 °C). Supernatant was then dried under vacuum centrifugation and reconstituted in 50 μL (mouse samples) or 17 μL (human samples) of methanol, and 2 μL was injected for uHPLC-Orbitrap analysis.

**Extraction of intracellular glutathione-conjugated NVP and 12-$D_3$NVP metabolites from primary mouse hepatocytes**

Fresh primary mouse hepatocytes were treated with vehicle (0.2% DMSO), 400 μM NVP, or 400 μM 12-$D_3$NVP for 8 hours in a 6-well format. Three wells of each treatment (720,000 cells total) were collected and pooled via cell scraping into PBS, followed by centrifugation (5 minutes, 500*g*, 4 °C). Cell pellets were flash frozen and stored at -80 °C prior to metabolite extraction. Pellets were lysed and metabolite extracted in 50 μL of 50% methanol. Samples were incubated for 10 minutes at room temperature. Centrifugation was used to pellet insoluble debris (10 minutes, 10,000*g*, 4 °C), and 25 μL of supernatant injected for uHPLC-Orbitrap analysis.

**Metabolism by individual c-DNA expressed cytochrome P450s**

NVP (10 μM) was incubated microsomes containing the following individual cDNA-expressed cytochrome P450 enzymes (Supersomes, BD Biosciences): CYP1A1, -1A2, -2A6, -2B6, -2C8, -2C9, -2C19, -2D6, -3A4, and -3A5. NVP was warmed in potassium phosphate buffer and an NADPH-

regeneration system (Corning, used as per manufacturer's protocol) for 5 minutes at 37 °C. Reactions were initiated with the addition of microsomes for final concentrations of 0.1 M potassium phosphate buffer, 100 nM P450, 10 μM NVP, final reaction volume of 100 μL, and a final vehicle concentration of 0.1% DMSO. Following a 30 minute incubation at 37 °C, reactions were stopped, centrifuged, and dried described above. Samples were reconstituted in 50 μL of methanol and 2 μL was injected for uHPLC-triple quadrupole analysis.

Microsomal NVP metabolism during co-incubation with P450 inhibitors

Human liver microsomes (0.5 mg/mL) were incubated in potassium phosphate buffer and NADPH-regenerating reagents, along with the following panel of P450 inhibitors: 20 μM furafylline (CYP1A2 inhibitor), 2 μM tranylcypromine (CYP2A6 inhibitor), 30 μM PPP (CYP2B6 inhibitor), 20 μM sulfaphenazole (CYP2C9 inhibitor), 10 μM (+)-N-3-benzyl-nirvanol (CYP2C19 inhibitor), 1 μM quinidine (CYP2D6 inhibitor), and 1 μM ketoconazole (CYP3A4 inhibitor). These compounds and concentrations were selected based on previous work regarding isoform selective cytochrome P450 inhibitors (Suzuki *et al.*, 2002; Khojasteh *et al.*, 2011). Following a 5 minute pre-incubation at 37 °C, NVP (10 μM) was added to initiate the reaction. The final reaction volume was 100 μL, with a final vehicle concentration of 0.2% DMSO. Following a 30 minute incubation at 37 °C reactions were stopped, centrifuged, and dried as described above. Samples were reconstituted in 50 μL methanol, and 2 μL was injected for uHPLC-Orbitrap analysis.

**Kinetics of 12-OHNVP production in liver microsomes**

Pilot experiments were performed to determine linearity of 12-OHNVP production with respect to time and microsomal protein concentration, from which the subsequent reaction conditions (2.5 mg/mL protein and 30 minute reaction times) were chosen. As above, NVP or 12-$D_3$NVP were warmed in potassium phosphate buffer and NADPH-regeneration system for 5 minutes at 37 °C. Following this, reactions were initiated through the addition of liver microsomes. Substrate concentrations of 1, 5, 10, 25, 50, 100, 200, or 400 µM NVP or 12-$D_3$NVP were tested in a final reaction volume of 250 µL, and a final vehicle concentration of 0.1% DMSO or 0.2% DMSO for 400 µM substrate reactions. Reactions were incubated at 37 °C for 30 minutes, after which time they were stopped, centrifuged, and supernatant dried as described above. Samples were reconstituted in 112.5 µL of methanol, and 2 µL was injected for Orbitrap uHPLC-MS/MS analysis. For quantification of 12-OHNVP formation, a standard curve of 12-OHNVP was prepared using the same method and microsome concentrations as the reactions, but with water in place of the NADPH-regeneration system. The following known final concentrations of 12-OHNVP standard were spiked into the samples in place of NVP or 12-$D_3$NVP: 1, 2, 5, 20, 50, 100, 200, 500, 1000, and 2000 nM. The 12-OHNVP peak area intensity of these samples were then used to calculate 12-OHNVP amounts in each reaction with NVP or 12-$D_3$NVP. The curve was fit using GraphPad prism software to a line with $1/Y^2$ weighting. An accuracy of ± 15% was observed for all standard curve points.

**Orbitrap detection of NVP and 12-$D_3$NVP metabolites**

Samples were injected for analysis using a Dionex 3000 ultra-high performance liquid chromatography (uHPLC) system coupled to a Thermo Fisher Q-Exactive high-resolution Orbitrap mass spectrometer. Samples were separated on a Waters X Bridge BEH C18 column (2.5 µm pore size, 50 mm long, and 2.1 mm internal diameter) using water with 0.1% formic acid (solvent A) and 100% acetonitrile with 0.1% formic acid (solvent B). A gradient of solvents was used for separation flowing at 750 µL/min during which the concentration of B increased from 5 to 15% over 1 minute, 15 to 18% over 2 minutes, increased immediately to 100% and held 100% for 30 seconds, and then decreased immediately to 5% and held at 5% for 1.5 minutes. The heated electrospray ionization source conditions were as follows: 3.5 kV spray voltage, 600 °C aux gas heater temperature (monooxygenated metabolites) or 350 °C (glucuronidated or glutathione conjugated metabolites), 60 sheath gas, 5 aux gas, 350 °C capillary temperature, and 60 S-Lens RF amplitude.

All metabolites were subjected to a tSIM scan in positive mode (resolution of 35,000, automatic gain control target of 5e4, maximum injection time of 100 ms) to generate high-resolution MS spectra and a PRM scan in positive mode (resolution of 35,000, automatic gain control target of 2e5, maximum injection time of 100 ms, and a normalized collision energy of 50 for monooxygenated metabolites and a three-step collision energy of 20, 35, and 50 for glucuronidated and glutathione conjugated metabolites) was performed to generate high-resolution MS/MS spectra. For all scans across the various metabolites the

quadrupole isolation was set to the compound accurate mass ± 0.5 m/z. For NVP monooxygenated metabolites, PRM fragment peak area was used for quantitation was in order to increase specificity for each of the three metabolites, and achieve baseline separation between metabolites in the chromatograms used for quantitation. The expected m/z for these metabolites were: 283.1190 (2-, 3-, or 12-OHNVP), 285.1315 (for 12-$OHD_2$NVP detection), or 286.1378 (for 2- or 3-$OHD_3$NVP detection). Extracted ion chromatograms (XICs) generated from the spectral intensities of the following specific high-resolution fragments (± 5ppm) and their peak areas monitored for quantitation of the monooxygenated metabolites: 161.0709 m/z for 2-OHNVP and 2-$OHD_3$NVP, 242.0798 m/z for 3-OHNVP, 245.0987 m/z for 3-$OHD_3$NVP, 223.1104 m/z for 12-OHNVP, and 225.1230 m/z for 12-$OHD_2$NVP. For O-glucuronidated or glutathione conjugated NVP metabolites, the expected accurate masses were: 459.1510 (O-GlucNVP), 572.1922 (glutathione-NVP), 462.1700 (O-Gluc$D_3$NVP), 575.2110 ± 0.5 m/z (glutathione-$D_3$NVP), 461.1636 (12-O-gluc$D_2$NVP), and 574.2048 (12-glutathione-$D_2$NVP). For quantitation of glucuronidated or glutathione metabolites, the XIC peak areas for the high-resolution accurate parent masses (± 5ppm) were observed. PRM scans of these metabolites were used only to look for identifying fragments that would provide structural confirmation.

**Triple-Quadrupole detection of NVP metabolites**

Sample was injected for analysis using a Dionex 3000 ultra-high performance liquid chromatography (uHPLC) system coupled to a Thermo Fisher TSQ Vantage triple quadrupole mass spectrometer. The sample was separated

on a Polaris C18 column (5 µm pore size, 100 mm long, and 2 mm internal diameter). Samples were separated using water with 0.1% formic acid (solvent A) and 100% acetonitrile with 0.1% formic acid (solvent B), using a gradient of solvents flowing at 400 µL/min during which the concentration of B increased from 5 to 15% over 1 minute, 15 to 21% over 5 minutes, and then dropped immediately back to 5% and then held at 5% for 1.5 minutes. The heated electrospray ionization source conditions were as follows: 5000 V spray voltage, 352 °C vaporizer temperature, 30 sheath gas, 25 aux gas, 390 °C capillary temperature, and 141 S-Lens RF amplitude. Positive mode SRM scans (scan with of 0.002 m/z, scan time of 0.1 sec, collision energy of 33, and quadrupole widths of 0.7 FWHM) were used to detect monooxygenated NVP metabolites, using the following specific transitions, as confirmed using authentic standards: 283.1 → 160.9 for 2-OHNVP, 283.1 → 241.9 for 3-OHNVP, and 283.1 → 223.0 for 12-OHNVP. Peak height was monitored as a measure of metabolite abundance.

**Cell death staining**

Primary mouse hepatocytes were plated on collagen coated coverslips as previously described (Heck, and treated in a 12-well format with vehicle (0.2% DMSO), 400 µM NVP, or 400 µM 12-$D_3$NVP for 8 hours. Staurosporin treatments at 10 µM were also included as a positive control for cell death activation. Primary hepatocytes were stained, imaged, and those images processed as previously described (Heck *et al.*, 2019).

**uHPLC-MS Proteomics Sample Preparation**

Fresh primary mouse hepatocytes were treated in a 6-well format with vehicle (0.2% DMSO), 400 μM NVP, or 400 μM 12-$D_3$NVP for 8 hours. Cryoplateable LIVERPOOL hepatocyte cultures were treated in a 12-well format with vehicle (0.1% DMSO), 10 μM NVP, or 10 μM 12-$D_3$NVP for 48 hours. Treated cells were harvested through cell scraping into PBS, followed by centrifugation (5 minutes, 500*g*, 4 °C) to pellet cells to be flash frozen and stored at -80 °C prior to sample preparation. Frozen samples were then thawed and re-suspended in 1X cell lysis buffer (Cell Signaling Technologies) supplements with 1X Halt Protease and Phosphatase Inhibitor Cocktail (Thermo Fisher Scientific), 0.5 mM phenylmethylsulfonyl fluoride (MilliporeSigma), and 0.5% sodium dodecyl sulfate. Cells were lysed via 30 passages through a 27-guage syringe needle, and clarified via centrifugation (10 minutes, 3000*g*, 4 °C). Protein concentration was quantified using a bicinchoninic acid assay (Pierce). Lysate (100 μg for mouse samples and 50 μg for human samples) was diluted to 1 mg/mL in 1X cell lysis buffer (Cell Signaling Technologies), supplemented with 0.5% sodium dodecyl sulfate. Dithiothreitol was added to a final concentration of 10 mM and the sample was incubated for 45 minutes at 50 °C. Iodoacetamide was added to a final concentration of 55 mM and the samples was incubated for 20 minutes protected from light. Protein was then precipitated through the addition of ice-cold acetone to a final concentration of 80%, followed by incubation for 1 hour at -20 °C. Protein was pelleted at 16,000*g* for 10 minutes at 4 °C, and the resulting pellet washed once with ice-cold 90% acetone. Pellet was re-suspended in 200

μL of digestion buffer (Pierce). Trypsin (in a ratio of 1:25 μg of trypsin to μg of sample) was added and the sample was digested overnight at 37 °C. Samples were flash frozen to stop the digestion.

Following digestion, samples were desalted using Oasis HLB 1cc Extraction Cartridges (Waters, according to the manufacturers protocol), and fractionated using an Agilent 3100 OFFGEL Fractionator with pH 3-10, twelve-well gel strips (according to the manufacturers protocol). Fractions were then pooled into six final fractions (fraction 1 with 2, 3 with 4, 5 with 6, 7 with 8, 9 with 10, and 11 with 12) and fractions desalted using Pierce C-18 Spin Columns (according to the manufacturers protocol). Eluent was dried under vacuum centrifugation and re-suspended (35 μL for mouse, 17.5 μL for human) of 5% acetonitrile and 0.1% formic acid.

**nanoLC-MS Proteomics Analysis**

Sample (5 μL) was injected for analysis using a Thermo Fisher Easy nLC nano-flow liquid chromatography system coupled to a Thermo Fisher Q-Exactive high-resolution Orbitrap mass spectrometer. The sample was separated on a Thermo Scientific Easy-Spray C18 Column (2 μm pore size, 150 mm long, and 0.050 mm internal diameter) equipped with a trap column (an Acclaim PepMap 100 C18 LC column with a 3 μm particle size, 150 mm long, and 0.075 mm internal diameter). Samples were separated using water with 0.1% formic acid (solvent A) and 80% acetonitrile with 0.1% formic acid (solvent B), using a gradient of solvents flowing at 300 nL/min during which the concentration of B increased from 2 to 24% over 60 minutes, 24 to 36% over 10 minutes, from 36 to

98% over one minute, and then held at 98% for 15 minutes. Samples were ionized at 300 °C and 200 V, with an S-lens RF level of 80. A full scan (resolution of 70,000, automatic gain control target of 3e6, maximum injection time of 40 ms, and scan range of 400 to 1600 m/z) coupled to a data-dependent $MS^2$ top 10 scan (resolution of 17,500, automatic gain control target of 5e4, maximum injection time of 150 ms, 0.8 m/z isolation window, normalized collision energy of 27, and dynamic exclusion period of 10 seconds) was performed to generate high-resolution parent and fragment masses of ionized peptides.

**Proteome Discoverer 2.1 Proteomics Data Analysis**

Raw files for sample fractions were pooled for analysis, with data processed and the consensus generated in Proteome Discoverer version 2.1. Spectra (with a precursor range of 350-5000 daltons, a minimum charge state of +2, and minimum signal to noise of 1.5) were processed and assigned to peptides using Sequest HT. The proteome fasta files used in analysis were Uniprot *Mus musculus* 10090, and *Homo sapiens* 9606 version 2016-05-11. The digestion enzyme was given as trypsin, with the allowance of up to two missed cleavage sites. Mass tolerances for precursor ions was 5 ppm and 0.05 Da for fragment ions. Assignment was performed based on b- and y- ions. The maximum number of dynamic modifications allowed for an identified peptide was three. The following dynamic modifications were included in analysis: methionine oxidation, deamidation of asparagine or glutamine, and n-terminal acetylation. Carbidomethyl cysteine was included as a static peptide modification. Assignments were validated using the Target Decoy Peptide Spectral Match

(PSM) Validator node, with a maximum/relaxed FDR of <0.05, and a strict FDR of <0.01. Peptide spectral matches demonstrating a ± 2 ppm a precision in mass/charge measurements across repeat scans qualified for relative quantitation based on precursor ion area detection.

In data consensus, PSMs were grouped with a site probability threshold of 25 and validated based on PSM level FDR calculation (<0.05 relaxed FDR, and <0.01 strict FDR). Only high confidence peptide assignments (<0.01 FDR) were included in protein identification analysis, with a minimum peptide length of 6 amino acids, counting only rank 1 peptides. Protein assignments were scored using the Protein FDR validator node (<0.05 relaxed FDR, and <0.01 strict FDR). Proteins were grouped using the strict parsimony principle. Protein relative quantitation in each sample is based on precursor ion area assignments generating in the data processing step, and included up to 10 unique and razor peptides for each protein.

Only high-confidence protein hits (FDR<0.01) of Uniprot master protein identifications are reported. Data was analyzed in Microsoft Excel and hits were determined to be significant via paired, two-tailed t-test (P<0.05), with an effect size (Cohen's d) cut off of 2. This alternative analysis to using multiple comparisons corrections has been previously suggested for low-power (small sample size), exploratory, relative-quantitation proteomics studies (Pascovici *et al.*, 2016). In identified hits, any missing quantitation values were filled using observed values for other biological replicate. After this adjustment, any hits that failed to remain significant (P<0.05) or have an effect size ≥2 were excluded from

analysis. Certain hits were not identified in any replicates of a given treatment and are listed as “not found with” a given treatment in the results.

### Statistical Analysis

Data analysis for all data sets except proteomics data was performed using GraphPad Prism, version 7.00. Throughout the text, fold changes are given as means of the ratios observed for each the individual experimental replicate, and reported with 95% confidence intervals (95% CI). Means of experimental replicate values are also reported throughout the text with their 95% CIs. Statistical significance was assayed using an unpaired, two-tailed t-test and P-values are reported as: * $P<0.05$, ** $P<0.01$, or *** $P<0.001$.

## Results

### Metabolism of NVP and 12-$D_3$NVP in primary hepatocyte culture

To assay the impact of twelfth-position deuteration on hepatic metabolism of NVP, we first developed a method to characterize the production of P450-dependent metabolites of NVP or 12-$D_3$NVP in the culture medium of primary hepatocytes treated with 10 μM of either of these compounds for 24 hours. In our initial method development we used C57BL/6J mouse hepatocytes, which have been previously employed as a model to study NVP hepatotoxicity (Sharma *et al.*, 2012). Using high resolution uHPLC-MS (Orbitrap) detection, and by comparison with known standards of monooxygenated NVP metabolites (Figure 1A), we were able to identify three monooxygenated metabolites of NVP formed in primary mouse hepatocytes: 2-OHNVP, 3-OHNVP, and 12-OHNVP (Figure

1B), as well as three main monooxygenated metabolites produced from 12-$D_3$NVP: 2-OH$D_3$NVP, 3-OH$D_3$NVP (Figure 1C), and 12-OH$D_2$NVP (Figure 1D). We also identified peaks corresponding to 2- and 3-OH$D_2$NVP, though the peak areas of these dideuterated metabolites were less than 10% of the trideuterated versions. Because of this, only the production of 12-OH$D_2$NVP, 2-OH$D_3$NVP, 3-OH$D_3$NVP were monitored in subsequent experiments with 12-$D_3$NVP. No peaks corresponding to 8-OHNVP were detected. These peaks were not found in vehicle-treated hepatocyte medium (data not shown). With these metabolite peaks identified, we developed specific MS/MS transitions to detect these metabolites in future assays of P450 metabolism of NVP and 12-$D_3$NVP (Figure 2). Monitoring these fragments for quantitation, as opposed to the high resolution parent masses, allowed for improved baseline separation of metabolite peaks in extracted ion chromatograms (XICs), especially for 12-OHNVP and 12-OH$D_2$NVP production (Figure 2 D and H). For simplicity, in the following results and discussion, comparisons of production of 12-OHNVP from NVP or 12-OH$D_2$NVP from 12-$D_3$NVP is referred to only as 12-OHNVP, with the deuteration for the product from 12-$D_3$NVP implied. The same abbreviation is used for 2-OHNVP vs. 2-OH$D_3$NVP and 2-OHNVP and 3-OH$D_3$NVP production from NVP and 12-$D_3$NVP, respectively.

Using this method, we compared the production of these three metabolites by primary human hepatocytes treated with either 10 μM of NVP or 12-$D_3$NVP for 24 or 48 hours. Levels of 12-OHNVP production with 12-$D_3$NVP decreased 10.6-fold (95% CI [6.7, 14.6]) at 24 hours and 13.2-fold (95% CI [11.2, 15.3]) at 48

hours, as compared to production with NVP (Figure 3A). Because of this reduction in 12-OHNVP production, we probed whether other P450-dependent metabolites of NVP would increase in response. No difference was observed in production of 2- or 3-OHNVP (Figure 3B and 3C), and as with mouse hepatocytes no peak corresponding to 8-OHNVP formation was identified (data not shown). At these same treatment times and concentrations, we assayed for differences in P450-dependent metabolism in C57BL/6J mice. As with human hepatocytes, we saw decreases in 12-OHNVP production: 4.6- (95% CI [3.6, 5.7]) and 4.0-fold (95% CI [2.7, 5.3]) at 24 and 48 hours of treatment, respectively (Figure 3D). Again, no difference was observed in either 2- or 3-OHNVP production (Figure 3E and 3F).

As previously mentioned, monooxygenated metabolites of NVP can be subsequently glucuronidated to form O-Glucuronide-NVP (O-GlucNVP) (Riska *et al.*, 1999). Because of this, we were interested in monitoring any impact of deuterium substitution on this subsequent metabolism of monooxygenated NVP. Again, we used C57Bl/6J hepatocytes in our initial method development for detection of these metabolites. One uHPLC-MS/MS peak corresponding to an O-GlucNVP metabolite was observed in the medium of primary mouse hepatocyte incubations with 10 μM NVP or 12-$D_3$NVP for 24 hours (Figure 4). This peak was not detected in vehicle-treated hepatocyte medium (data not shown). In incubations with 12-$D_3$NVP, the high-resolution accurate mass of this peak was that of a trideuterated O-glucuronidated metabolite (O-Gluc$D_3$NVP, 462.1700 m/z), which suggests that this metabolite is likely from 2- or 3-OHNVP

glucuronidation, as these are the two metabolites that retain all three deuterium atoms following metabolism by cytochrome P450s. In our treatments of primary human and primary mouse hepatocytes with 10 μM NVP or 12-$D_3$NVP, no difference was observed in the levels of this O-GlucNVP metabolite (Figure 5).

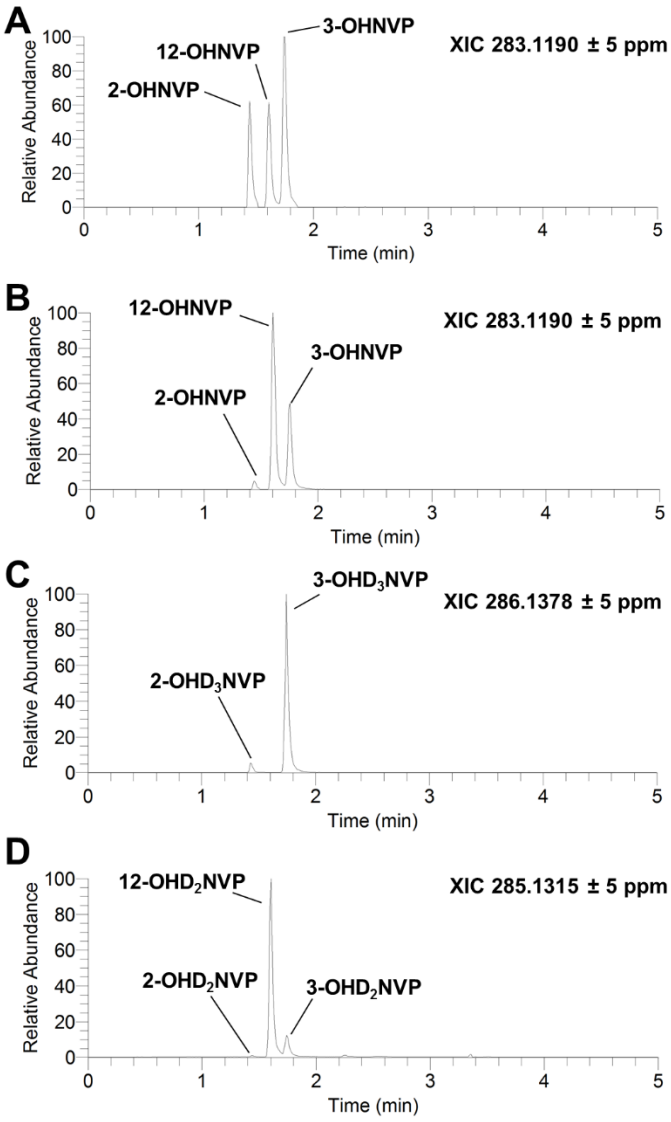


**Figure 1. Characterization of P450-dependent NVP and 12-$D_3$NVP metabolite formation in primary mouse hepatocytes.** Fresh primary mouse hepatocytes from male C57BL/6J mice were cultured and treated with 10 μM NVP or 12-$D_3$NVP for 24 hours. Metabolites were extracted from the medium from these treatments and subjected to uHPLC-MS (Orbitrap) analysis. The following high resolution ions were observed to assay for the presence of P450 metabolites: 238.1190 ± 5 ppm for monooxygenated, undeuterated NVP,

286.1378 ± 5 ppm for monooxygenated, trideuterated NVP, and 285.1315 ± 5 ppm for monooxygenated, dideuterated NVP. Representative extracted ion chromatograms (XICs) from this analysis are shown for a mix of authentic standards for undeuterated 2- 3- and 12-OHNVP (A, each at 50 nM), monooxygenated, undeuterated metabolites formed during incubations with NVP (B), monooxygenated, trideuterated metabolites formed during incubations with 12-$D_3$NVP (C), and monooxygenated, dideuterated metabolites formed during incubations with 12-$D_3$NVP (D). Results are representations of four experimental replicates.

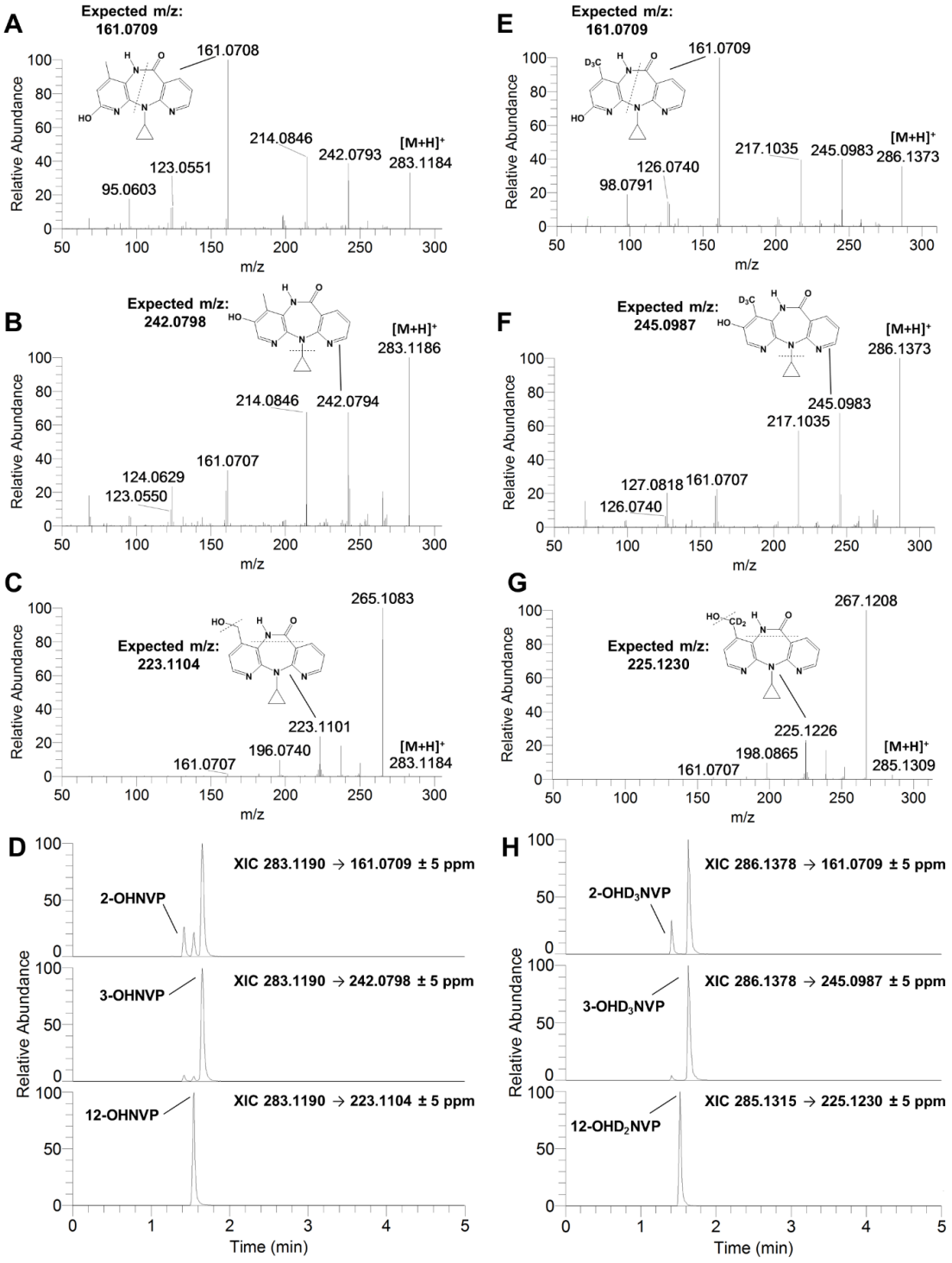


**Figure 2. Fragment selection for uHPLC-MS/MS based quantitation of monooxygenated NVP and 12-D$_3$NVP metabolites.** Fresh primary mouse hepatocytes from male C57BL/6J mice were cultured and treated with 10 μM

NVP or 12-$D_3$NVP for 24 hours. Metabolites were extracted from the medium from these treatments and subjected to uHPLC-MS/MS (Orbitrap) analysis. Representative fragmentation spectra are shown for the following metabolites from NVP incubations: 2-OHNVP (A), 3-OHNVP (B), and 12-OHNVP (C), with the selected fragmentation ions used for quantitation and their proposed sights of fragmentation highlighted. The extracted ion chromatograms (XICs) of these fragments from incubations with NVP are shown, with the metabolite highlighted that is quantified with each mass transition (D). Representative fragmentation spectra are also shown for the following metabolites from 12-$D_3$NVP incubations: 2-OH$D_3$NVP (E), 3-OH$D_3$NVP (F), and 12-OH$D_2$NVP (G), with the selected fragmentation ions used for quantitation and their proposed sights of fragmentation highlighted. The extracted ion chromatograms (XICs) of these fragments from incubations with 12-$D_3$NVP are shown (H). Results are representations of four experimental replicates.

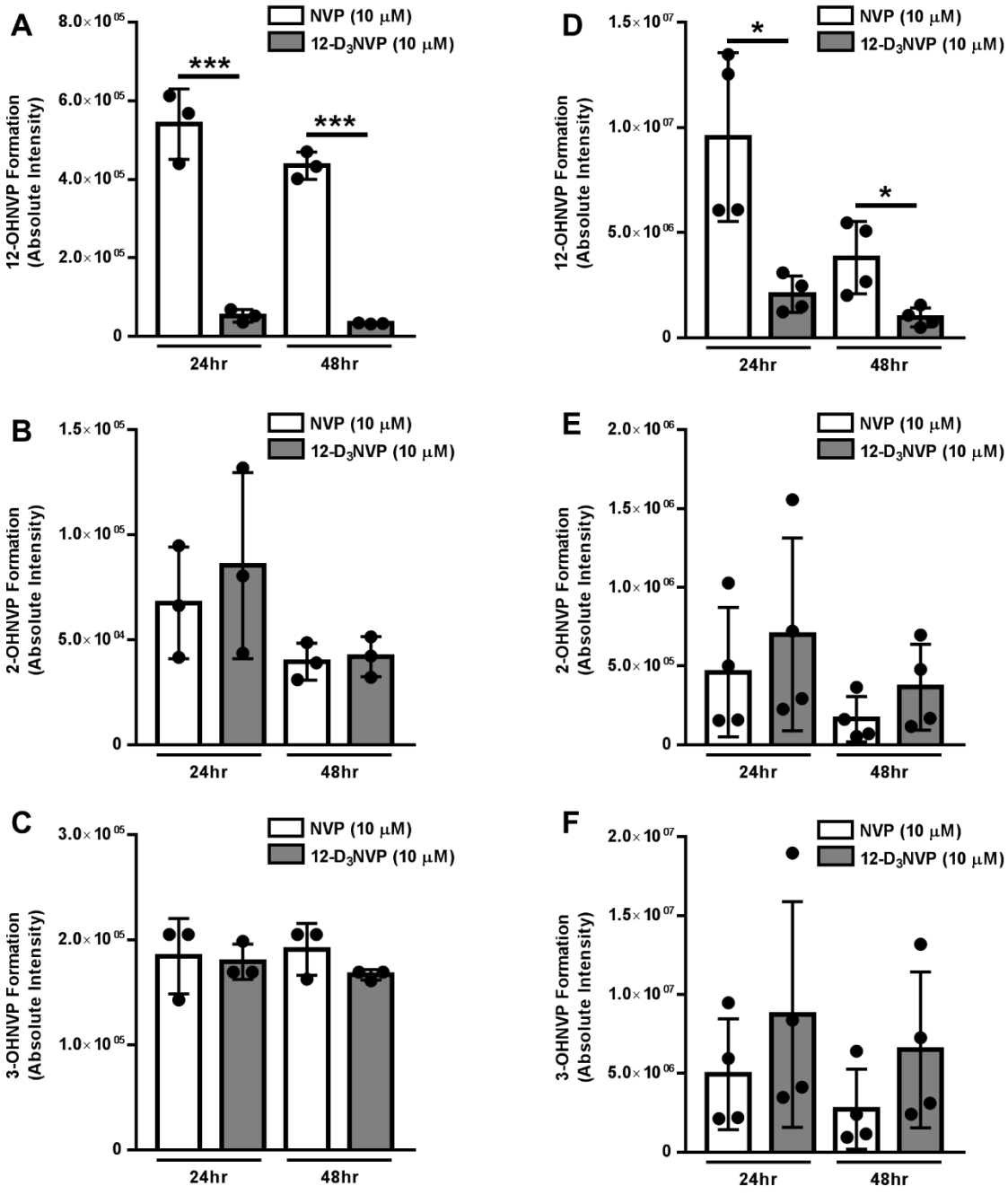


**Figure 3. NVP and 12-D$_3$NVP cytochrome P450-dependent metabolism in primary human and mouse hepatocytes.** Cryopreserved primary human hepatocytes (A-C) and fresh primary mouse hepatocytes (D-F) were incubated with 10 μM NVP or 12-D$_3$NVP for 24 or 48 hours. Cytochrome P450 metabolites extracted from hepatocyte culture medium were measured using uHPLC-MS/MS

(Orbitrap) detection. 12-OHNVP (A,D), 2-OHNVP (B,E), and 3-OHNVP (C,F) were monitored using MS/MS scans for the following transitions: 283.1190 → 223.1104 *m*/*z* (12-OHNVP), 285.1315 → 225.1230 *m*/*z* (12-$OHD_2$NVP), 283.1190 → 161.0709 *m*/*z* (12-OHNVP), 285.1315 → 161.0709 *m*/*z* (2-$OHD_3$NVP), 283.1190 → 242.0798 *m*/*z* (3-OHNVP), and 285.1315 → 245.0987 *m*/*z* (3-$OHD_3$NVP). Data are representative of the mean ± standard deviation of three (human) or four (mouse) experimental replicates. Significant differences between metabolite production with NVP and 12-$D_3$NVP were determined using an unpaired t-test generating two-tailed P values (* $P<0.05$ and *** $P < 0.001$).

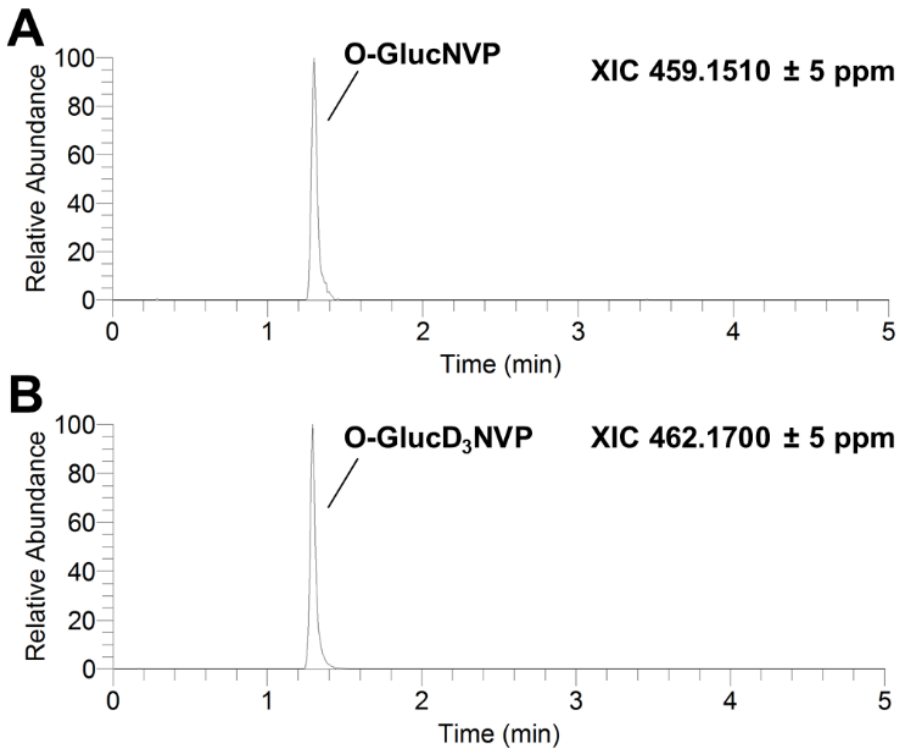


**Figure 4. Extracted ion chromatograms of O-glucuronidated NVP and 12-$D_3$NVP metabolite formation in primary mouse hepatocytes.** Fresh primary mouse hepatocytes from male C57BL/6J mice were cultured and treated with 10 μM NVP or 12-$D_3$NVP for 24 hours. Metabolites were extracted from the cell culture medium and subjected to uHPLC-MS (Orbitrap) analysis. The following high resolution ions were observed to assay for the presence of P450 metabolites: 459.1510 ± 5 ppm for O-glucuronidated, undeuterated NVP (O-GlucNVP) and 462.1700 ± 5 ppm for O-glucuronidated, trideuterated NVP (O-Gluc$D_3$NVP). Representative extracted ion chromatograms (XICs) from this analysis are shown for O-GlucNVP formed during incubations with NVP (A) and O-Gluc$D_3$NVP formed during incubations with 12-$D_3$NVP (B). Results are representations of four experimental replicates.

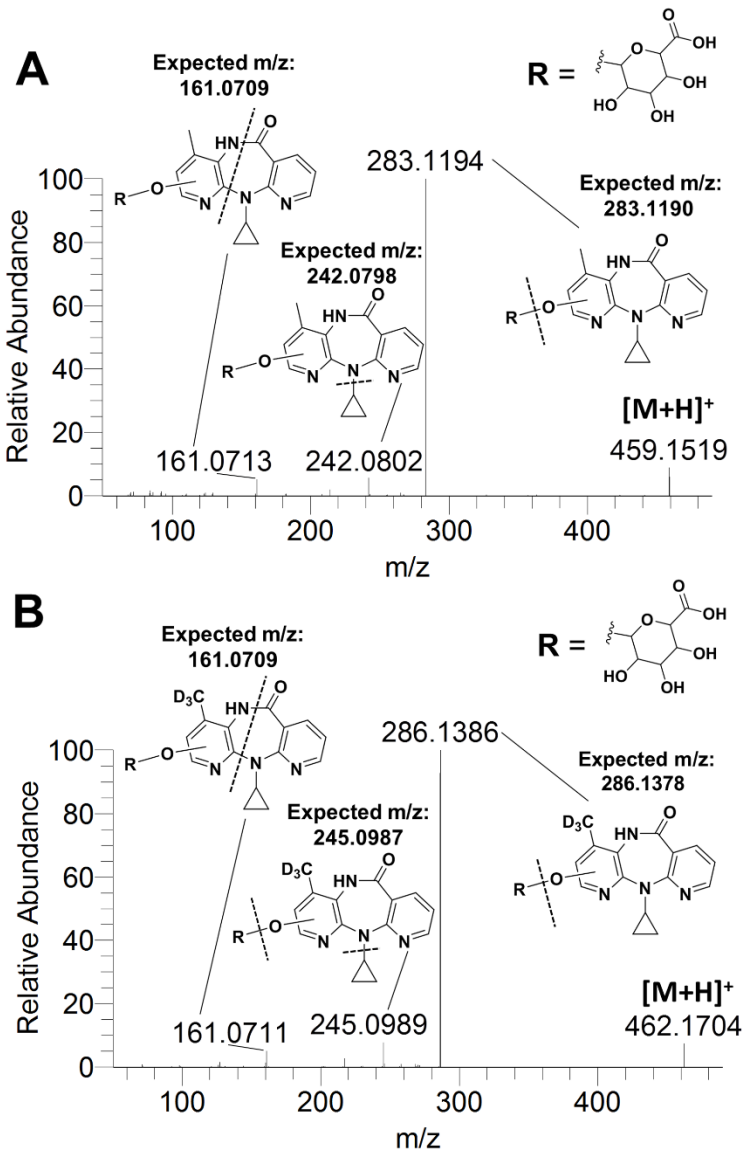


**Figure 5. Representative fragmentation spectra for an O-glucuronidated NVP and 12-$D_3$NVP metabolite formed in primary mouse hepatocytes.** Fresh primary mouse hepatocytes from male C57BL/6J mice were cultured and treated with 10 μM NVP or 12-$D_3$NVP for 24 hours. Metabolites were extracted from the cell culture medium and subjected to uHPLC-MS/MS (Orbitrap) analysis. Fragmentation scans for the following ions were performed: 459.1510 ± 5 ppm for O-glucuronidated, undeuterated NVP (O-GlucNVP) and 462.1700 ± 5 ppm for

O-glucuronidated, trideuterated NVP (O-Gluc$D_3$NVP). Representative fragmentation spectra for these ions are shown are shown for O-GlucNVP formed during incubations with NVP (A) and O-Gluc$D_3$NVP formed during incubations with 12-$D_3$NVP (B). The high resolution parent mass is indicated as [$M+H^+$], and the high resolution fragments used for structural confirmation are indicated, along with their predicted sites of fragmentation. Results are representations of four experimental replicates.

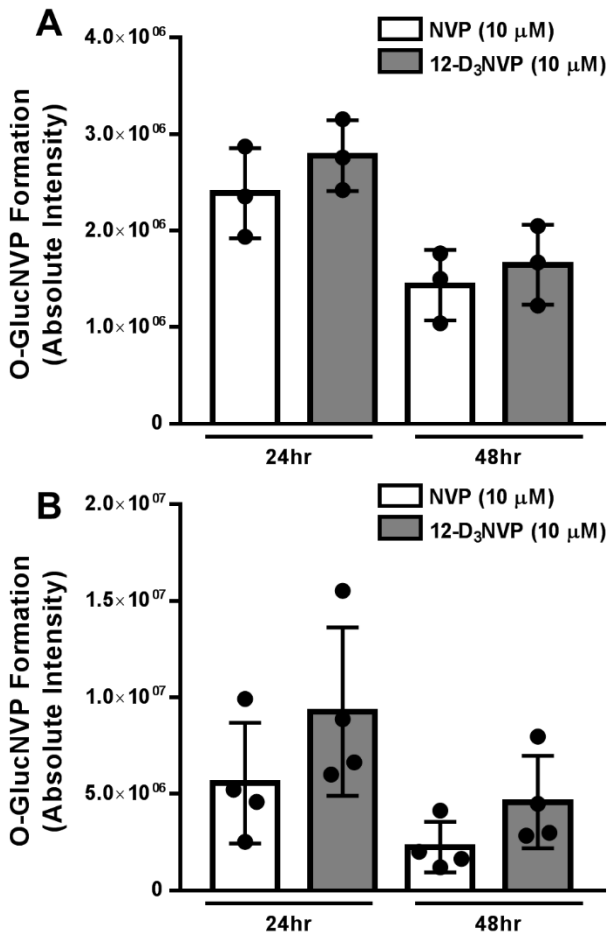


**Figure 6. O-glucuronidated NVP and 12-$D_3$NVP formation in primary human and mouse hepatocytes.** Cryopreserved primary human hepatocytes (A) and fresh primary mouse hepatocytes (B) were incubated with 10 μM NVP or 12-$D_3$NVP for 24 or 48 hours. O-glucuronidated metabolites extracted from hepatocyte culture medium were measured using uHPLC-MS (Orbitrap) detection. The peak area of the XICs for the following high resolution ions were observed to assay metabolite formation: 459.1510 ± 5 ppm for O-glucuronidated, undeuterated NVP (O-GlucNVP) and 462.1700 ± 5 ppm for O-glucuronidated, trideuterated NVP (O-Gluc$D_3$NVP). Data are representative of the mean ± standard deviation of three (human) or four (mouse) experimental replicates.

**Identifying human cytochrome P450s involved in the metabolism of NVP**

Given our observed reduction in P450 formation of 12-OHNVP with 12-$D_3$NVP as compared to NVP, we became interested in which human P450s isoforms are responsible for the formation of 12-OHNVP. We performed incubations of NVP (10 μM) with individual human cytochrome P450 enzymes (100 nM active enzyme), and NADPH regenerating reagents. We employed a panel of ten cytochrome P450 enzymes commonly implicated in drug metabolism (Rendic and Guengerich, 2015). As in our incubations with hepatocytes, peaks corresponding to 2-, 3- and 12-OHNVP were observed in these incubations, and no peak corresponding to 8-OHNVP was observed (data not shown). Using the unique fragments identified for these metabolites, uHPLC-MS/MS (triple quadrupole) detection was employed to quantify 2-, 3-, and 12-OHNVP in these incubations. For 12-OHNVP (Figure 6A), all but one P450 tested (CYP3A5) formed this metabolite, with CYP2C19 producing the highest levels. CYP3A4 produced the highest levels of 2-OHNVP (Figure 6B) and CYP2B6 produced the highest levels of 3-OHNVP (Figure 6C)

Cytochrome P450 isoforms do not exist in equal concentrations within the human liver. In order to assay the contribution of these P450s in model that is more representative of the relative abundances of P450 isoforms in the human liver, we measured monooxygenated NVP metabolite formation in human liver microsomes. Liver microsomes are endoplasmic retuculum fractions from pooled-donor human liver homogenate, representing the diversity and relative abundances of P450s in the hepatic endoplasmic reticulum (Knights *et al.*, 2016)

We performed one hour co-incubations with liver microsomes (0.5 mg/mL), NADPH regenrating reagents, and NVP (10 μM), with and without the addition of small molecule P450 inhibitors at the following concentrations specific to indicated P450 isoform: 20 μM furafylline (CYP1A2 inhibitor), 2 μM tranylcypromine (CYP2A6 inhibitor), 30 μM 2-phenyl-2-(1-piperidinyl)propane (PPP, a CYP2B6 inhibitor), 20 μM sulfaphenazole (CYP2C9 inhibitor), 10 μM (+) N-3-Benzyl-nirvanol (CYP2C19 inhibitor), 1 μM quinidine (CYP2D6 inhibitor), or 1 μM ketoconazole (CYP3A inhibitor). Using uHPLC-MS/MS (Orbitrap) detection, we monitored the formation of 12-, 2- and 3-OHNVP in these incubations (Figure 7A, B, and C, respectively). Interestingly, no P450 inhibitor was able to reduce the formation of 12-OHNVP, including (+)-N-3-benzyl-nirvanol, a CYP2C19 inhibitor (Figure 7A). P450 production of 2-OHNVP was inhibited by ketoconozole, a CYP3A inhibitor (Figure 7B), and 3-OHNVP production was inhibited by PPP, a CYP2B6 inhibitor (Figure 7C).

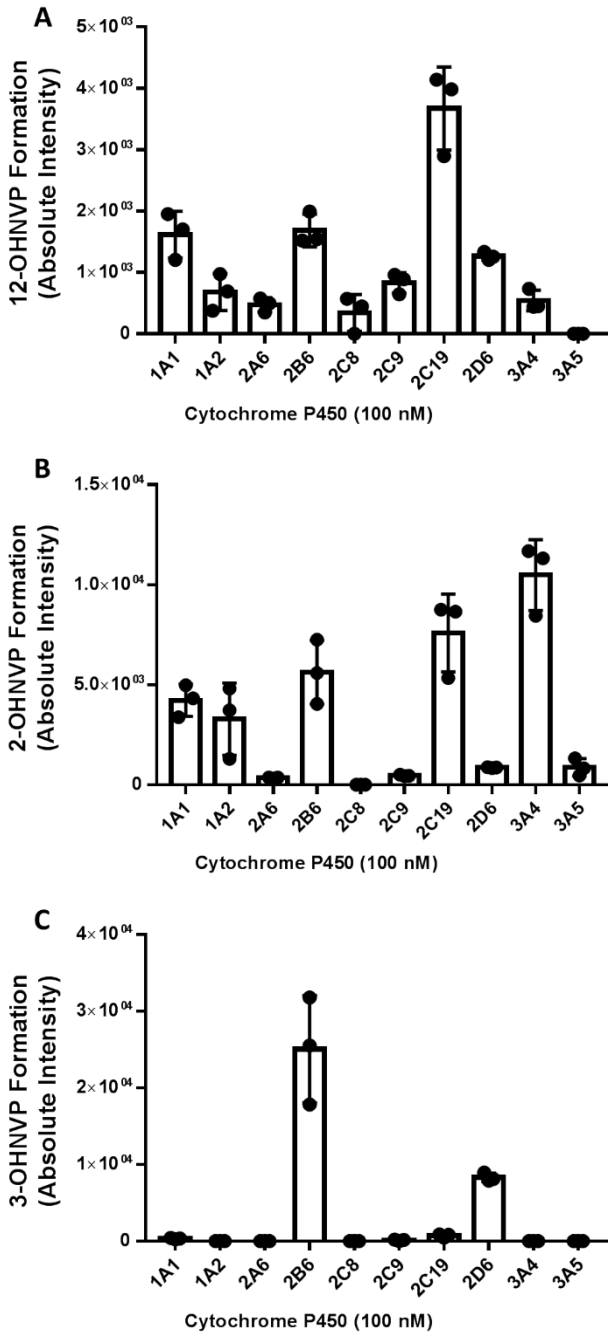


**Figure 7. NVP monooxygenated metabolite produced during incubations with individual cDNA-expressed human P450 enzymes.** Insect cell microsomes containing one the following c-DNA expressed cytochrome P450s (100 nM): CYP1A1, -1A2, -2A6, -2B6, -2D6, -2C8, -2C9, -2C19, -3A4, and -3A5, were incubated with NVP (10 μM) and NADPH regenerating reagents for 30

minutes. 12-OHNVP (A), 2-OHNVP (B), and 3-OHNVP (C) were extracted from these incubations and measured using uHPLC-MS/MS (triple quadrupole) detection for the following transitions: 283.1 → 223.0 *m*/*z* (12-OHNVP), 283.1 → 160.9 *m*/*z* (2-OHNVP), and 283.1 → 241.9 *m*/*z* (3-OHNVP). Data are representative of the mean ± standard deviation of three experimental replicates.

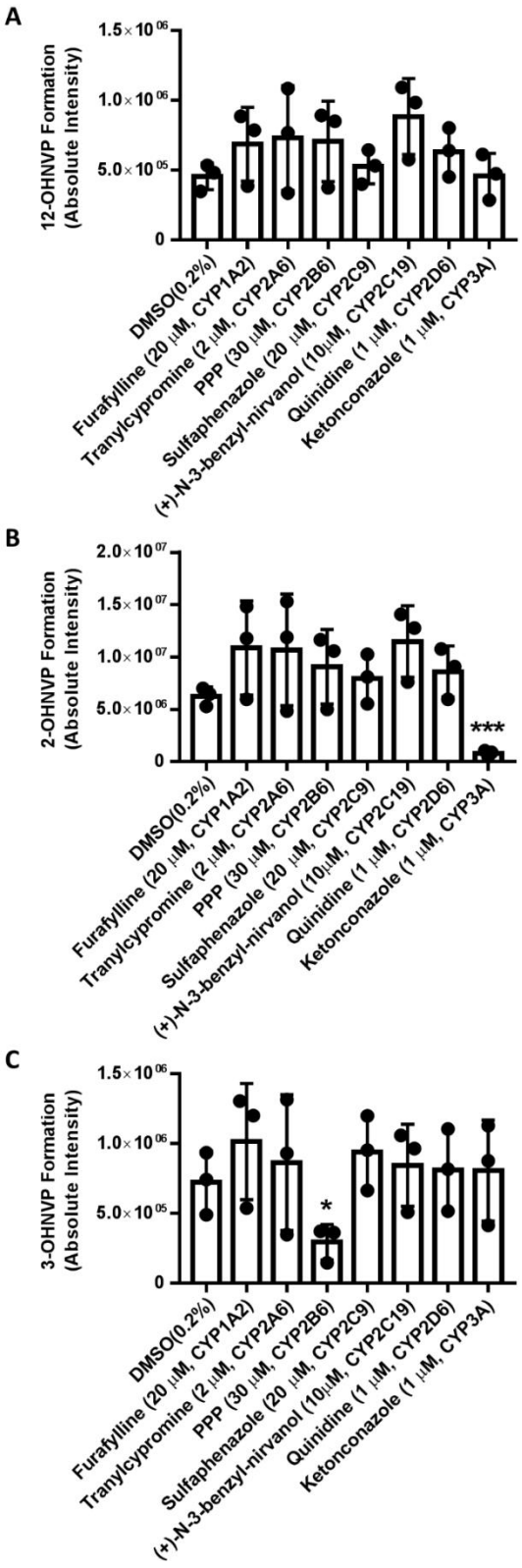
A
12-OHNVP Formation (Absolute Intensity)
1.5×10 06
1.0×10 06
5.0×10 05
0
DMSO(0.2%)
Furafylline (20 μM, CYP1A2)
Tranylcypromine (2 μM, CYP2A6)
PPP (30 μM, CYP2B6)
Sulfaphenazole (20 μM, CYP2C9)
(+)-N-3-benzyl-nirvanol (10μM, CYP2C19)
Quinidine (1 μM, CYP2D6)
Ketonconazole (1 μM, CYP3A)
B
2-OHNVP Formation (Absolute Intensity)
2.0×10 07
1.5×10 07
1.0×10 07
5.0×10 06
0
***
DMSO(0.2%)
Furafylline (20 μM, CYP1A2)
Tranylcypromine (2 μM, CYP2A6)
PPP (30 μM, CYP2B6)
Sulfaphenazole (20 μM, CYP2C9)
(+)-N-3-benzyl-nirvanol (10μM, CYP2C19)
Quinidine (1 μM, CYP2D6)
Ketonconazole (1 μM, CYP3A)
C
3-OHNVP Formation (Absolute Intensity)
1.5×10 06
1.0×10 06
5.0×10 05
0
*
DMSO(0.2%)
Furafylline (20 μM, CYP1A2)
Tranylcypromine (2 μM, CYP2A6)
PPP (30 μM, CYP2B6)
Sulfaphenazole (20 μM, CYP2C9)
(+)-N-3-benzyl-nirvanol (10μM, CYP2C19)
Quinidine (1 μM, CYP2D6)
Ketonconazole (1 μM, CYP3A)

**Figure 8. NVP cytochrome P450-dependent metabolism in human liver microsomes during co-incubations with cytochrome P450 inhibitors.** Liver microsomes (0.5 mg/mL) prepared from human liver were incubated with NVP (10 μM) and NADPH-regenerating reagents for one hour either with additional vehicle as a control (0.2% DMSO) or with the following Cytochrome P450 inhibitors: 20 μM furafylline (CYP1A2 inhibitor), 2 μM tranylcypromine (CYP2A6 inhibitor), 30 μM PPP (CYP2B6 inhibitor), 20 μM sulfaphenazole (CYP2C9 inhibitor), 10 μM (+)-N-3-benzyl-nirvanol (CYP2C19 inhibitor), 1 μM quinidine (CYP2D6 inhibitor), or 1 μM ketoconazole (CYP3A inhibitor). Metabolites were measured using uHPLC-MS/MS (Orbitrap) detection. 12-OHNVP (A), 2-OHNVP (B), and 3-OHNVP (C) were monitored using MS/MS scans for the following transitions: 283.1190 → 223.1104 *m*/*z* (12-OHNVP), 283.1190 → 161.0709 *m*/*z* (12-OHNVP), and 283.1190 → 242.0798 *m*/*z* (3-OHNVP). Data are representative of the mean ± standard deviation of three experimental replicates. Significant differences in inhibitor containing incubations to vehicle control incubations were determined using an unpaired t-test generating two-tailed P values (* $P < 0.05$ and *** $P < 0.001$).

**Quantifying the kinetic isotope effect of twelfth-position deuteration of NVP on 12-OHNVP production in human liver microsomes**

No single P450 isoform produced 12-OHNVP and no P450 inhibitor was able to inhibit liver microsome production of this metabolite at therapeutically relevant (10 μM) concentrations of NVP. Because of this, we decided to quantify the kinetic isotope effect of NVP trideuteration on twelfth position oxygen insertion by P450s using human liver microsomes. Preliminary incubations were performed in microsomes to determine optimal microsomal protein concentrations and incubation time points to obtain linear rates of 12-OHNVP formation from NVP (data not shown). Liver microsomes (2.5 mg/mL) were incubated with NADPH regenerating reagents and a range of concentrations (1-400 μM) of either NVP or 12-$D_3$NVP for 30 minutes. We were unable to achieve saturation of the rate of 12-OHNVP production even with up to 400 μM NVP, and beyond this concentration NVP solubility became limiting (data not shown). Because of this, we monitored the rate of 12-OHNVP production, using uHPLC-MS/MS Orbitrap detection, with lower concentraions of NVP and 12-$D_3$NVP (0, 1, 5, 10, 25 and 50 μM), where the curve of rate of 12-OHNVP production vs. substrate concentration maintained linearity for both NVP and 12-$D_3$NVP. To do this, we employed a standard curve of 12-OHNVP prepared in equal concentrations of human liver microsomes, without NADPH regenerating reagents.

12-OHNVP was quantifiable in incubations with all concentrations of NVP, in incubations with 5, 10, 25 and 50 μM of 12-$D_3$NVP (Figure 8A). The catalytic

efficiency ($K_{cat}/K_m$, the slope of the rate vs. substrate concentration line at non-saturating conditions) of 12-OHNVP formation with both NVP and 12-$D_3$NVP, was 83.7 (95% CI [78.2, 89.1]) $M^{-1}$ $min^{-1}$, and 9.2 (95% CI [8.1, 10.3]) $M^{-1}$ $min^{-}$ respectively (Figure 8A). The average fold change (NVP/12-$D_3$NVP) in $K_{cat}/K_m$ was 9.1 (95% CI [7.4, 10.9]). The fold change in rate of 12-OHNVP production, known as the observed kinetic isotope effect, with 12-$D_3$NVP as compared to NVP across all concentrations tested was 10.1 (95% CI [9.4, 10.8]).

As with our human hepatocyte incubations we wanted to observe whether decreased production of 12-OHNVP in liver microsomes would result in increases in the production of other P450 metabolites of NVP. No significant change was observed in 2- or 3-OHNVP formation with 50 μM of 12-$D_3$NVP vs NVP (Figure 8B and 8C, respectively), or with any of the other substrate concentrations tested (5, 10, 25, 100, 200, 400 μM, data not shown).

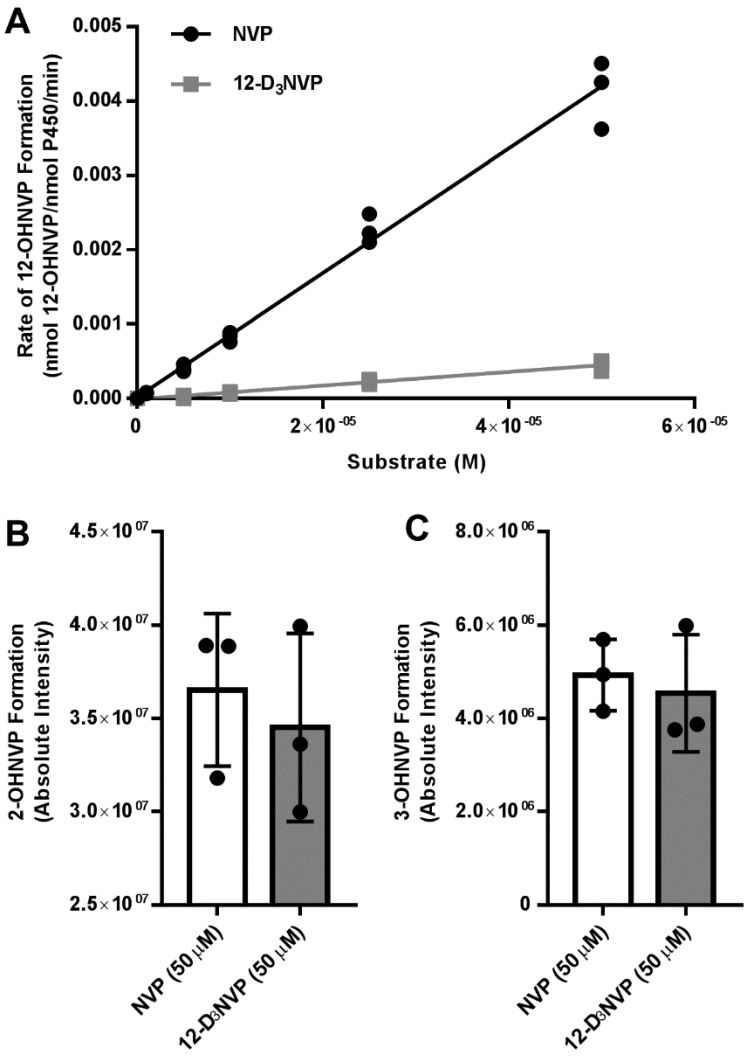


**Figure 9. Rate of 12-OHNVP production, as well as 2- and 3-OHNVP formation, from NVP and 12-D$_3$NVP in human liver microsome incubations.** Liver microsomes (2.5 mg/mL) prepared from pooled human donor livers were incubated with a range of concentrations of NVP (0, 1, 5, 10, 25, and 50 μM) or 12-D$_3$NVP (0, 5, 10, 25 and 50 μM) and NADPH regenerating reagents for 30 minutes. Cytochrome P450 metabolites extracted from these incubations were measured using uHPLC-MS/MS (Orbitrap) detection. Metabolites were monitored using MS/MS scans for the following transitions: 283.1190 → 223.1104 *m*/*z* (12-

OHNVP), 285.1315 → 225.1230 *m*/*z* (12-OHD$_2$NVP), 283.1190 → 161.0709 *m*/*z* (12-OHNVP), 285.1315 → 161.0709 *m*/*z* (2-OHD$_3$NVP), 283.1190 → 242.0798 *m*/*z* (3-OHNVP), and 285.1315 → 245.0987 *m*/*z* (3-OHD$_3$NVP). The rate of formation of 12-OHNVP (A) was quantified by comparing peak areas of 12-OHNVP or 12-OHD$_2$NVP to those of a standard curve of 12-OHNVP prepared in liver microsomal incubations without NADPH regenerating reagents. Formation of 2-OHNVP (B) and 3-OHNVP(C) from 50 μM of NVP or 12-D$_3$NVP is also shown. For rates of 12-OHNVP production, all data points are shown, in addition to results of linear curve fitting for the graphs of rate vs. substrate concentration. For 2- and 3-OHNVP production, data are representative of the mean ± standard deviation of three experimental replicates.

**Hepatocyte viability during treatments with NVP and 12-$D_3$NVP**

With our observed reduction in hepatocyte formation of 12-OHNVP with 12-$D_3$NVP, we probed whether there is a difference in hepatocyte viability during treatments with NVP vs. 12-$D_3$NVP. Primary mouse hepatocytes were treated with 400 μM of NVP or 12-$D_3$NVP for 8 hours, and their viability assayed using ethidium bromide (EtBr)/acridine orange (AcrO) co-staining, and compared to treatment with vehicle alone (Figure 9A and 9B). EtBr positive nuclei were observed as a marker for cell death. Staurosporin (10 μM, 8 hours) treatments were used as a positive control (data not shown). During treatment with NVP, the percentage of EtBr- positive cell nucleii was 52.6% (95% CI [37.0, 68.2]), which is noteably higher than the 19.0% (95% CI [9.5, 28.4]) observed for vehicle treatments. The percentage of EtBr-positive cell nucleii in treatments with 12-$D_3$NVP was 36.8% (95% CI [25.3, 48.2]), a modest reduction from levels in treatments with NVP, though still elevated above vehicle control.

Given the high treatment concentrations needed to induce cell death, we wanted to compare NVP and 12-$D_3$NVP metabolite formation in these incubations. The differences in metabolism between NVP and 12-$D_3$NVP observed with lower (10 μM) hepatocyte treatment incubations may be differ at these higher concentrations. Production of 12-OHNVP was reduced 3.5-fold (95% CI [3.2, 3.8]) with 12-$D_3$NVP as compared to NVP (Figure 9C) and though differences between 2- and 3-OHNVP formation did not rise to the level of statistical significance, the formation of both of these metabolites trended towards an increase with 12-$D_3$NVP as compared to NVP. Given this trend, we

also measured the formation of the downstream O-GlucNVP metabolite, likely formed from 2- or 3-OHNVP, and observed an 2.8-fold (95% CI [1.9, 3.4]) increase with 12-$D_3$NVP as compared to NVP (Figure 9D). With this observed increase, we became interested in quantifying other subsequent metabolites of mono-oxygenated NVP. Glutathione conjugation has been previously observed on both the 3- and 12- positions (Dekker *et al.*, 2016). We were able to profile one glutathione cojugated metabolite in our primary mouse hepatocyte incubations (Figures 11 and 12). Given that with 12-$D_3$NVP this metabolite retains all three deuteriums (Figures 11 and 12), we propose that this is likely 3-glutathione-NVP, rather than 12-glutathione-NVP, which would only have two deuteriums remaining following the metabolism by P450s, sulfotransferases, and glutathione-s-transferases necessary to produce 12-glutathione-NVP. Interestingly, during these treatments, we observed a 3.0-fold increase (95% CI [0.486, 5.514]) in this glutathione-conjugated metabolite with 12-$D_3$NVP as compared to NVP.

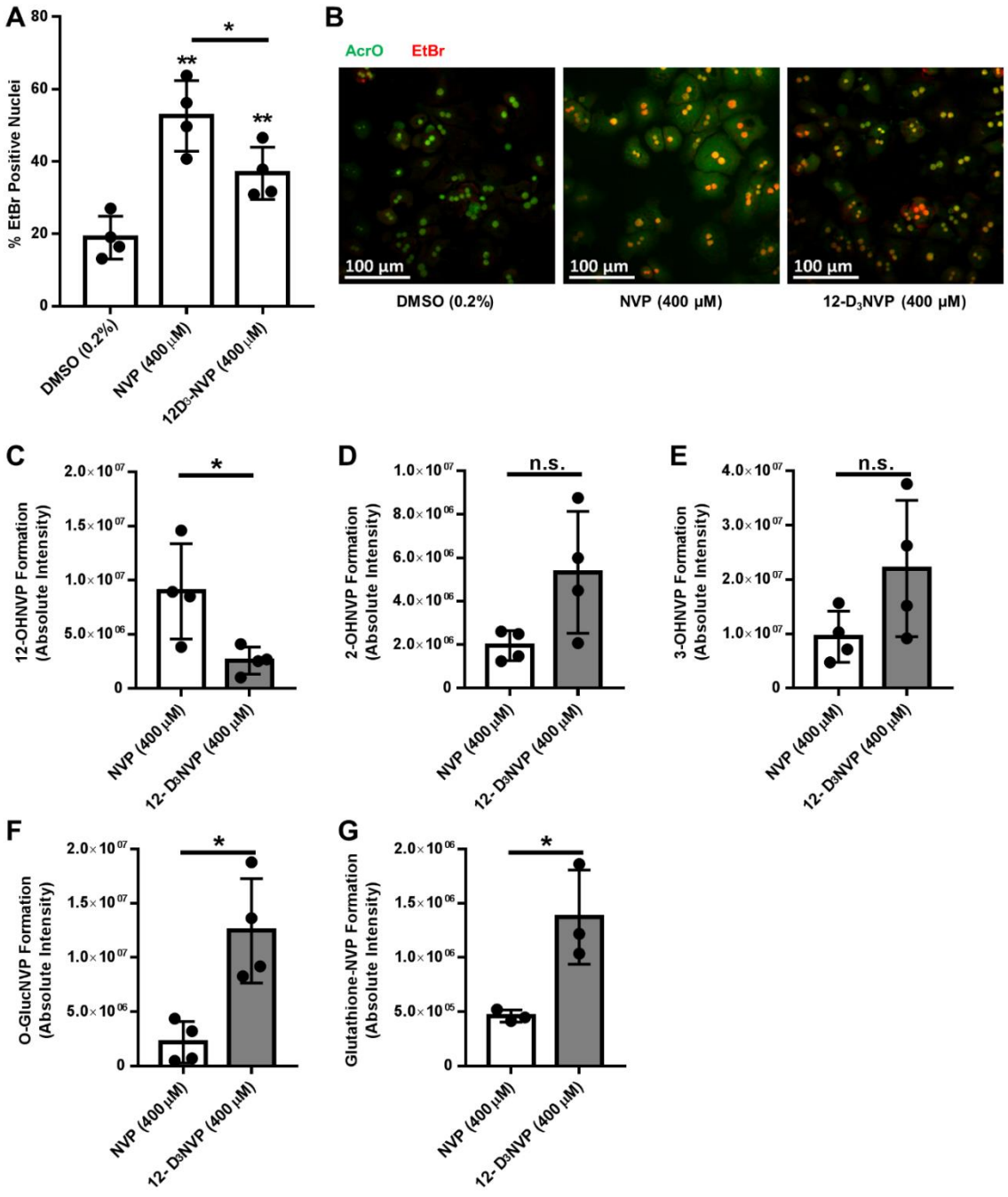


**Figure 10. EtBr/AcrO viability staining and metabolite formation in primary mouse hepatocytes treated with NVP or 12-D$_3$NVP.** Fresh primary mouse hepatocytes were incubated with vehicle (0.02% DMSO), 400 µM NVP, or 400 µM 12-D$_3$NVP for 8 hours. Quantitation of nuclear EtBr incorporation from EtBr/AcrO viability co-staining (A), as well as representative images of EtBr/AcrO

co-staining (B) are shown for these incubations. Cytochrome P450 metabolites extracted from hepatocyte culture medium were measured using uHPLC-MS/MS (Q-Exactive) detection. 12-OHNVP (C), 2-OHNVP (D), and 3-OHNVP (E) were monitored using MS/MS scans for the following transitions: 283.1190 → 223.1104 *m*/*z* (12-OHNVP), 285.1315 → 225.1230 *m*/*z* (12-$OHD_2$NVP), 283.1190 → 161.0709 *m*/*z* (12-OHNVP), 285.1315 → 161.0709 *m*/*z* (2-$OHD_3$NVP), 283.1190 → 242.0798 *m*/*z* (3-OHNVP), and 285.1315 → 245.0987 *m*/*z* (3-$OHD_3$NVP). One O-glucuronidated metabolite (F) was extracted from the cell culture medium and subjected to uHPLC-MS (Orbitrap) analysis. The following high resolution ions were observed to assay for the presence of O-glucuronidated metabolite: 459.1510 ± 5 ppm for O-glucuronidated, undeuterated NVP (O-GlucNVP) and 462.1700 ± 5 ppm for O-glucuronidated, trideuterated NVP (O-Gluc$D_3$NVP). Data are representative of the mean ± standard deviation of four experimental replicates. Significant differences from vehicle (A) or for the indicated comparisons (A, C, D, E, F) was determined using an unpaired t-test generating two-tailed P values (* $P < 0.05$; ** $P < 0.01$).

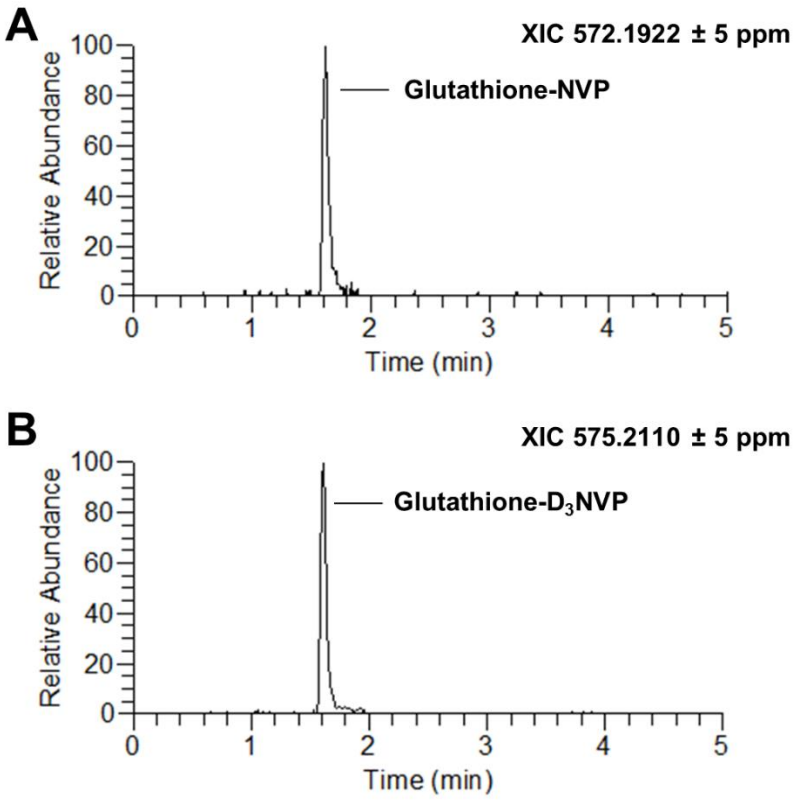


**Figure 11. Extracted ion chromatograms of a glutathione conjugated NVP and 12-$D_3$NVP metabolite formed in primary mouse hepatocytes.** Fresh primary mouse hepatocytes from male C57BL/6J mice were cultured and treated with 10 μM NVP or 12-$D_3$NVP for 24 hours. Metabolites were extracted from isolated cell pellets and subjected to uHPLC-MS (Orbitrap) analysis. The following high resolution ions were observed to assay for the presence of P450 metabolites: 572.1922 ± 5 ppm for glutathione conjugated, undeuterated NVP (Glutathione-NVP) and 575.2110 ± 5 ppm for glutathione conjugated, trideuterated NVP (Glutathione-$D_3$NVP). Representative extracted ion chromatograms (XICs) from this analysis are shown for glutathione conjugates formed during incubations with NVP (A) and with 12-$D_3$NVP (B). Results are representations of four experimental replicates.

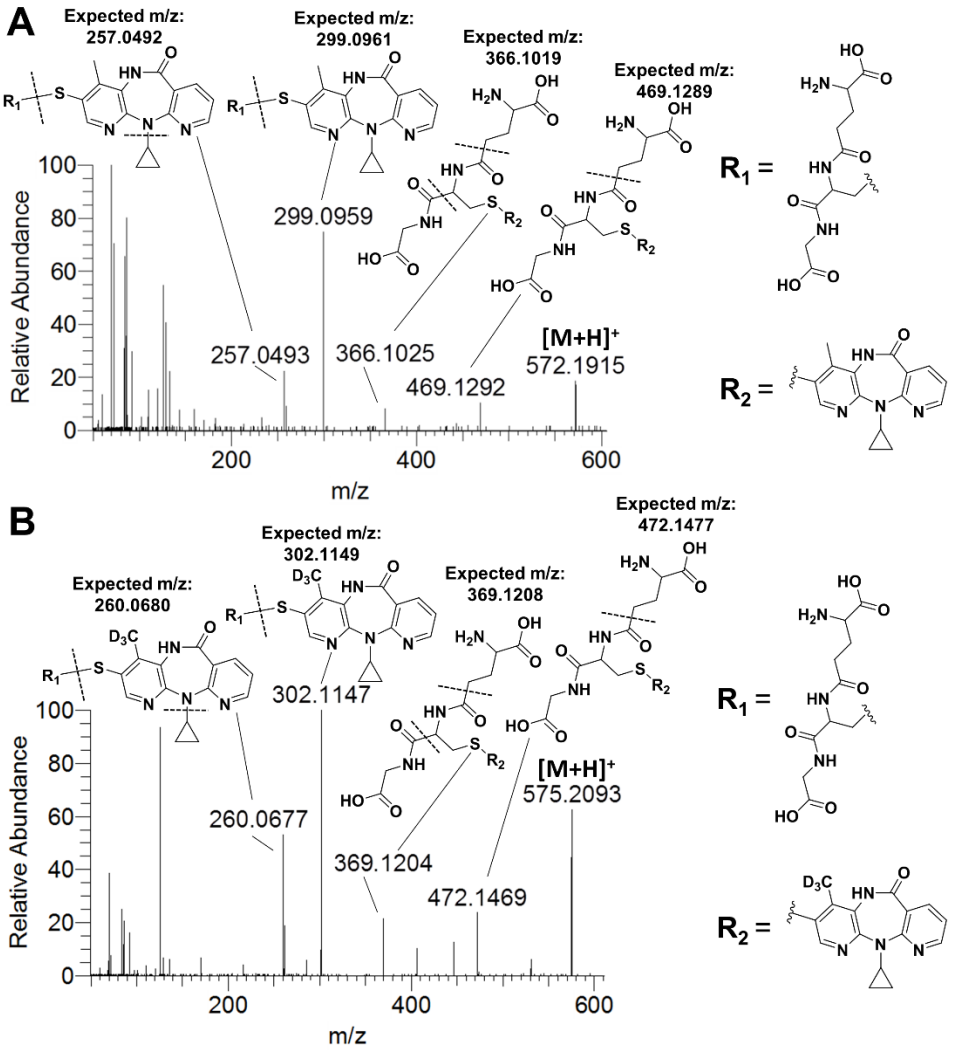


**Figure 12. Representative fragmentation spectra for a glutathione conjugated NVP and 12-D$_3$NVP metabolite formed in primary mouse hepatocytes.** Fresh primary mouse hepatocytes from male C57BL/6J mice were cultured and treated with 10 μM NVP or 12-D$_3$NVP for 24 hours. Metabolites were extracted from isolated cell pellets and subjected to uHPLC-MS/MS (Orbitrap) analysis. Fragmentation scans for the following ions were performed: 572.1922 ± 5 ppm for glutathione conjugated, undeuterated NVP (Glutathione-NVP) and 575.2110 ± 5 ppm for glutathione conjugated, trideuterated NVP (Glutathione-D$_3$NVP). Representative fragmentation spectra for these ions are

shown are shown for glutathione conjugates formed during incubations with NVP (A) and 12-$D_3$NVP (B). The high resolution parent mass is indicated as [$M+H^+$], and the high resolution fragments used for structural confirmation are indicated, along with their predicted sites of fragmentation. Results are representations of four experimental replicates.

**Relative-quantitation proteomics analysis of NVP and 12-$D_3$NVP treated hepatocytes**

The molecular mechanisms underlying NVP-induced hepatocyte death are poorly understood. In addition, though deuterium substitution in this case is intended to slow metabolism at a specific position, it can also lead to other unintended consequencecs such as increases in other metabolites, as we have observed at high concentrations, and even altered parent drug exposure, as has been previously observed in rats dosed with NVP and 12-$D_3$NVP (Chen *et al.*, 2008). This may result in alternative cell signalling in response to exposure to NVP vs. 12-$D_3$NVP. To better understand differential responses to these two compounds, we performed relative-quantitation label-free proteomics analysis of primary mouse heptocytes treated with vehicle (0.2% DMSO), 400 μM NVP, or 400 μM 12-$D_3$NVP for 8 hours. In addition, to assess potential changes at more therapeutically relevant concentrations in a human model, we also performed this analysis on primary human hepatocytes treated with with vehicle (0.1% DMSO), 10 μM NVP, or 10 μM 12-$D_3$NVP for a longer treatment duration (48 hours). We looked for protein changes with NVP or 12-$D_3$NVP treatment alone, but also between NVP and 12-$D_3$NVP. For the purposes of making easier visual comparisons, changes greater in magnitude than ±2.0-fold across the above comparisons are are shown in Table 1 (mouse hepatocyte treatments) and Table 2 (human hepatocyte treatments). All significant protein changes, regardless of magnitude, are shown in Tables 3-5 (mouse hepatocyte treatments) and Tables 6-8 (human hepatocyte treatments). Comparisons of housekeeping proteins actin

and glyceraldehyde-3-phosphate dehydrogenase are also shown in Tabels 3-8. No change in these housekeeping proteins was observed across any of the treatments. In treament of mouse hepatocytes for 8 hours, 7 proteins were elevated or decreased more than 3-fold with 400 μM NVP (as compared to vehicle), 9 with 400 μM 12-$D_3$NVP (as compared to vehicle), and 9 between 400 μM NVP and 12-$D_3$NVP treaments (Table 1). In treament of human hepatocytes treated for 48 hours, 3 proteins were elevated or decreased more than 3-fold with 10 μM NVP (as compared to vehicle), 7 with 10 μM 12-$D_3$NVP (as compared to vehicle), and 8 between 10 μM NVP and 12-$D_3$NVP treaments (Table 2).

The largest observed change was a 15.96-fold increase in the expression of mitochondrial pyruvate carrier protein 1 (*MPC1*) during treatment of human hepatocytes with 12-$D_3$NVP as compared to vehicle. An 8.32-fold increase the the mitochondrial 39S ribosome protein L23 (*MRPL23*) was also observed with 12-$D_3$NVP treatment in human hepatocytes, as compared to NVP treatment. Interestingly one protein was differentially expressed in mouse hepatocytes treated with 12-$D_3$NVP as compared to both vehicle and NVP: increased insulin-like growth factor-binding protein 1 (*Igfbp1*, 4.18-fold higher than vehicle and 4.70-fold higher than with NVP treatment). Two cytochrome P450 enzymes, CYP2D6 and CYP2C9 were both decreased during 12-$D_3$NVP treatment in human hepatocytes as compared to NVP, by around 1.92- and 2.06- fold, respectively (Table 8). Most of the observed changes with NVP vs. 12-$D_3$NVP were unique to either of these compounds. In addition, among all of the identified

changes in human hepatocytes there appears to be an abundance of mitochrondrial proteins (Tables 2 and 6-8).

| Protein Changes with NVP Treatment (in comparison to Vehicle) | | | | |
|---|---|---|---|---|
| **UniProt Accession** | **UniProt Entry** | **Gene Name** | **Fold Change** | **P-Value** |
| Q91VC3 | Eukaryotic initiation factor 4A-III | *Eif4a3* | -2.02 ± 0.12 | 0.0047 |
| Q9Z1N5 | Spliceosome RNA helicase Ddx39b | *Ddx39b* | -2.15 ± 0.16 | 0.0381 |
| Q91W92 | Cdc42 effector protein 1 | *Cdc42ep1* | -2.54 ± 0.05 | 0.0039 |
| P13597 | Intercellular adhesion molecule 1 | *Icam1* | -2.85 ± 0.01 | 0.0001 |
| Q9DC13 | Lysosomal membrane glycoprotein 1, isoform CRA_a | *Lamp1* | -3.24 ± 0.19 | 0.0336 |
| P70318 | Nucleolysin TIAR | *Tial1* | Not found with NVP | 0.0047 |
| D3Z5N6 | Zinc finger protein ubi-d4 | *Dpf2* | Not found with NVP | 0.0038 |
| **Protein Changes with 12-$D_3$NVP Treatment (in comparison to Vehicle)** | | | | |
| Q8BKT7 | THO complex subunit 5 homolog | *Thoc5* | Not found with DMSO | 0.0072 |
| A2AIL4 | NADH dehydrogenase (ubiquinone) complex I, assembly factor 6 | *Ndufaf6* | Not found with DMSO | 0.0089 |
| P47876 | Insulin-like growth factor-binding protein 1 | *Igfbp1* | 4.18 ± 1.16 | 0.0179 |
| O35405 | Phospholipase D3 | *Pld3* | 3.36 ± 0.98 | 0.0250 |
| Q9DAS9 | Guanine nucleotide-binding protein G(I)/G(S)/G(O) subunit gamma-12 | *Gng12* | 2.41 ± 0.98 | 0.0408 |
| B9EKL6 | MCG114106 | *Ptp4a1* | -2.16 ± 0.2 | 0.0179 |
| Q921I1 | Serotransferrin | *Tf* | -2.22 ± 0.07 | 0.0057 |
| Q3UUI3 | Acyl-coenzyme A thioesterase THEM4 | *Them4* | -3.18 ± 0.16 | 0.0460 |
| P15116 | Cadherin-2 | *Cdh2* | Not found with 12-$D_3$NVP | 0.0385 |
| **Changes with 12-$D_3$NVP Treatment (in comparison to NVP)** | | | | |
| **UniProt Accession** | **UniProt Entry** | **Gene Name** | **Fold Change** | **P-Value** |
| P47876 | Insulin-like growth factor-binding protein 1 | *Igfbp1* | 4.7 ± 1.38 | 0.0048 |
| E9QPI2 | Putative methyltransferase NSUN7 | *Nsun7* | 3.89 ± 2.73 | 0.0244 |
| Q642L7 | MCG13441 | *Rps27a* | 3.03 ± 2.51 | 0.0144 |
| D3Z5F7 | Protein Gm20521 | *Gm20521* | 2.64 ± 0.79 | 0.0079 |
| P70441 | Na(+)/H(+) exchange regulatory cofactor NHE-RF1 | *Slc9a3r1* | 2.5 ± 0.86 | 0.0319 |
| O08600 | Endonuclease G, mitochondrial | *Endog* | 2.07 ± 0.47 | 0.0336 |
| Q6A0A9 | Constitutive coactivator of PPAR-gamma-like protein 1 | *Fam120A* | 2.06 ± 0.6 | 0.0204 |
| Q3KNM2 | E3 ubiquitin-protein ligase MARCH5 | *March5* | -2.14 ± 0.17 | 0.0061 |
| Q6ZWY3 | 40S ribosomal protein S27-like | *Rps27l* | -5.67 ± 0.08 | 0.0416 |

**Table 1. Relative-quantitation proteomics analysis of protein expression changes with NVP and 12-$D_3$NVP treatment of primary mouse hepatocytes.** Freshly isolated primary mouse hepatocytes were treated for 8 hours with vehicle (0.2% DMSO), 400 μM NVP, or 400 μM 12-$D_3$NVP. Cell lysate was then prepared for and subjected to Top10 nanoLC-MS based proteomics, with data analysis performed in Proteome Discoverer 2.1, using Sequest HT for peptide spectral matching/protein identification and precursor ion area detection for relative quantitation. Up to 10 unique or razor peptides were used in protein precursor ion-based quantitation. Relative quantitation changes over 2- fold (ratio of means) are shown for treatment with NVP as compared to vehicle (top panel), with 12-$D_3$NVP as compared to vehicle (middle panel), and with 12-$D_3$NVP as compared to NVP (bottom panel). UniProt proteome *Mus musculus* 10090 was used for protein identification profiling, with UniProt accession numbers, protein entry (protein name), and gene name's provided. P-values were generated using un-paired t-test and effect size calculated using Cohen's d equation. Data are representative of four biological replicates.

| Protein Changes with NVP Treatment (in comparison to Vehicle) | | | | |
|---|---|---|---|---|
| **UniProt Accession** | **UniProt Entry** | **Gene Name** | **Fold Change** | **P-Value** |
| Q13098 | Isoform 3 of COP9 signalosome complex subunit 1 | *GPS1* | 2.06 ± 0.26 | 0.0289 |
| Q13190 | Syntaxin-5 | *STX5* | 2.02 ± 0.39 | 0.0183 |
| P36543 | V-type proton ATPase subunit E 1 | *ATP6V1E1* | -2.16 ± 0.25 | 0.0460 |
| **Protein Changes with 12-$D_3$NVP Treatment (in comparison to Vehicle)** | | | | |
| Q9Y5U8 | Mitochondrial pyruvate carrier 1 | *MPC1* | 15.96 ± 11.14 | 0.0015 |
| Q16718 | NADH dehydrogenase [ubiquinone] 1 alpha subcomplex subunit 5 | *NDUFA5* | -2.14 ± 0.1 | 0.0247 |
| Q92552 | Isoform 2 of 28S ribosomal protein S27, mitochondrial | *MRPS27* | -2.4 ± 0.17 | 0.0490 |
| P61457 | Pterin-4-alpha-carbinolamine dehydratase | *PCBD1* | -2.63 ± 0.17 | 0.0042 |
| O15127 | Secretory carrier-associated membrane protein 2 | *SCAMP2* | -2.68 ± 0.05 | 0.0380 |
| Q7L8L6 | FAST kinase domain-containing protein 5, mitochondrial | *FASTKD5* | -4.73 ± 0.06 | 0.0456 |
| Q96K37 | Solute carrier family 35 member E1 | *SLC35E1* | Not Found in 12-$D_3$NVP | 0.0151 |
| **Changes with 12-$D_3$NVP Treatment (in comparison to NVP)** | | | | |
| **UniProt Accession** | **UniProt Entry** | **Gene Name** | **Fold Change** | **P-Value** |
| Q16540 | 39S ribosomal protein L23, mitochondrial | *MRPL23* | 8.32 ± 2.21 | 0.0159 |
| Q8N163 | Cell cycle and apoptosis regulator protein 2 | *CCAR2* | -2.05 ± 0.09 | 0.0164 |
| Q9UJ68 | Mitochondrial peptide methionine sulfoxide reductase | *MSRA* | -2.05 ± 0.14 | 0.0358 |
| P11712 | Cytochrome P450 2C9 | *CYP2C9* | -2.06 ± 0.16 | 0.0498 |
| Q9NYL9 | Tropomodulin-3 | *TMOD3* | -2.1 ± 0.01 | 0.0356 |
| Q93096 | Protein tyrosine phosphatase type IVA 1 | *PTP4A1* | -2.42 ± 0.17 | 0.0466 |
| Q9Y2D5 | Isoform 2 of A-kinase anchor protein 2 | *AKAP2* | -2.67 ± 0.06 | 0.0249 |
| Q9Y3B2 | Exosome complex component csl4 | *EXOSC1* | -2.73 ± 0.09 | 0.0086 |

**Table 2. Relative-quantitation proteomics analysis of protein expression changes with NVP and 12-$D_3$NVP treatment of cryopreserved human hepatocytes.** Cryopreserved pooled-donor (10, mixed-sex) primary human hepatocytes were treated for 48 hours with vehicle (0.1% DMSO), 10 μM NVP, or 10 μM 12-$D_3$NVP. Cell lysate was then prepared for and subjected to Top10 nanoLC-MS based proteomics, with data analysis performed in Proteome Discoverer 2.1, using Sequest HT for peptide spectral matching/protein identification and precursor ion area detection for relative quantitation. Up to 10 unique or razor peptides were used in protein precursor ion-based quantitation. Relative quantitation changes over 2- fold (ratio of means) are shown for treatment with NVP as compared to vehicle (top panel), with 12-$D_3$NVP as compared to vehicle (middle panel), and with 12-$D_3$NVP as compared to NVP (bottom panel). UniProt proteome *Homo sapiens* 9606 was used for protein identification profiling, with UniProt accession numbers, protein entry (protein name), and gene name's provided. P-values were generated using un-paired t-test and effect size calculated using Cohen's d equation. Data are representative of experiments with three different 10-donor pools of hepatocytes.

| Protein Changes with NVP Treatment (in comparison to Vehicle) | | | | |
|---|---|---|---|---|
| **UniProt Accession** | **UniProt Entry** | **Gene Name** | **Fold Change** | **P-Value** |
| P70404 | Isocitrate dehydrogenase [NAD] subunit gamma 1, mitochondrial | *Idh3g* | 1.8 ± 0.36 | 0.0071 |
| P60710 | Actin, cytoplasmic 1 | *Actb* | 1.15 ± 0.64 | 0.8847 |
| A0A0A0MQF6 | Glyceraldehyde-3-phosphate dehydrogenase | *Gapdh* | -1.01 ± 0.33 | 0.8643 |
| Q9DBG7 | Signal recognition particle receptor subunit alpha | *Srpra* | -1.27 ± 0.1 | 0.0408 |
| Q9D710 | Thioredoxin-related transmembrane protein 2 | *Tmx2* | -1.39 ± 0.1 | 0.0310 |
| Q569Z6 | Thyroid hormone receptor-associated protein 3 | *Thrap3* | -1.46 ± 0.09 | 0.0064 |
| Q9DB05 | Alpha-soluble NSF attachment protein | *Napa* | -1.48 ± 0.09 | 0.0108 |
| Q8C2T9 | Putative uncharacterized protein | *Ik* | -1.51 ± 0.19 | 0.0484 |
| A1L2Z3 | C230096C10Rik protein | *Emc1* | -1.52 ± 0.13 | 0.0404 |
| Q3UMF0 | Cordon-bleu protein-like 1 | *Cobll1* | -1.58 ± 0.18 | 0.0477 |
| Q8BFP9 | Pyruvate dehydrogenase (acetyl-transferring)] kinase isozyme 1, mitochondrial | *Pdk1* | -1.66 ± 0.09 | 0.0394 |
| Q3TKM9 | Actin-related protein 2/3 complex subunit 5 | *Arpc5* | -1.69 ± 0.1 | 0.0061 |
| Q542U7 | LSM6 homolog, U6 small nuclear RNA associated (S. cerevisiae) | *Lsm6* | -1.72 ± 0.22 | 0.0292 |
| Q91VC3 | Eukaryotic initiation factor 4A-III | *Eif4a3* | -2.02 ± 0.12 | 0.0047 |
| Q9Z1N5 | Spliceosome RNA helicase Ddx39b | *Ddx39b* | -2.15 ± 0.16 | 0.0381 |
| Q91W92 | Cdc42 effector protein 1 | *Cdc42ep1* | -2.54 ± 0.05 | 0.0039 |
| P13597 | Intercellular adhesion molecule 1 | *Icam1* | -2.85 ± 0.01 | 0.0001 |
| Q9DC13 | Lysosomal membrane glycoprotein 1, isoform CRA_a | *Lamp1* | -3.24 ± 0.19 | 0.0336 |
| P70318 | Nucleolysin TIAR | *Tial1* | Not found with NVP | 0.0047 |
| D3Z5N6 | Zinc finger protein ubi-d4 | *Dpf2* | Not found with NVP | 0.0038 |

**Table 3. Relative-quantitation proteomics analysis of protein expression changes with NVP treatment of primary mouse hepatocytes.** Freshly isolated primary mouse hepatocytes were treated for 8 hours with vehicle (0.2% DMSO) or 400 μM NVP. Cell lysate was then prepared for and subjected to Top10 nanoLC-MS based proteomics, with data analysis performed in Proteome Discoverer 2.1, using Sequest HT for peptide spectral matching/protein identification and precursor ion area detection for relative quantitation. Up to 10 unique or razor peptides were used in protein precursor ion-based quantitation. Statistically significant relative-quantitation changes are shown for treatment with NVP as compared to vehicle, as well as the results for housekeeping proteins actin and GAPDH. UniProt proteome *Mus musculus* 10090 was used for protein identification profiling, with UniProt accession numbers, protein entry (protein name), and gene name's provided. P-values were generated using un-paired t-test and effect size calculated using Cohen's d equation. Data are representative of four biological replicates.

| Protein Changes with 12-$D_3$NVP Treatment (in comparison to Vehicle) | | | | |
|---|---|---|---|---|
| **UniProt Accession** | **UniProt Entry** | **Gene Name** | **Fold Change** | **P-Value** |
| Q8BKT7 | THO complex subunit 5 homolog | *Thoc5* | Not found with DMSO | 0.0072 |
| A2AIL4 | NADH dehydrogenase (ubiquinone) complex I, assembly factor 6 | *Ndufaf6* | Not found with DMSO | 0.0089 |
| P47876 | Insulin-like growth factor-binding protein 1 | *Igfbp1* | 4.18 ± 1.16 | 0.0179 |
| O35405 | Phospholipase D3 | *Pld3* | 3.36 ± 0.98 | 0.0250 |
| Q9DAS9 | Guanine nucleotide-binding protein G(I)/G(S)/G(O) subunit gamma-12 | *Gng12* | 2.41 ± 0.98 | 0.0408 |
| Q3TJ01 | tRNA-splicing ligase RtcB homolog | *Rtcb* | 1.65 ± 0.47 | 0.0340 |
| Q3TND1 | Peptidyl-prolyl cis-trans isomerase | *Fkbp2* | 1.57 ± 0.31 | 0.0295 |
| P60710 | Actin, cytoplasmic 1 | *Actb* | 1.19 ± 0.68 | 0.7786 |
| A0A0A0MQF6 | Glyceraldehyde-3-phosphate dehydrogenase | *Gapdh* | 1.11 ± 0.53 | 0.6387 |
| P13597 | Intercellular adhesion molecule 1 | *Icam1* | -1.36 ± 0.03 | 0.0015 |
| Q3TEX7 | Putative uncharacterized protein | *Mfn2* | -1.45 ± 0.09 | 0.0266 |
| P11352 | Glutathione peroxidase 1 | *Gpx1* | -1.5 ± 0.03 | 0.0028 |
| Q9DBG7 | Signal recognition particle receptor subunit alpha | *Srpra* | -1.58 ± 0.17 | 0.0225 |
| Q14C24 | MCG14259, isoform CRA_a | *U2af1* | -1.95 ± 0.13 | 0.0042 |
| B9EKL6 | MCG114106 | *Ptp4a1* | -2.16 ± 0.2 | 0.0179 |
| Q921I1 | Serotransferrin | *Tf* | -2.22 ± 0.07 | 0.0057 |
| Q3UUI3 | Acyl-coenzyme A thioesterase THEM4 | *Them4* | -3.18 ± 0.16 | 0.0460 |
| P15116 | Cadherin-2 | *Cdh2* | Not found with 12-$D_3$NVP | 0.0385 |

**Table 4. Relative-quantitation proteomics analysis of protein expression changes with 12-$D_3$NVP treatment of primary mouse hepatocytes.** Freshly isolated primary mouse hepatocytes were treated for 8 hours with vehicle (0.2% DMSO) or 400 μM 12-$D_3$NVP. Cell lysate was then prepared for and subjected to Top10 nanoLC-MS based proteomics, with data analysis performed in Proteome Discoverer 2.1, using Sequest HT for peptide spectral matching/protein identification and precursor ion area detection for relative quantitation. Up to 10 unique or razor peptides were used in protein precursor ion-based quantitation. Statistically significant relative-quantitation changes are shown for treatment with 12-$D_3$NVP as compared to vehicle, as well as the results for housekeeping proteins actin and GAPDH. UniProt proteome *Mus musculus* 10090 was used for protein identification profiling, with UniProt accession numbers, protein entry (protein name), and gene name's provided. P-values were generated using un-paired t-test and effect size calculated using Cohen's d equation. Data are representative of four biological replicates.

| Changes with 12-$D_3$NVP Treatment (in comparison to NVP) | | | | |
|---|---|---|---|---|
| **UniProt Accession** | **UniProt Entry** | **Gene Name** | **Fold Change** | **P-Value** |
| P47876 | Insulin-like growth factor-binding protein 1 | *Igfbp1* | 4.7 ± 1.38 | 0.0048 |
| E9QPI2 | Putative methyltransferase NSUN7 | *Nsun7* | 3.89 ± 2.73 | 0.0244 |
| Q642L7 | MCG13441 | *Rps27a* | 3.03 ± 2.51 | 0.0144 |
| D3Z5F7 | Protein Gm20521 | *Gm20521* | 2.64 ± 0.79 | 0.0079 |
| P70441 | Na(+)/H(+) exchange regulatory cofactor NHE-RF1 | *Slc9a3r1* | 2.5 ± 0.86 | 0.0319 |
| O08600 | Endonuclease G, mitochondrial | *Endog* | 2.07 ± 0.47 | 0.0336 |
| Q6A0A9 | Constitutive coactivator of PPAR-gamma-like protein 1 | *Fam120A* | 2.06 ± 0.6 | 0.0204 |
| Q91XE4 | N-acyl-aromatic-L-amino acid amidohydrolase (carboxylate-forming) | *Acy3* | 1.6 ± 0.07 | 0.0067 |
| Q8K2C6 | NAD-dependent protein deacylase sirtuin-5, mitochondrial | *Sirt5* | 1.56 ± 0.29 | 0.0481 |
| Q3TMX5 | Arginine-rich, mutated in early stage tumors, isoform CRA_b | *Manf* | 1.3 ± 0.06 | 0.0066 |
| A0A0A0MQF6 | Glyceraldehyde-3-phosphate dehydrogenase | *Gapdh* | 1.4 ± 1.01 | 0.7024 |
| P60710 | Actin, cytoplasmic 1 | *Actb* | 1.05 ± 0.4 | 0.7289 |
| Q4VBG1 | DEAD (Asp-Glu-Ala-Asp) box polypeptide 47 | *Ddx47* | -1.5 ± 0.1 | 0.0094 |
| Q921I1 | Serotransferrin | *Tf* | -1.52 ± 0.17 | 0.0440 |
| B2RT89 | Predicted gene, EG434674 | *Slc22a28* | -1.66 ± 0.16 | 0.0287 |
| Q99N96 | 39S ribosomal protein L1, mitochondrial | *Mrpl1* | -1.87 ± 0.19 | 0.0295 |
| Q4VA32 | Thioesterase superfamily member 2 | *Acot13* | -1.97 ± 0.16 | 0.0055 |
| Q3KNM2 | E3 ubiquitin-protein ligase MARCH5 | *March5* | -2.14 ± 0.17 | 0.0061 |
| Q6ZWY3 | 40S ribosomal protein S27-like | *Rps27l* | -5.67 ± 0.08 | 0.0416 |

**Table 5. Relative-quantitation proteomics analysis of protein expression changes with 12-$D_3$NVP treatment, as compared to NVP, of primary mouse hepatocytes.** Freshly isolated primary mouse hepatocytes were treated for 8 hours with 400 μM NVP or 12-$D_3$NVP. Cell lysate was then prepared for and subjected to Top10 nanoLC-MS based proteomics, with data analysis performed in Proteome Discoverer 2.1, using Sequest HT for peptide spectral matching/protein identification and precursor ion area detection for relative quantitation. Up to 10 unique or razor peptides were used in protein precursor ion-based quantitation. Statistically significant relative-quantitation changes are shown for treatment with 12-$D_3$NVP as compared to NVP, as well as the results for housekeeping proteins actin and GAPDH. UniProt proteome *Mus musculus* 10090 was used for protein identification profiling, with UniProt accession numbers, protein entry (protein name), and gene name's provided. P-values were generated using un-paired t-test and effect size calculated using Cohen's d equation. Data are representative of four biological replicates. Protein identifications that were only detected one of the two treatments, across all replicates, are also included for discussion, though in highlighted incidences (*) they did not rise to the level of statistical significance.

| Protein Changes with NVP Treatment (in comparison to Vehicle) | | | | |
|---|---|---|---|---|
| **UniProt Accession** | **UniProt Entry** | **Gene Name** | **Fold Change** | **P-Value** |
| Q13098 | Isoform 3 of COP9 signalosome complex subunit 1 | *GPS1* | 2.06 ± 0.26 | 0.0289 |
| Q13190 | Syntaxin-5 | *STX5* | 2.02 ± 0.39 | 0.0183 |
| O95298 | NADH dehydrogenase [ubiquinone] 1 subunit C2 | *NDUFC2* | 1.91 ± 0.23 | 0.0135 |
| Q96I59 | Pprobable asparagine--tRNA ligase, mitochondrial | *NARS2* | 1.88 ± 0.06 | 0.0263 |
| Q9UQ53 | Isoform 3 of Alpha-1,3-mannosyl-glycoprotein 4-beta-N-acetylglucosaminyltransferase B | *MGAT4B* | 1.87 ± 0.45 | 0.0339 |
| Q14320 | Protein FAM50A | *FAM50A* | 1.82 ± 0.12 | 0.0387 |
| Q14117 | Dihydropyrimidinase | *DPYS* | 1.73 ± 0.15 | 0.0359 |
| P15907 | Beta-galactoside alpha-2,6-sialyltransferase 1 | *ST6GAL1* | 1.65 ± 0.33 | 0.0371 |
| O95197 | Isoform 3 of Reticulon-3 | *RTN3* | 1.62 ± 0.04 | 0.0111 |
| P63208 | S-phase kinase-associated protein 1 | *SKP1* | 1.59 ± 0.15 | 0.0298 |
| Q9Y3B2 | Exosome complex component csl4 | *EXOSC1* | 1.55 ± 0.17 | 0.0181 |
| Q9BVV7 | Mitochondrial import inner membrane translocase subunit TIM21 | *TIMM21* | 1.52 ± 0.18 | 0.0368 |
| P28072 | Proteasome subunit beta type-6 | *PSMB6* | 1.44 ± 0.09 | 0.0241 |
| Q9ULA0 | Aspartyl aminopeptidase | *DNPEP* | 1.42 ± 0.06 | 0.0075 |
| Q9HD45 | Transmembrane 9 superfamily member 3 | *TM9SF3* | 1.41 ± 0.1 | 0.0258 |
| Q9H6R3 | Acyl-CoA synthetase short-chain family member 3, mitochondrial | *ACSS3* | 1.31 ± 0.11 | 0.0214 |
| O15382 | Branched-chain-amino-acid aminotransferase, mitochondrial | *BCAT2* | 1.3 ± 0.09 | 0.0270 |
| Q9NX47 | E3 ubiquitin-protein ligase MARCH5 | *MARCH5* | 1.3 ± 0.13 | 0.0489 |
| Q5JTZ9 | Alanine--tRNA ligase, mitochondrial | *AARS2* | 1.21 ± 0.06 | 0.0202 |
| Q6P1M0 | Long-chain fatty acid transport protein 4 | *SLC27A4* | 1.17 ± 0.01 | 0.0019 |
| P04406 | Glyceraldehyde-3-phosphate dehydrogenase | *GAPDH* | 1.18 ± 0.13 | 0.2236 |
| P60709 | Actin, cytoplasmic 1 | *ACTB* | 1.03 ± 0.3 | 0.9894 |
| P56182 | Ribosomal RNA processing protein 1 homolog A | *RRP1* | -1.32 ± 0.07 | 0.0402 |
| P36543 | V-type proton ATPase subunit E 1 | *ATP6V1E1* | -2.16 ± 0.25 | 0.0460 |

**Table 6. Relative-quantitation proteomics analysis of protein expression changes with NVP treatment of cryopreserved human hepatocytes.**

Cryopreserved pooled-donor (10, mixed-sex) primary human hepatocytes were treated for 48 hours with vehicle (0.1% DMSO) or 10 μM NVP. Cell lysate was then prepared for and subjected to Top10 nanoLC-MS based proteomics, with data analysis performed in Proteome Discoverer 2.1, using Sequest HT for peptide spectral matching/protein identification and precursor ion area detection for relative quantitation. Up to 10 unique or razor peptides were used in protein precursor ion-based quantitation. Statistically significant relative quantitation changes are shown for treatment with NVP as compared to vehicle, as well as the results for housekeeping proteins actin and GAPDH. UniProt proteome *Homo sapiens* 9606 was used for protein identification profiling, with UniProt accession numbers, protein entry (protein name), and gene name's provided. P-values were generated using un-paired t-test and effect size calculated using Cohen's d equation. Data are representative of experiments with three different 10-donor pools of hepatocytes. Protein identifications that were only detected one of the two treatments, across all replicates, are also included for discussion, though in highlighted incidences (*) they did not rise to the level of statistical significance.

| Protein Changes with 12-$D_3$NVP Treatment (in comparison to Vehicle) | | | | |
|---|---|---|---|---|
| **UniProt Accession** | **UniProt Entry** | **Gene Name** | **Fold Change** | **P-Value** |
| Q9Y5U8 | Mitochondrial pyruvate carrier 1 | *MPC1* | 15.96 ± 11.14 | 0.0015 |
| P60059 | Protein transport protein Sec61 subunit gamma | *SEC61G* | 1.96 ± 0.21 | 0.0285 |
| Q96CU9 | FAD-dependent oxidoreductase domain-containing protein 1 | *FOXRED1* | 1.95 ± 0.27 | 0.0343 |
| Q15397 | Pumilio homolog 3 | *PUM3* | 1.94 ± 0.37 | 0.0320 |
| P33261 | Cytochrome P450 2C19 | *CYP2C19* | 1.79 ± 0.12 | 0.0339 |
| Q8WUK0 | Phosphatidylglycerophosphatase and protein-tyrosine phosphatase 1 | *PTPMT1* | 1.74 ± 0.01 | 0.0225 |
| P60709 | Actin, cytoplasmic 1 | *ACTB* | -1.13 ± 0.06 | 0.1272 |
| P04406 | Glyceraldehyde-3-phosphate dehydrogenase | *GAPDH* | -1.17 ± 0.11 | 0.1835 |
| P16152 | Carbonyl reductase [NADPH] 1 | *CBR1* | -1.25 ± 0.04 | 0.0082 |
| O94973 | AP-2 complex subunit alpha-2 | *AP2A2* | -1.3 ± 0.07 | 0.0373 |
| Q02252 | Methylmalonate-semialdehyde dehydrogenase [acylating], mitochondrial | *ALDH6A1* | -1.32 ± 0.06 | 0.0229 |
| P42765 | 3-ketoacyl-CoA thiolase, mitochondrial | *ACAA2* | -1.33 ± 0.02 | 0.0244 |
| Q9ULC5 | Isoform 2 of Long-chain-fatty-acid--CoA ligase 5 | *ACSL5* | -1.36 ± 0.09 | 0.0371 |
| P61604 | 10 kDa heat shock protein, mitochondrial | *HSPE1* | -1.38 ± 0.06 | 0.0291 |
| P26440 | Isovaleryl-CoA dehydrogenase, mitochondrial | *IVD* | -1.39 ± 0.09 | 0.0349 |
| Q13243 | Serine/arginine-rich splicing factor 5 | *SRSF5* | -1.45 ± 0.06 | 0.0035 |
| Q6YN16 | Hydroxysteroid dehydrogenase-like protein 2 | *HSDL2* | -1.46 ± 0.05 | 0.0052 |
| Q96I99 | Succinyl-CoA ligase [GDP-forming] subunit beta, mitochondrial | *SUCLG2* | -1.48 ± 0.1 | 0.0302 |
| Q9UJZ1 | Stomatin-like protein 2, mitochondrial | *STOML2* | -1.53 ± 0.1 | 0.0441 |
| Q9BYG3 | MKI67 FHA domain-interacting nucleolar phosphoprotein | *NIFK* | -1.54 ± 0.08 | 0.0188 |
| Q9BYT8 | Neurolysin, mitochondrial | *NLN* | -1.57 ± 0.13 | 0.0332 |
| P51398 | 28S ribosomal protein S29, mitochondrial | *DAP3* | -1.62 ± 0.03 | 0.0109 |
| O95297 | Myelin protein zero-like protein 1 | *MPZL1* | -1.64 ± 0.03 | 0.0039 |
| O00515 | Ladinin-1 | *LAD1* | -1.66 ± 0.09 | 0.0068 |
| O14561 | Acyl carrier protein, mitochondrial | *NDUFAB1* | -1.7 ± 0.15 | 0.0456 |
| Q07020 | 60S ribosomal protein L18 | *RPL18* | -1.77 ± 0.15 | 0.0336 |
| Q15392 | Delta(24)-sterol reductase | *DHCR24* | -1.85 ± 0.15 | 0.0397 |
| Q92734 | Protein TFG | *TFG* | -1.87 ± 0.04 | 0.0497 |
| P62995 | Transformer-2 protein homolog beta | *TRA2B* | -1.94 ± 0.08 | 0.0067 |
| P62241 | 40S ribosomal protein S8 | *RPS8* | -1.98 ± 0.16 | 0.0067 |
| Q9UL25 | Ras-related protein Rab-21 | *RAB21* | -1.99 ± 0.03 | 0.0482 |
| Q16718 | NADH dehydrogenase [ubiquinone] 1 alpha subcomplex subunit 5 | *NDUFA5* | -2.14 ± 0.1 | 0.0247 |
| Q92552 | Isoform 2 of 28S ribosomal protein S27, mitochondrial | *MRPS27* | -2.4 ± 0.17 | 0.0490 |
| P61457 | Pterin-4-alpha-carbinolamine dehydratase | *PCBD1* | -2.63 ± 0.17 | 0.0042 |
| O15127 | Secretory carrier-associated membrane protein 2 | *SCAMP2* | -2.68 ± 0.05 | 0.0380 |
| Q7L8L6 | FAST kinase domain-containing protein 5, mitochondrial | *FASTKD5* | -4.73 ± 0.06 | 0.0456 |
| Q96K37 | Solute carrier family 35 member E1 | *SLC35E1* | Not Found in 12-D3NVP | 0.0151 |

**Table 7. Relative-quantitation proteomics analysis of protein expression changes with 12-$D_3$NVP treatment of cryopreserved human hepatocytes.** Cryopreserved pooled-donor (10, mixed-sex) primary human hepatocytes were treated for 48 hours with vehicle (0.1% DMSO) or 10 μM 12-$D_3$NVP. Cell lysate was then prepared for and subjected to Top10 nanoLC-MS based proteomics, with data analysis performed in Proteome Discoverer 2.1, using Sequest HT for peptide spectral matching/protein identification and precursor ion area detection for relative quantitation. Up to 10 unique or razor peptides were used in protein precursor ion-based quantitation. Statistically significant relative quantitation changes are shown for treatment with 12-$D_3$NVP as compared to vehicle, as well as the results for housekeeping proteins actin and GAPDH. UniProt proteome *Homo sapiens* 9606 was used for protein identification profiling, with UniProt accession numbers, protein entry (protein name), and gene name's provided. P-values were generated using un-paired t-test and effect size calculated using Cohen's d equation. Data are representative of experiments with three different 10-donor pools of hepatocytes. Protein identifications that were only detected one of the two treatments, across all replicates, are also included for discussion, though in highlighted incidences (*) they did not rise to the level of statistical significance.

| Changes with 12-$D_3$NVP Treatment (in comparison to NVP) | | | | |
|---|---|---|---|---|
| **UniProt Accession** | **UniProt Entry** | **Gene Name** | **Fold Change** | **P-Value** |
| Q16540 | 39S ribosomal protein L23, mitochondrial | *MRPL23* | 8.32 ± 2.21 | 0.0159 |
| Q8NI60 | Atypical kinase ADCK3, mitochondrial | *COQ8A* | 1.95 ± 0.2 | 0.0168 |
| Q9HA77 | Probable cysteine--tRNA ligase, mitochondrial | *CARS2* | 1.85 ± 0.2 | 0.0041 |
| Q14498 | RNA-binding protein 39 | *RBM39* | 1.7 ± 0.2 | 0.0339 |
| Q9Y2H5 | Pleckstrin homology domain-containing family A member 6 | *PLEKHA6* | 1.59 ± 0.05 | 0.0188 |
| Q8IYS2 | Isoform 2 of Uncharacterized protein KIAA2013 | *KIAA2013* | 1.36 ± 0.01 | 0.0051 |
| P60709 | Actin, cytoplasmic 1 | *ACTB* | -1.09 ± 0.19 | 0.4937 |
| P04406 | Glyceraldehyde-3-phosphate dehydrogenase | *GAPDH* | -1.35 ± 0.16 | 0.1836 |
| P34897 | Serine hydroxymethyltransferase, mitochondrial | *SHMT2* | -1.28 ± 0.05 | 0.0225 |
| P08574 | Cytochrome c1, heme protein, mitochondrial | *CYC1* | -1.4 ± 0.09 | 0.0478 |
| Q15046 | Isoform Mitochondrial of Lysine--tRNA ligase | *KARS* | -1.42 ± 0.06 | 0.0490 |
| Q96I24 | Far upstream element-binding protein 3 | *FUBP3* | -1.47 ± 0.03 | 0.0198 |
| P00167 | Cytochrome b5 | *CYB5A* | -1.5 ± 0.11 | 0.0361 |
| Q13438 | Protein os-9 | *OS9* | -1.53 ± 0.09 | 0.0187 |
| Q9Y315 | deoxyribose-phosphate aldolase | *DERA* | -1.63 ± 0.06 | 0.0229 |
| Q4G176 | Acyl-CoA synthetase family member 3, mitochondrial | *ACSF3* | -1.63 ± 0.09 | 0.0278 |
| P82979 | SAP domain-containing ribonucleoprotein | *SARNP* | -1.65 ± 0.07 | 0.0043 |
| O75431 | Metaxin-2 | *MTX2* | -1.67 ± 0.09 | 0.0465 |
| Q9H6R4 | Nucleolar protein 6 | *NOL6* | -1.85 ± 0.12 | 0.0121 |
| P13716 | Isoform 2 of Delta-aminolevulinic acid dehydratase | *ALAD* | -1.86 ± 0.08 | 0.0467 |
| O15321 | Transmembrane 9 superfamily member 1 | *TM9SF1* | -1.86 ± 0.08 | 0.0366 |
| P10635 | Cytochrome P450 2D6 | *CYP2D6* | -1.92 ± 0.07 | 0.0317 |
| Q9BVK6 | Transmembrane emp24 domain-containing protein 9 | *TMED9* | -1.93 ± 0.14 | 0.0218 |
| Q8N163 | Cell cycle and apoptosis regulator protein 2 | *CCAR2* | -2.05 ± 0.09 | 0.0164 |
| Q9UJ68 | Mitochondrial peptide methionine sulfoxide reductase | *MSRA* | -2.05 ± 0.14 | 0.0358 |
| P11712 | Cytochrome P450 2C9 | *CYP2C9* | -2.06 ± 0.16 | 0.0498 |
| Q9NYL9 | Tropomodulin-3 | *TMOD3* | -2.1 ± 0.01 | 0.0356 |
| Q93096 | Protein tyrosine phosphatase type IVA 1 | *PTP4A1* | -2.42 ± 0.17 | 0.0466 |
| Q9Y2D5 | Isoform 2 of A-kinase anchor protein 2 | *AKAP2* | -2.67 ± 0.06 | 0.0249 |
| Q9Y3B2 | Exosome complex component csl4 | *EXOSC1* | -2.73 ± 0.09 | 0.0086 |

**Table 8. Relative-quantitation proteomics analysis of protein expression changes with 12-$D_3$NVP treatment, as compared to NVP, of cryopreserved human hepatocytes.** Cryopreserved pooled-donor (10, mixed-sex) primary human hepatocytes were treated for 48 hours with 10 μM NVP or 12-$D_3$NVP. Cell lysate was then prepared for and subjected to Top10 nanoLC-MS based proteomics, with data analysis performed in Proteome Discoverer 2.1, using Sequest HT for peptide spectral matching/protein identification and precursor ion area detection for relative quantitation. Up to 10 unique or razor peptides were used in protein precursor ion-based quantitation. Statistically significant relative quantitation changes are shown for treatment with 12-$D_3$NVP as compared to NVP, as well as the results for housekeeping proteins actin and GAPDH. UniProt proteome *Homo sapiens* 9606 was used for protein identification profiling, with UniProt accession numbers, protein entry (protein name), and gene name's provided. P-values were generated using un-paired t-test and effect size calculated using Cohen's d equation. Data are representative of experiments with three different 10-donor pools of hepatocytes. Protein identifications that were only detected one of the two treatments, across all replicates, are also included for discussion, though in highlighted incidences (*) they did not rise to the level of statistical significance.

## Discussion

With this work, through the use of high resolution uHPLC-MS/MS analyses, we have assayed differences in the P450 metabolism of NVP and 12-$D_3$NVP in primary hepatocytes. At clinically relevant concentrations (10 μM) of these compounds we observed a 10.6-fold reduction in 12-OHNVP production in primary human hepatocytes and a lesser 4.6-fold reduction in C57Bl/6J primary mouse heptocytes. These results demonstrate that trideuteration at the twelfth position NVP is an effective method of reducing hepatic production of the potentially toxic 12-OHNVP metabolite, in both a human hepatocyte model and in a model organism previously employed in the study of NVP toxicities (Sharma *et al.*, 2012; Sharma *et al.*, 2013).

In an effort to concentrate on potential impacts of this deuterium substitution for specific P450 isoforms, we assayed the contribution of various human P450s in the production 12-OHNVP. We found that all but one P450 tested produced detectable 12-OHNVP and that no P450 isoform-specific inhibitor reduced the production of this metabolite in liver microsomes incubated with 10 μM NVP. We were able to demonstrate that CYP3A4 is the isform responsible for 2-OHNVP produciton and CYP2B6 for 3-OHNVP production. In initial work characterizing the P450 metabolism of NVP, similar results were observed using a smaller sampling (four) of human P450s. *Erickson et al. (1999)* observed 12-OHVNP production by multiple P450s, and no impact of antibody-based P450 inhibition on 12-OHNVP production during incubations with 25 μM NVP. However, there was an impact on the production of 12-OHNVP from anti-

CYP3A4 with 400 μM NVP and from ketoconozole (CYP3A inhibitor) with 100 μM NVP. From their work, Erickson *et al.* concluded that several P450s may contribute to 12-OHNVP formation at lower, more clinically relevant concentrations of NVP. They also attributed 2-OHNVP to the CYP3A subfamily and 3-OHNVP to CYP2B6 subfamily (Erickson *et al.*, 1999). Though we could have continued with a more extensive characterization by varying substrate concentrations or trying different modes of inhibition, we felt these results supported quantitation of the kinetic isotope effect of twelfth position deuterium substitution in a multi-P450 system such as human liver microsomes.

To quantify the kinetic isotope effect of this substitution, we performed non-competitive intermolecular experiments with NVP and 12-$D_3$NVP. Terminology estabilished by Norththrop (1982) is used to distinguish the different parameters observed in this work (Northrop, 1982). In human liver micosome incubations, we have demonstrated a marked (9.1-fold) reduction of the catalytic efficiency of P450 production of 12-OHNVP as a result of twelfth-position deuterium substitution, abbreviated commonly as $^{D}(V/K)$. In addition we have quantified a primary, normal observed kinetic isotope effect ($^{D}K$), of this substition on human P450 metabolism to be 10.1-fold. Both of which correspond with the reduction in 12-OHNVP production observed with human hepatocyte incubations (10.6-fold at 24 hours with 10 μM substrate). We were unable to calculate intrinsic kinetic isotope effect ($^{D}k$), which is a measure of the impact on the P450 hydrogen bond-breaking step specifically (Guengerich, 2017). However, it is our understanding that our observed $^{D}(V/K)$ is fairly high considering the same

measurements for other P450 reactions: 2-3 (Yun *et al.*, 2000), 3.1-3.18 (Guengerich *et al.*, 2002), 4.5 (Bell-Parikh and Guengerich, 1999), 5-11 (Pallan *et al.*, 2015), and >10 (Yun *et al.*, 2000). Of note, one previous study observed $^{D}V/K$ to be 10.9 in microsomal incubations, but only 3.7 in CYP2E1-specific incubations (Chowdhury *et al.*, 2012). In the future it would be interesting to survey the diversity of kinetic isotope effects for 12-OHNVP from 12-$D_3$NVP across different isoforms, given that NVP appears to be a substrate for multiple different P450s.

Interestingly, we observed no change in 2-OHNVP or 3-OHNVP, or in one glucuronidated metabolite, which we propose to be either 2- or 3-O-glucNVP, during 24 and 48 hour hepatocyte incubations with 10 μM 12-$D_3$NVP as compared to NVP. This was consistent across human and C57Bl/6J primary hepatocytes. In incubations with human liver microsomes we also did not observed any change in the production of 2- or 3-OHNVP, at substrate concentrations ranging from 5-400 μM. We found this intriguing, as metabolic switching, in which other drug metabolite levels increase in response to decreased metabolism at one position, has been kown to occur with deuterium substitution (Kim *et al.*, 2014; Stringer *et al.*, 2014; Sun *et al.*, 2018; Ucal *et al.*, 2018).This may be due to differences in P450 contributions to metabolism at these different positions of the NVP scaffold. Since we did not see a significant decrease in 12-OHNVP with inhibitors that reduced production of 2-OHNVP and 3-OHNVP, this suggests that the enzymes responsible for 2- and 3-OHNVP production (CYP3A4 and CYP2B6, respectively) may not play a large role in the

conversion of NVP to 12-OHNVP. With that, modifying the dynamics of this specific conversion may not impact formation of the rates of CYP3A4/CYP2B6 production of 2- or 3-OHNVP. However, it is worth noting that at high concentrations of NVP or 12-$D_3$NVP in primary mouse hepatocytes we did observed a trend towards an increase in 2- and 3-OHNVP, as well as increased O-GlucNVP formation. This difference from results with high concentration incubations in human liver microsomes may be a result of species differences (at higher concentrations in mice there is a mouse P450 that forms all three metabolites, and therefore is subject to switching), differences in incubation times (short term incubations with micrsomes versus long-term hepatocyte culture incubations), system complexity (multiple classes of drug metabolizing enzymes working simultaneously in hepatocytes versus only P450 activity in our liver microsome incubations), or more likely some combination of all of these factors. Previously, in rats treated with NVP and 12-$D_3$NVP, a reduction in circulating concentrations of 12-$D_3$NVP (as compared to NVP) was observed (Chen *et al.*, 2008). This suggests the possibility of metabolic switching, resulting in faster drug clearance, in this model of toxicity.

Here we have also assayed for differences in hepatocyte death with NVP and 12-$D_3$NVP. Unfortunately, as with other *in vitro* work involving NVP, we had to use high supra-therapeutic concentrations to observe any cell death with NVP (Fang and Beland, 2013; Marinho *et al.*, 2016; Pinheiro *et al.*, 2017). We did see a modest reduction in C57Bl/6J hepatocyte death with 12-$D_3$NVP as compared to NVP, though the clinical implications in this degree of change are difficult to

ascertain (from 52.6% of cells dead/dying with NVP to 36.8% with 12-$D_3$NVP). It may be that 12-OHNVP production is playing a role given that we did observe a reduction, but given the high concentrations needed to stimulate cell death and the small degree of decrease, future experimentation is needed. Selection of model organism may also play a role in the observed outcomes. Previous work regarding the liver toxicity of these compounds demonstrated that while C57Bl/6 mice did experience mild hepatotoxicity with NVP, it was exacerbated in rat models. However, it was demonstrated that treatment of C57Bl/6 liver microsomes resulted in NVP-protein adducts, and that this was lessened with 12-$D_3$NVP (Sharma *et al.*, 2012) The use of human hepatocyte cell culture models, like spheroid culture, that allow for long term, low-concentration incubations (Bell *et al.*, 2016), as well as co-culture with immune cells (Granitzny *et al.*, 2017) may be useful in profiling NVP-induced hepatotoxicity, especially given the proposed involvement of immune hypersensitivity.

In order to understand differences in hepatocyte response to NVP and 12-$D_3$NVP we employed relative quantitation proteomics analysis on primary mouse hepatocytes and human hepatocytes treated with these compounds. For both treatment sets, more (greater than 3-fold in magnitude) differentially expressed proteins were observed for NVP vs.12-$D_3$NVP than for either treatement compared to vehicle alone. Interestingly, many of the observed changes with either NVP or 12-$D_3$NVP were unique to these individual compounds, and not shared across NVP and12-$D_3$NVP treatment. One difference of note was a significant increase in IGFBP-1 with treatment 12-$D_3$NVP (4.18-fold higher than

with vehicle, and 4.70-fold higher than with NVP). Increases in this protein have been found in the serum of patients with advanced liver fibrosis and it has been demonstrated to be elevated in general during hepatic stress (Hagström *et al.*, 2017). In general, differences in hepatocyte response, beyond metabolic impacts between NVP and 12-$D_3$NVP treatment are useful to consider in using this trideuterated compound as way to probe the impacts of P450 metabolism on NVP toxicities.

Across all protein changes, many indentified with either NVP or 12-$D_3$NVP were mitrochondrial components. This suggestes that perhaps mitochondrial dysregulation may play a role in the toxicities of NVP or 12-$D_3$NVP. Previously, mitochondrial damage during rat treatment with NVP has been observed (Sastry *et al.*, 2018), and in treatments of HepG2 cells (Paemanee *et al.*, 2017). The implications of the various changes observed warrents futher exploration. One example, FASTKD5 (which was significantly decreased in human primary hepatocytes treated with 12-$D_3$NVP), has been previously demonstrated to be involved in non-canonical mitochondrial mRNA processing. FASTKD5 silencing resulted in assembly defects of complex IV of the electron transport chain (Antonicka and Shoubridge, 2015).

In this work we have demonstrated that deuterium substitution is effective at controlling hepatic P450 production of 12-OHNVP in both human and C57Bl/6J mouse hepatocytes. We have measured a high observed kinetic isotope effect of this substitution on production of 12-OHNVP in human liver microsomes. Metabolic switching was only observed during high concentration

incubations with mouse primary hepatocytes. That being said, only a modest reduction from NVP-induced primary mouse hepatocyte cell death was observed with 12-$D_3$NVP, and in proteomics analysis unique proteomic shifts were detected with 12-$D_3$NVP. Taken together, this trideuterated compound is very effective at reducing P450 metabolism to NVP, though unintended effects, such as metabolic switching and differential impacts on hepatocyte protein expression should be taken into consideration when using this deuterated compound and others to study drug-induced hepatotoxicity.

## References

Centers for Disease Control and Prevetion (CDC) (2001) Serious adverse events attributed to nevirapine regimens for postexposure prophylaxis after HIV exposures--worldwide, 1997-2000. *MMWR Morb Mortal Wkly Rep* **49**:1153-1156.

Antonicka H and Shoubridge EA (2015) Mitochondrial RNA Granules Are Centers for Posttranscriptional RNA Processing and Ribosome Biogenesis. *Cell Rep* **10**:920-932.

Antunes AM, Godinho AL, Martins IL, Justino GC, Beland FA and Marques MM (2010) Amino acid adduct formation by the nevirapine metabolite, 12-hydroxynevirapine--a possible factor in nevirapine toxicity. *Chem Res Toxicol* **23**:888-899.

Bell CC, Hendriks DF, Moro SM, Ellis E, Walsh J, Renblom A, Fredriksson Puigvert L, Dankers AC, Jacobs F, Snoeys J, Sison-Young RL, Jenkins RE, Nordling Å, Mkrtchian S, Park BK, Kitteringham NR, Goldring CE, Lauschke VM and Ingelman-Sundberg M (2016) Characterization of primary human hepatocyte spheroids as a model system for drug-induced liver injury, liver function and disease. *Sci Rep* **6**:25187.

Bell-Parikh LC and Guengerich FP (1999) Kinetics of cytochrome P450 2E1-catalyzed oxidation of ethanol to acetic acid via acetaldehyde. *J Biol Chem* **274**:23833-23840.

Buyse S, Vibert E, Sebagh M, Antonini T, Ichai P, Castaing D, Samuel D and Duclos-Vallée JC (2006) Liver transplantation for fulminant hepatitis related to nevirapine therapy. *Liver Transpl* **12**:1880-1882.

Caixas U, Antunes AM, Marinho AT, Godinho AL, Grilo NM, Marques MM, Oliveira MC, Branco T, Monteiro EC and Pereira SA (2012) Evidence for nevirapine bioactivation in man: searching for the first step in the mechanism of nevirapine toxicity. *Toxicology* **301**:33-39.

Carr A, Vella S, de Jong MD, Sorice F, Imrie A, Boucher CA and Cooper DA (1996) A controlled trial of nevirapine plus zidovudine versus zidovudine alone in p24 antigenaemic HIV-infected patients. The Dutch-Italian-Australian Nevirapine Study Group. *AIDS* **10**:635-641.

Chen J, Mannargudi BM, Xu L and Uetrecht J (2008) Demonstration of the metabolic pathway responsible for nevirapine-induced skin rash. *Chem Res Toxicol* **21**:1862-1870.

Chowdhury G, Calcutt MW, Nagy LD and Guengerich FP (2012) Oxidation of methyl and ethyl nitrosamines by cytochrome P450 2E1 and 2B1. *Biochemistry* **51**:9995-10007.

Dekker SJ, Zhang Y, Vos JC, Vermeulen NP and Commandeur JN (2016) Different Reactive Metabolites of Nevirapine Require Distinct Glutathione S-Transferase Isoforms for Bioinactivation. *Chem Res Toxicol* **29**:2136-2144.

Erickson DA, Mather G, Trager WF, Levy RH and Keirns JJ (1999) Characterization of the in vitro biotransformation of the HIV-1 reverse

transcriptase inhibitor nevirapine by human hepatic cytochromes P-450. *Drug Metab Dispos* **27**:1488-1495.

Fang JL and Beland FA (2013) Differential responses of human hepatocytes to the non-nucleoside HIV-1 reverse transcriptase inhibitor nevirapine. *J Toxicol Sci* **38**:741-752.

Granitzny A, Knebel J, Müller M, Braun A, Steinberg P, Dasenbrock C and Hansen T (2017) Evaluation of a human in vitro hepatocyte-NPC co-culture model for the prediction of idiosyncratic drug-induced liver injury: A pilot study. *Toxicol Rep* **4**:89-103.

Guengerich FP (2017) Kinetic Deuterium Isotope Effects in Cytochrome P450 Reactions. *Methods Enzymol* **596**:217-238.

Guengerich FP, Miller GP, Hanna IH, Sato H and Martin MV (2002) Oxidation of methoxyphenethylamines by cytochrome P450 2D6. Analysis of rate-limiting steps. *J Biol Chem* **277**:33711-33719.

Hagström H, Stål P, Hultcrantz R, Brismar K and Ansurudeen I (2017) IGFBP-1 and IGF-I as markers for advanced fibrosis in NAFLD - a pilot study. *Scand J Gastroenterol* **52**:1427-1434.

Heck CJS, Hamlin AN and Bumpus NN (2019) Efavirenz and Efavirenz-like Compounds Activate Human, Murine, and Macaque Hepatic IRE1. *Mol Pharmacol* **95**:183-195.

Huang S, Taylor NL, Ströher E, Fenske R and Millar AH (2013) Succinate dehydrogenase assembly factor 2 is needed for assembly and activity of

mitochondrial complex II and for normal root elongation in Arabidopsis. *Plant J* **73**:429-441.

Jao J, Sturdevant M, del Rio Martin J, Schiano T, Fiel MI and Huprikar S (2010) Nevirapine-induced stevens johnson-syndrome and fulminant hepatic failure requiring liver transplantation. *Am J Transplant* **10**:1713-1716.

Khojasteh SC, Prabhu S, Kenny JR, Halladay JS and Lu AY (2011) Chemical inhibitors of cytochrome P450 isoforms in human liver microsomes: a re-evaluation of P450 isoform selectivity. *Eur J Drug Metab Pharmacokinet* **36**:1-16.

Kim D, Cha GS, Nagy LD, Yun CH and Guengerich FP (2014) Kinetic analysis of lauric acid hydroxylation by human cytochrome P450 4A11. *Biochemistry* **53**:6161-6172.

Knights KM, Stresser DM, Miners JO and Crespi CL (2016) In Vitro Drug Metabolism Using Liver Microsomes. *Curr Protoc Pharmacol* **74**:7.8.1-7.8.24.

Lee P, Peng H, Gelbart T and Beutler E (2004) The IL-6- and lipopolysaccharide-induced transcription of hepcidin in HFE-, transferrin receptor 2-, and beta 2-microglobulin-deficient hepatocytes. *Proc Natl Acad Sci U S A* **101**:9263-9265.

Maniar JK, Shah SR, Verma R, Kamath R, Gupte P and Maniar A (2006) Nevirapine-induced fulminant hepatitis. *J Assoc Physicians India* **54**:957-958.

Marinho AT, Dias CG, Pinheiro PF, Lemos AR, Antunes AM, Marques MM, Monteiro EC, Miranda JP and Pereira SA (2016) Nevirapine modulation of paraoxonase-1 in the liver: An in vitro three-model approach. *Eur J Pharm Sci* **82**:147-153.

Marinho AT, Rodrigues PM, Caixas U, Antunes AM, Branco T, Harjivan SG, Marques MM, Monteiro EC and Pereira SA (2014) Differences in nevirapine biotransformation as a factor for its sex-dependent dimorphic profile of adverse drug reactions. *J Antimicrob Chemother* **69**:476-482.

Northrop DB (1982) Deuterium and tritium kinetic isotope effects on initial rates. *Methods Enzymol* **87**:607-625.

Paemanee A, Sornjai W, Kittisenachai S, Sirinonthanawech N, Roytrakul S, Wongtrakul J and Smith DR (2017) Nevirapine induced mitochondrial dysfunction in HepG2 cells. *Sci Rep* **7**:9194.

Pallan PS, Wang C, Lei L, Yoshimoto FK, Auchus RJ, Waterman MR, Guengerich FP and Egli M (2015) Human Cytochrome P450 21A2, the Major Steroid 21-Hydroxylase: STRUCTURE OF THE ENZYME·PROGESTERONE SUBSTRATE COMPLEX AND RATE-LIMITING C-H BOND CLEAVAGE. *J Biol Chem* **290**:13128-13143.

Pascovici D, Handler DC, Wu JX and Haynes PA (2016) Multiple testing corrections in quantitative proteomics: A useful but blunt tool. *Proteomics* **16**:2448-2453.

Pinheiro PF, Pereira SA, Harjivan SG, Martins IL, Marinho AT, Cipriano M, Jacob CC, Oliveira NG, Castro MF, Marques MM, Antunes AMM and Miranda JP

(2017) Hepatocyte spheroids as a competent in vitro system for drug biotransformation studies: nevirapine as a bioactivation case study. *Arch Toxicol* **91**:1199-1211.

Pollard RB, Robinson P and Dransfield K (1998) Safety profile of nevirapine, a nonnucleoside reverse transcriptase inhibitor for the treatment of human immunodeficiency virus infection. *Clin Ther* **20**:1071-1092.

Rendic S and Guengerich FP (2015) Survey of Human Oxidoreductases and Cytochrome P450 Enzymes Involved in the Metabolism of Xenobiotic and Natural Chemicals. *Chem Res Toxicol* **28**:38-42.

Riska P, Lamson M, MacGregor T, Sabo J, Hattox S, Pav J and Keirns J (1999) Disposition and biotransformation of the antiretroviral drug nevirapine in humans. *Drug Metab Dispos* **27**:895-901.

Sanne I, Mommeja-Marin H, Hinkle J, Bartlett JA, Lederman MM, Maartens G, Wakeford C, Shaw A, Quinn J, Gish RG and Rousseau F (2005) Severe hepatotoxicity associated with nevirapine use in HIV-infected subjects. *J Infect Dis* **191**:825-829.

Sastry J, Mohammed H, Campos MM, Uetrecht J and Abu-Asab M (2018) Nevirapine-induced liver lipid-SER inclusions and other ultrastructural aberrations. *Ultrastruct Pathol* **42**:108-115.

Sharma AM, Klarskov K and Uetrecht J (2013) Nevirapine bioactivation and covalent binding in the skin. *Chem Res Toxicol* **26**:410-421.

Sharma AM, Li Y, Novalen M, Hayes MA and Uetrecht J (2012) Bioactivation of nevirapine to a reactive quinone methide: implications for liver injury. *Chem Res Toxicol* **25**:1708-1719.

Srivastava A, Lian LY, Maggs JL, Chaponda M, Pirmohamed M, Williams DP and Park BK (2010) Quantifying the metabolic activation of nevirapine in patients by integrated applications of NMR and mass spectrometries. *Drug Metab Dispos* **38**:122-132.

Stringer RA, Williams G, Picard F, Sohal B, Kretz O, McKenna J and Krauser JA (2014) Application of a deuterium replacement strategy to modulate the pharmacokinetics of 7-(3,5-dimethyl-1H-1,2,4-triazol-1-yl)-3-(4-methoxy-2-methylphenyl)-2,6-dimethylpyrazolo[5,1-b]oxazole, a novel CRF1 antagonist. *Drug Metab Dispos* **42**:954-962.

Sun H, Piotrowski DW, Orr STM, Warmus JS, Wolford AC, Coffey SB, Futatsugi K, Zhang Y and Vaz ADN (2018) Deuterium isotope effects in drug pharmacokinetics II: Substrate-dependence of the reaction mechanism influences outcome for cytochrome P450 cleared drugs. *PLoS One* **13**:e0206279.

Suzuki H, Kneller MB, Haining RL, Trager WF and Rettie AE (2002) (+)-N-3-Benzyl-nirvanol and (-)-N-3-benzyl-phenobarbital: new potent and selective in vitro inhibitors of CYP2C19. *Drug Metab Dispos* **30**:235-239.

Ucal S, Häkkinen MR, Alanne AL, Alhonen L, Vepsäläinen J, Keinänen TA and Hyvönen MT (2018) Controlling of. *Biochem J* **475**:663-676.

Usach I, Melis V and Peris JE (2013) Non-nucleoside reverse transcriptase inhibitors: a review on pharmacokinetics, pharmacodynamics, safety and tolerability. *J Int AIDS Soc* **16**:1-14.

Wen B, Chen Y and Fitch WL (2009) Metabolic activation of nevirapine in human liver microsomes: dehydrogenation and inactivation of cytochrome P450 3A4. *Drug Metab Dispos* **37**:1557-1562.

WHO (2017) WHO Model List of Essential Medicines- 20th Edition, in, World Health Organization, http://www.who.int/medicines/publications/essentialmedicines/en/.

Wit FW, Kesselring AM, Gras L, Richter C, van der Ende ME, Brinkman K, Lange JM, de Wolf F and Reiss P (2008) Discontinuation of nevirapine because of hypersensitivity reactions in patients with prior treatment experience, compared with treatment-naive patients: the ATHENA cohort study. *Clin Infect Dis* **46**:933-940.

Yun CH, Miller GP and Guengerich FP (2000) Rate-determining steps in phenacetin oxidations by human cytochrome P450 1A2 and selected mutants. *Biochemistry* **39**:11319-11329.

Zhang C, Wang W, Zhou M, Han Y, Xie J, Qiu Z, Guo F, Li Y, Wang H, Ghanem KG and Li T (2013) The interaction of CD4 T-cell count and nevirapine hepatotoxicity in China: a change in national treatment guidelines may be warranted. *J Acquir Immune Defic Syndr* **62**:540-545.

## Chapter 4: Final Discussion

Since their discovery, 57 different human cytochrome P450s have been identified, and it has been observed that cytochrome P450 monooxygenase enzymes play a role in the metabolism of ~75% of approved drugs. Following the insertion of oxygen by a cytochrome P450, a new molecular entity is created that could have potential cytotoxic effects. It has previously been demonstrated that P450 metabolism can generate toxic metabolites, with one well characterized example being the metabolism of the widely used analgesic acetaminophen by CYP2E1. The first generation non-nucleoside reverse transcriptase inhibitors efavirenz (EFV) and nevirapine (NVP) are used in the treatment of HIV despite causing hepatotoxicity in patients. These two drugs are both extensively metabolized by cytochrome P450s, such that their main monooxygenated metabolites reach micromolar concentrations in patient circulation. These two drugs present an interesting opportunity to probe the contributions of cytochrome P450 metabolite formation in the development of drug-induced hepatotoxicity.

Exposure to the cytochrome P450 metabolite 8-hydroxy-EFV (8-OHEFV) has been previously demonstrated to play a role in both EFV-induced hepatotoxicity and neurotoxicity. Both EFV and 8-OHEFV have been shown to activate hepatocyte death in a JNK-dependent manner. We probed whether these compounds activate IRE1α-XBP1 signaling in primary human and mouse hepatocytes, as this pathway has been demonstrated under certain stimuli to contribute to hepatocyte death progression. We demonstrated that EFV and 8-OHEFV activated IRE1α-XBP1. In addition this activation appears to play a role

in the toxicity of EFV, as inhibition of IRE1α-XBP1 with the small molecule inhibitor STF083010 reduced EFV-induced primary mouse hepatocyte death levels. We extended our investigation of IRE1α-XBP1 activation to include a panel of sixteen analogs with discreet changes in the EFV scaffold. Interestingly, analogs 3 and 14 were also strong activators, though cell death with analog 3 was not abrogated by STF083010 treatment, and cell death with analog 14 was not observed. These results demonstrate that IRE1α-XBP1 plays a role in hepatocyte cell death with EFV. And though 8-OHEFV did activate IRE1α-XBP1, it did so to a much lesser magnitude than EFV, suggesting potential divergence in signaling pathway activation between these two compounds. We have also demonstrated the impact of discreet, single atom changes to the EFV scaffold to impact compound toxicity and IRE1α-XBP1 activation.

Cytochrome P450 formation of 12-hydroxy-NVP (12-OHNVP) has been implicated in the hepatotoxicity and skin toxicity of NVP. Previous work with a trideuterated version of NVP (12-$D_3$NVP), which was intended to reduce P450 formation of 12-OHNVP through the kinetic isotope effect, has demonstrated a reduction in skin toxicity and in liver protein-NVP adduct formation with equimolar amounts of 12-$D_3$NVP as compared to NVP. With that, we became interested in profiling the impact of this trideuteration on hepatic P450 metabolism of NVP. At clinically relevant concentrations, we demonstrated a large 10.6-fold reduction in the production of 12-OHNVP in primary human and mouse hepatocyte cultures treated with 12-$D_3$NVP as compared to NVP, with no impact on the formation of other P450 metabolites (2- and 3-OHNVP) or in a downstream metabolite of

monooxygenated NVP, O-glucuronidated-NVP. We performed characterization of different human P450 isoforms in the metabolism of NVP and concluded that multiple P450s are contributing to the formation of 12-OHNVP, while 2-OHNVP is produced mainly by CYP3A4 and 3-OHNVP by CYP2B6. We quantified the observed kinetic isotope effect, $^{D}V$, of this substitution on 12-OHNVP production in human liver microsomes to be 10.1. Despite this large change, only a moderate reduction in hepatocyte cell death was observed with 12-$D_3$NVP as compared to NVP. In addition, we observed evidence of metabolic switching at high concentrations of NVP/12-$D_3$NVP needed to induced hepatocyte death, as well as significant changes in protein expression profiles during treatment with these two compounds. We have demonstrated that deuterium substitution on NVP is a very effective measure of modulating P450 metabolism, but given the high concentrations needed to study hepatocyte death, metabolic switching may be observed, and that during treatment with both high and low concentrations of drug, cells display differential protein expression with deuterated and undeuterated NVP.

Taken together this work demonstrates that toxic drugs and drug P450-dependent metabolites may activate differential cell signaling mechanisms, as was observed with EFV and 8-OHEFV. In addition, though deuterium is an effective strategy for modulating P450 metabolite production in order to study drug-metabolite induced hepatotoxicity, there may be unintended consequences to this deuterium substitution, as was observed with NVP and 12-$D_3$NVP. Through the use of first generation non-nucleoside reverse transcriptase

inhibitors as a tool to study drug and drug metabolite toxicities, this work has furthered our understanding in the contributions of P450 metabolites in the toxicities of both EFV and NVP. We have also demonstrated both differential responses to drug and P450 metabolite as well as effective strategies to study the question of P450 contribution to drug toxicity.

# Curriculum Vitae: Carley J.S. Heck

1518 Park Avenue, Apartment 203S (267) 515-3761

Baltimore, MD 21217 check4@jhmi.edu

carley.js.heck@gmail.com

## Professional Summary

- Pharmacology Ph.D. with a strong foundation in drug metabolism
- National Science Foundation Graduate Research Fellow
- Experienced in mass spectrometry of small molecules and peptides
- Diverse technical knowledge and experience in working with hepatic models for assessing drug metabolism and toxicity
- Strong history of presentation of work through presentations and publications
- First-hand experience in industry science through Amgen internship

## Education

**Johns Hopkins School of Medicine**, Baltimore, MD **August 2014 - Present**

- Ph.D. Candidate in the Department of Pharmacology and Molecular Sciences
- Principle Investigator: Dr. Namandjé Bumpus
- Expected Graduation: June 28th, 2019
- GPA: 3.95 (calculated)

**Shippensburg University of Pennsylvania**, Shippensburg, PA **August 2010 - May 2014**

- Bachelor of Science in Biology, Minor in Biochemistry
- GPA: 3.9, Graduated Summa Cum Laude

## Relevant Positions Held

**Amgen, Inc.**, South San Francisco, CA **June - September 2017**

Position: Intern, Pharmacokinetics and Drug Metabolism

**USAMRIID, Frederick, MD June - August 2013, January - May 2014**

Position: Intern, Toxicology

## Fellowships

**National Science Foundation Graduate Research Fellow June 2016 - Present**

Cell Biology, NSF GRFP DGE-1232825

## Publications

**Heck, CJS**, HK Seneviratne, and NN Bumpus. (2019). Twelfth-Position Deuteration Decreases Cytochrome P450 Production of 12-hydroxy-Nevirapine through the Kinetic Isotope Effect **.** *Manuscript in Preparation.*

Seneviratne, HK, **CJS Heck**, AN Hamlin, and NN Bumpus. (2019) Simultaneous spatial mapping of tenofovir, emtricitabine and efavirenz in mouse tissues using matrix-assisted laser desorption/ionization mass spectrometry imaging. *Manuscript in Preparation.*

**Heck, CJS,** AN Hamlin, and NN Bumpus. (2019). Efavirenz and Efavirenz-like Compounds Activate Human, Murine, and Macaque Hepatic IRE1α-XBP1. *Mol Pharmacol*. 95:183-195.

Narayanan, B, JM Lade, **CJS Heck,** KD Dietz, H Wade, and NN Bumpus. (2018). Probing Ligand Structure-Activity Relationships in Pregnane X Receptor (PXR): Efavirenz and 8-Hydroxyefavirenz Exhibit Divergence in Activation. *ChemMedChem*. 13:736-747

## Research Experience

**Cytochrome P450 Metabolism and Hepatotoxicity of the HIV non-nucleoside reverse-transcriptase inhibitors Efavirenz and Nevirapine**

*Current thesis research, Johns Hopkins School of Medicine, Department of Pharmacology and Molecular Sciences*

*Principle Investigator:* Dr. Namandjé Bumpus

Technical experience:

- Mass spectrometry analysis of drugs, drug metabolites, and peptides
- Triple Quadrupole and Orbitrap (high-resolution) Mass Spectrometry
- uHPLC-MS quantitative assay development and implementation
- nanoLC-MS proteomics workflow development and implementation
- Proteome Discoverer data analysis
- Extraction, detection, and quantitation of drugs/drug metabolites in various biological matrices (cells, microsomal assays, plasma, and culture medium)
- *In vitro* (microsomal) drug biotransformation characterization

- Measuring kinetics of drug metabolism
- General molecular biology techniques (PCR, western blotting, cloning)
- Bright-field and fluorescent microscopy
- Recombinant protein purification from bacterial expression systems
- Primary hepatocyte isolation and culture
- *In vivo* mouse dosing, handling, and dissection
- Participation in collaborative efforts with labs at Johns Hopkins University, Emory University, and the DIVA clinical trial team at the University of Melbourne
- Preparation of manuscripts for publication
- Data collection, management, analysis, and presentation locally and internationally

**Development of an *in vitro* Active Hepatic Drug Uptake Assay for the Purpose of *in silico* PK Modeling using Simcyp**

*June - September 2017, Amgen, Inc., Pharmacokinetics and Drug Metabolism*

*Supervisor:* Dr. Zhican Wang

Technical experience:

- uHPLC-MS analysis (triple quadrupole) of small molecules
- Hepatic uptake assay development
- Cryopreserved hepatocyte culture
- SimCyp *in silico* drug clearance modeling

- Data collection, management, analysis, and presentation at on-site and cross-site meetings

**Development of MERS-CoV 3-Chymotrypsin-like protease activity assay based on MALDI-IMS analysis of protein activity towards peptide microarrays**

*January - May 2014, USAMRIID, Toxicology Department*

*Principle Investigator*: Dr. Robert E. Ulrich

Technical experience:

- Recombinant protein purification
- Arrayjet microarray printing
- MALDI-TOF imaging mass spectrometry
- Data collection, management, analysis, and presentation

**Determining the Ligand and Confirming Surface Expression of Human G Protein-Coupled Receptor GP133**

*September 2013 - April 2014, Shippensburg University Chemistry Department*

*Faculty Advisor:* Dr. Thomas Frielle

Technical experience*:*

- Transfection
- Culturing of COS7 cells
- Immunofluorescent staining
- Data collection, management, analysis, and presentation

**Screening of Potential Small Molecule Inhibitors of *Variola major* H1 Phosphatase and Human Dual Specificity Phosphatase 14**

*June - August 2013, USAMRIID, Toxicology Department*

*Supervisor:* Dr. Megan E. Hogan

*Principle Investigator:* Dr. Robert E. Ulrich

Technical experience:

- Recombinant protein purification
- Arrayjet microarray printing
- Absorbance-based enzyme activity assays
- Surface plasmon resonance
- Data collection, management, analysis, and presentation

**Sequencing, Overexpression, and Gene Expression Analysis of Autophagy Related Genes in Glioma Cells**

*September 2012 - December 2013, Shippensburg University Biology Department*

*Faculty Advisors:* Dr. Sherri Bergsten and Dr. Lucinda Elliott

Technical experience:

- PCR and cloning
- Culturing of SNB19 glioblastoma cells
- Data collection, management, analysis, and presentation

## Abstracts Accepted for Presentation

**Twelfth-position deuterium substitution decreases cytochrome P450-dependent production of 12-hydroxy nevirapine.**

Heck, CJS, HK Seneviratne, and NN Bumpus.

Poster at Microsomes and Drug Oxidations 2018 (Kanazawa, Japan).

**Activation of X-Box Binding Protein 1 Splicing Contributes to Efavirenz-mediated Hepatocyte Death.**

Heck, CJS, AN Hamlin, and NN Bumpus

Poster at Experimental Biology 2018 (San Diego, CA).

Selected for Graduate Student Poster Competition

**Site-Specific Deuteration Decreases Cytochrome P450 Production of 12-Hydroxy-Nevirapine through the Kinetic Isotope Effect.**

Heck, CJS, HK Seneviratne, and NN Bumpus.

Poster at Experimental Biology 2018 (San Diego, CA).

**Efavirenz Treatment Activates XBP1 Splicing in Primary Hepatocytes: a Comparison Across Species and an Investigation into the Role of PXR.**

Heck, CJS and NN Bumpus.

Poster at Experimental Biology 2017 (Chicago, IL).

Selected for Graduate Student Poster Competition

**Efavirenz Treatment in Primary Mouse Hepatocytes Results in Splicing of XBP1.**

Heck, CJS and NN Bumpus.

Poster at Microsomal Drug Oxidations 2016 (Davis, CA).

Selected for Graduate Student Poster Competition

**Development of an activity assay for the Middle Eastern Respiratory Syndrome coronavirus 3-Chymotrypsin-like Protease.**

Heck, CJS, T Glaros, B Zhao, and RG Ulrich.

Poster at the NCI at Frederick 2014 Spring Research Festival (Frederick, MD).

**Plasma membrane-specific expression of human G-protein coupled receptor GP133.**

Heck, CJS and T Frielle.

Poster at ACS National Meeting 2014 (Dallas, TX).

**Examining the Effectiveness of Potential Small Molecule Inhibitors of *Variola major* H1 (VH1) Phosphatase and Human Dual Specificity Phosphatase 14 (DUSP14).**

Heck, CJS, M Hogan, B Zhao, and RG Ulrich.

Poster at the Summer 2013 NCI Frederick Student Poster Session (Frederick, MD).

**Expression, Cloning, and Sequencing of Atg4c Variant 1 and p62 Autophagy related cDNA from Glioma Cells**

Heck, CJS, E Shadle, J Sergent, J Rauchut, L Elliott, and S Bergsten.

Poster at the 2013 Shippensburg University Celebration of Student Research (Shippensburg, PA).

## Awards and Honors

| | |
|---|---|
| Molecular Pharmacology Highlighted Trainee Author | February 2019 |
| ASPET Karl H. Beyer, Jr. Travel Award | 2018 |
| Scheinberg Travel Award | 2016 |
| Shippensburg University Website Advertising Campaign: “Scholarship” Student | 2013 |

Commonwealth of Pennsylvania University Biologists Outstanding Student Award 2013

Shippensburg University Board of Governors Scholarship 2010-2014

Taylor N. Seitzinger Memorial Scholarship 2010-2011

Esther H. Ludwig Scholarship 2010-2014

## Professional Society Memberships

American Society for Pharmacology and Experimental Therapeutics **October 2016 - Present**

## Current Volunteering and Leadership Positions

**Pharmacology Student Initiative** **January 2015 - Present**

Position: Founding member and Officer

Description: Organize academic and social events, as well as community outreach initiatives in the Johns Hopkins Pharmacology and Molecular Sciences department to facilitate student and faculty interaction, as well as foster camaraderie and community involvement

**Destination Imagination** **January 2017 - Present**

Position: Volunteer Appraiser

Description: Coordinate creative problem-solving challenges for K-12$^{th}$ grade teams